The role of glial cells in the regulation of energy homeostasis

Ph.D. Thesis

Anett Stiftné Szilvásy-Szabó

Semmelweis University
János Szentágothai Ph.D. School of Neuroscience

Institute of Experimental Medicine
Hungarian Academy of Sciences

Supervisor:	Csaba Fekete, M.D., D.Sc.
Official reviewers:	Árpád Dobolyi, D.Sc.
	Balázs Gaszner, M.D., Ph.D.
Head of the Final Examination Committee:	András Csillag, M.D., D.Sc.
Members of the Final Examination Committee:	Krisztina Kovács, D.Sc.
	Attila Patócs, M.D., Ph.D.

Budapest
2018

Table of contents

Abbreviations

2-DG	2-deoxy-D-glucose
A20	tumor necrosis factor alpha-induced protein 3
ABC	avidin-biotin peroxidase complex
aCSF	artificial cerebrospinal fluid
ACTH	adrenocorticotropic hormone
AgRP	agouti-related peptide
ARC	hypothalamic arcuate nucleus
CART	cocaine- and amphetamine-regulated transcript
CCK	cholecystokinin
CNS	central nervous system
CPM	counts per million
CSF	cerebrospinal fluid
CSF1R	colony stimulating factor 1 receptor
CVOs	circumventricular organs
Cx43	connexin 43
DAB	diaminobenzidine
DAPI	4',6-diamidino-2-phenylindole
DARP-32	dopamine- and cyclic adenosine-monophosphate-regulated phosphoprotein
DEPC	diethylpyrocarbonate
DMN	dorsomedial hypothalamic nucleus
ERK	extracellular regulated kinase
FFAs	free fatty acids
GABA	gamma-aminobutyric acid
GFAP	glial fibrillary acidic protein
GHSR	growth hormone secretagogue receptor
GK	glucokinase
GLP-1	glucagon-like peptide 1
GLUT1	glucose transporter 1
GLUT2	glucose transporter 2
HFD	high-fat diet

Iba1	ionized calcium-binding adapter molecule 1
IGLE	intraganglionic laminar endings
Ikbkb	inhibitor of nuclear factor kappa-B kinase subunit beta
Ikbke	inhibitor of nuclear factor kappa-B kinase subunit epsilon
Il6	interleukin 6
ISH	*in situ* hybridization
K_{ATP}	ATP-inhibited potassium channel
KO	knock out
LCM	laser capture microdissection
LepR	leptin receptor
LH	lateral hypothalamic area
LY	Lucifer yellow
MCR3	melanocortin receptor 3
MCR4	melanocortin receptor 4
ME	median eminence
NF-κB	nuclear factor kappa B
NGS	next-generation sequencing
NHS	normal horse serum
NPY	neuropeptide Y
NSC	neural stem cell
NTS	nucleus tractus solitarii
PB	phosphate buffer
PBS	phosphate buffered saline
PC1	prohormone convertase 1
PC2	prohormone convertase 2
PFA	paraformaldehyde
PI3K	phosphatidylinositol-3-kinase
POMC	proopiomelanocortin
PVN	hypothalamic paraventricular nucleus
PYY	peptide YY
SOCS3	suppressor of cytokine signaling 3
STAT3	signal transducer and activator of transcription 3

TLR	toll-like receptor
TNFα	tumor necrosis factor alpha
TRH	thyrotropin-releasing hormone
TSH	thyroid stimulating hormone
VEGF-A	vascular endothelial growth factor A
VMN	ventromedial nucleus of the hypotahalmus
WAT	white adipose tissue

1. Introduction

1.1. The key components of the energy homeostasis

The perception of the status of energy stores and the quality and quantity of the consumed food by the central nervous system (CNS) plays crucial role in the regulation of energy homeostasis (Morton et al., 2006, Schwartz et al., 2000). This regulation is guided by the communication between the peripheral organs and the brain. The two main routes of this communication are the peripheral nerves (primarily the vagus nerve) and the blood circulation. The vagus nerve mediates the effects of some gastrointestinal hormones and the information from chemo- and mechanosensors of the gastrointestinal tract towards the nucleus tractus solitarii (NTS) in the brainstem (Li, 2007). The primary central target of peripheral, blood-derived energy homeostasis-related hormones is the hypothalamic arcuate nucleus (ARC), but these hormones can also directly influence other brain regions including the NTS (Kanoski et al., 2014) (*Figure 1*).

1.2. The role of vagus nerve in the mediation of the energy homeostasis-related signals

The vagus nerve represents the longest nerve of the autonomic nervous system and is involved in the regulation of the heart, lungs and the digestive tract. The sensory fibers of the vagus nerve convey afferent information from the mechano- and chemoreceptors of the gastrointestinal tract and mediates information about changes of local hormonal signals to the NTS (Schwartz et al., 2000).

The vagal afferent fibers can be found within all layers of the stomach and the small intestine, however, their location and morphology strongly influences their modality to mechanical or chemical stimuli. The intraganglionic laminar endings (IGLEs) are embedded between the longitudinal and circular smooth muscle layers (Berthoud and Powley, 1992) and being sensitive for both contractions and distensions, IGLEs represent the first candidates to sense the gastric distension after food consumption. Besides stomach, IGLEs can be also found in the small intestine. The intramuscular arrays represent another type of vagus nerve ending either establishing parallel bundles

to the lamina muscularis externa or sphincter regions of the stomach (Berthoud and Powley, 1992) and their function is to sense the length of the stomach (Phillips and Powley, 2000). The mucosal afferents are both mechano- and chemosensitive components of the vagal sensory machinery. These afferents extend through the submucosal layer and can respond to mediators released from the enteroendocrine cells (Page et al., 2002).

In addition, the vagus nerve can also sense changes of certain hormones by expressing receptors for gastrointestinal hormones, like cholecystokinin (CCK), glucagon-like peptide 1 (GLP-1) and peptide YY (PYY) by which the mechanosensitivity of the vagal afferent fibers also can be modulated (Kentish and Page, 2014). The enteroendocrine cells of the intestine secrete CCK, which acting through the CCK-receptors of the vagal afferents inhibits gastric emptying and food intake (Glatzle et al., 2003). GLP-1 released from the intestinal L-cells was shown to activate both gastric and jejunal vagal afferents (Gaisano et al., 2010) resulting in decreased food intake. The L-cell derived PYY can act through PYY-receptors present on both the intestinal vagal afferents and on neurons of the ARC, indicating, that PYY can reduce food intake via the combination of more pathways (Broberger et al., 1997, Burdyga et al., 2008).

Thus, vagal afferents mediate the mechanical, chemical and hormonal information of the gastrointestinal tract and serve information about the quality and quantity of the consumed food to the NTS which integrates the food-related information. Besides the NTS, the brainstem contains other fields involved in the vagal sensory complex establishing the dorsovagal complex, including the chemosenory area, the circumventricular area postrema (AP) and the dorsal motor nucleus of the vagus, which integrates the motor and secretory drive of the gastro-intestinal tract (Young, 2012).

1.3. The role of blood-born signals in the mediation of energy homeostasis-related information

In order to regulate the food intake and energy expenditure, the brain has to sense the nutritional status and the condition of the peripheral energy stores. Blood-transported signals, like nutrients, such as glucose, amino and fatty acids, nutrition-dependent gastrointestinal hormones, like GLP-1, PYY, CCK and ghrelin or adiposity signals, like

the white adipose tissue (WAT) derived leptin and the pancreatic insulin (Berthoud, 2008, Schwartz et al., 2000), play critical role in this process.

The main feature of adiposity signals is that their circulating level is proportional to the size of the adipose tissue and other energy stores. The first described adipostatic hormone was the insulin. **Insulin** is produced by the pancreatic beta cells after carbohydrate intake (Begg and Woods, 2012). Its level is very quickly regulated by the circulating glucose levels. Thus insulin level is decreased during fasting and very quickly increased after food intake (Begg and Woods, 2012). This glucose induced regulation is, however, superimposed on a longer term regulation that makes the circulating insulin level proportional to the size of adipose depots (Woods, 2013). Insulin acts through its receptor that is a member of the tyrosine kinase receptor family (Ebina et al., 1985, Ullrich et al., 1985). High level of insulin receptor is expressed in the skeletal muscle, where insulin supports the glucose uptake by the cells as energy source, resulting in decreased blood glucose level (Boucher et al., 2014). In the liver, insulin also promotes the uptake and the transformation of glucose to glycogen via glycogenesis and to fat via lipogenesis, moreover, insulin has opposite effect as glucagon, by inhibiting gluconeogenesis (Saltiel and Kahn, 2001). Similarly to skeletal muscle and liver, insulin regulates the uptake of glucose by the adipose tissue, promoting the development of fat depots (Mitrou et al., 2013). Since the changes of the insulin level in the CSF is relatively slow, it cannot follow the fast, glucose level induced fluctuation of the circulating insulin level. Therefore, it is likely, that the central insulin level is primarily regulated by the size of the adipose tissue. While peripheral administration of insulin indirectly stimulates food intake due to its hypoglycemic effect, insulin exerts opposite effects in the brain: it inhibits food intake and stimulates energy expenditure (Woods et al., 1979).

In 1994, the gene coding another adiposity signal, leptin, was identified (Zhang et al., 1994). **Leptin** is predominantly produced by the adipocytes of the WAT (Flier, 1998) and as an adipostatic hormone, the circulating level of leptin is proportional to the size of the WAT (Schwartz et al., 2000). Leptin was identified as the hormone missing from the obese ob/ob mouse line (Halaas et al., 1995). Administration of leptin to rodents with normal body weight results in inhibition of food intake and decrease of body weight (Halaas et al., 1995). Leptin also regulates energy expenditure as both central

and peripheral leptin administration markedly stimulates the basal energy expenditure. While leptin has potent anorexigenic effect in animals with normal body weight, obese rodents and humans have high leptin level and develop leptin resistance (Zhou and Rui, 2013). Therefore, leptin is crucial for the normal regulation of energy homeostasis, but cannot be used to treat obesity. In humans, the mutation of leptin gene causes similar obese phenotype than in rodents (Farooqi et al., 1998).

GLP-1 is a food intake-related peptide secreted by the L-cells of the small intestine (Herrmann et al., 1995). In addition, GLP-1 is also synthesized in a neuronal group of the NTS (Herrmann et al., 1995). By acting in the pancreas, GLP-1 induces insulin secretion, while it inhibits glucagon release (Holst, 2007), thus, GLP-1 has a crucial role in the regulation of glucose homeostasis. Peripheral as well as central administration of GLP-1 was proved to inhibit food intake and increase energy expenditure (Gutzwiller et al., 1999, Tang-Christensen et al., 1996). Analogues of the hormone, like exendine-4 and liraglutide were also shown to reduce body weight both in rodents and humans (Edwards et al., 2001, Hayes et al., 2011). GLP-1 and its analogues are able to cross the blood-brain barrier (BBB) (Hunter and Holscher, 2012) and GLP-1 receptors have been shown to be present in several brain regions involved in the regulation of energy homeostasis (Cork et al., 2015). These data together suggest that GLP-1 have important role in the regulation of energy homeostasis. GLP-1 has, however, a very short half-life raising the question whether peripheral GLP-1 may reach the CNS in effective dose. However, the high amount of GLP-1 receptor in the ARC, where relatively few GLP-1 axons can be found suggests that peripheral GLP-1 may influence this nucleus (Personal observation). This effect of GLP-1 may be enhanced by inhibition of the GLP-1 degrading dipeptidyl peptidase-4 or by administration of the agonists of GLP-1 with longer half-time. These strategies are widely used in the treatment of type 2 diabetes and investigated as the targets in the treatment of obesity (Dailey and Moran, 2013, Lovshin and Drucker, 2009)

PYY is a 36-amino acid peptide released from the distal segments of the gastrointestinal tract, predominantly from the ileum and colon (Tatemoto, 1982). The main function of PYY is to inhibit gastric motility and to promote the absorption of water and electrolytes in the colon (Liu et al., 1996). PYY is secreted from the gut into the blood circulation in a nutrient-dependent manner. During fasting, PYY level is low, however,

during food intake the PYY level is rising (Adrian et al., 1985). It has been shown that intraperitoneal injection of the predominant circulating form, the $PYY_{3-36,}$ decreases food intake in rats (Batterham et al., 2002). Additionally, peripheral infusion of PYY_{3-36} reduces the appetite of non-obese humans (Batterham et al., 2002). Moreover, PYY knock out (KO) mice are hyperphagic, their food consumption is significantly higher and show increased subcutaneous and visceral adiposity (Batterham et al., 2006). These data all confirm the anorexigenic nature of PYY.

CCK is secreted from the enteroendocrine I cells of the small intestine and it has an important role in the regulation of the exocrine pancreatic secretion, in the modulation of gastric motility and the digestion of fat by increasing the release of bile from the gallbladder (Sayegh, 2013, Stengel and Tache, 2011). The secretion of CCK occurs in a nutrition dependent manner, the peak of the CCK level can be observed 15 min after the start of the meal in human (Stengel and Tache, 2011). The anorexigenic feature of CCK was shown several years ago by central administration of the peptide that markedly reduced the amount of the consumed food. CCK was also shown to decrease food intake in humans (Goebel-Stengel et al., 2012, Smith et al., 1981). The CCK_{58} isoform decreases the consumed food during one meal; nevertheless, it cannot reduce the daily food intake, as intraperitoneal injection of the peptide increases the frequency of meals (Goebel-Stengel et al., 2012). While, other nutrition dependent hormones regulate food intake via crossing the BBB, the main pathway that mediates the effects of CCK is the vagus nerve-NTS pathway (Smith et al., 1981).

The common feature of the above mentioned gastrointestinal hormones is their anorexigenic effect, however, in 1999 a new gastrointestinal peptide, ghrelin was discovered with opposite effect (Kojima et al., 1999, Nakazato et al., 2001).

Ghrelin was shown to be secreted from the mucosa of the stomach (Date et al., 2000) before and during nutrition and to have potent effect on appetite (Cummings et al., 2001). The serum level of ghrelin is the highest just before the expected meal time and decreases after food consumption (Tschop et al., 2001). Ghrelin was named after its ability to bind to the growth hormone secretagogue receptor (GHSR) and to stimulate the secretion of growth hormone (Kojima et al., 1999). Both central and peripheral administration of ghrelin was shown to increase food intake, moreover it results in body

weight gain (Tschop et al., 2000). Additionally, intraperitoneal injection of ghrelin significantly increases the appetite of humans (Wren et al., 2001). According to these data, ghrelin is the only peripheral hormone with orexigenic effect (Iwakura et al., 2015). Besides regulating food intake, ghrelin also decreases energy expenditure and the two processes together lead to the increase of the WAT (Davies et al., 2009).

Figure 1: Schematic illustration of the peripheral adiposity and satiety signals regulating energy homeostasis

Adiposity signals like leptin and insulin from the adipose tissue and pancreas, respectively and satiety signals like the anorexigenic GLP-1, PYY and the orexigenic ghrelin from the gastrointestinal tract are released into the blood and delivered to the neurons of the ARC. The ARC contains first order neurons of the regulation of energy homeostasis. These neurons sense the peripheral signals, integrate with neuronal inputs and transmit this information toward second order neuronal groups, like neurons of the LH and PVN. The other energy expenditure-related sensory area of the brain is the NTS integrating the information carried by the vagus nerve from the gastrointestinal tract. The descending pathways from the hypothalamus can change the sensitivity of the NTS neurons to the vagal afferents.

Abbreviations: PVN –hypothalamic paraventricular nucleus; LH – lateral hypothalamic area; ARC – arcuate nucleus; NTS – nucleus tractus solitarii; CCK – cholecysokinin; GLP-1 – glucagon-like peptide 1; PYY – peptide YY.

Modified from (Schwartz et al., 2000)

The central melanocortin system

The central melanocortin system plays a crucial role in the regulation of energy homeostasis including the mediation of the peripheral signals toward the brain (Cone, 2005, Ellacott and Cone, 2006). The melanocortin system is composed of the 5 melanocortin receptors (MCRs) and their ligands the proopiomelanocortin (POMC) derived peptide agonists and the endogenous antagonists, like the agouti-related peptide (AGRP). The melanocortin system of the brain includes the POMC expressing neurons of the ARC and the NTS, the AGRP neurons of the ARC and the downstream targets of these neuronal groups expressing MCRs (Cone, 2005).

The elements of the melanocortin system. The POMC serves as a precursor that is cleaved by prohormone convertase enzymes resulting in smaller tissue-specific melanocortin peptides. The melanocortin receptor family consists of 5 7-transmembrane G protein-coupled receptors that have different tissue specific expression pattern and different affinity for their agonists, melanocortins and antagonists, like AgRP. The agonists of the different receptors are listed in the order of their affinity. Modified from (Dib et al., 2017).
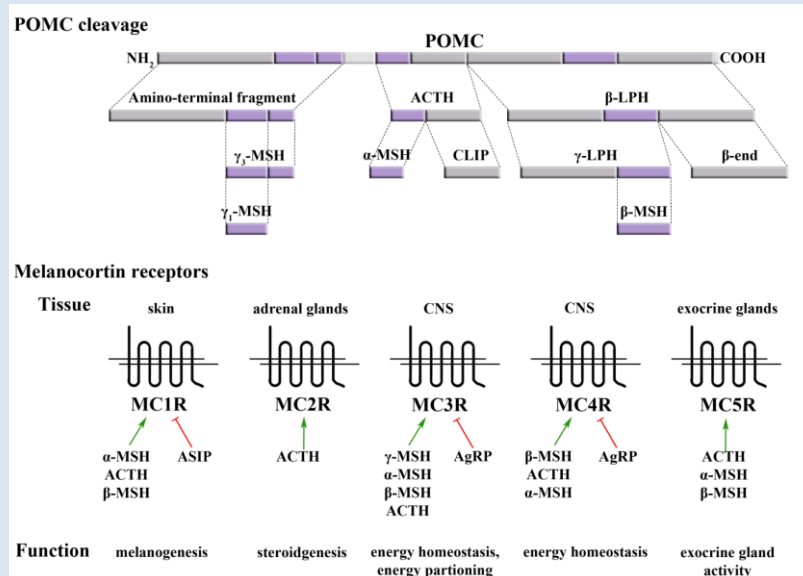
The role of the melanocortin system in the regulation of energy homeostasis has been shown by genetic lesions of this signaling pathway. Deletion of the *POMC* gene in mice results in obesity (Yaswen et al., 1999), moreover, the loss of either melanocortin receptor 3 or 4 (MCR3 or MCR4) also cause obese phenotype (Butler et al., 2000, Huszar et al., 1997).Similarly to rodents, deficiency of the human melanocortin system has been shown to lead to failures in the regulation of energy homeostasis and thus obesity (Farooqi et al., 2000, Krude et al., 1998).

1.4. The role of ARC in the regulation of feeding and energy metabolism

The main central target of the above mentioned energy homeostasis related peripheral hormones is the ARC, containing several elements of the central melanocortin system. The ARC is located in the vicinity of the BBB free median eminence (ME). This way, blood-derived hormones and metabolites can easily reach the neurons in this brain area.

The ARC contains at least two feeding-related neuronal populations: the proopiomelanocortin (POMC) and cocaine- and amphetamine-regulated transcript (CART) synthesizing anorexigenic neurons and the neuropeptide Y (NPY), agouti-related peptide (AgRP) and gamma-aminobutyric acid (GABA) producing orexigenic cell population (Blouet and Schwartz, 2010, Hillebrand et al., 2002). The two distinct neuronal groups are located in different parts of the ARC, while the POMC/CART neurons reside in the more lateral parts of the ARC; the NPY/AgRP neurons are located in the ventromedial part of the nucleus. These two neuronal groups have antagonistic effects in the regulation of food intake and energy expenditure (Ollmann et al., 1997).

1.4.1. The anorexigenic cell population of the ARC

The anorexigenic neuronal group of the ARC co-synthesizes two peptide precursors, the POMC and CART (Dhillo et al., 2002, Fekete et al., 2000c).

Proteolytic cleavage of POMC results in biological active peptides that plays crucial role in the regulation of energy homeostasis (See detailes in *The central melanocortin system* textbox). The role of POMC is widely investigated by animal models. *Pomc*-null mutant mice have early onset obesity, failure in the adrenal development, and alteration in hair pigmentation (Challis et al., 2004, Yaswen et al., 1999). Neuronal specific deletion of POMC results in similar obesity phenotype without effects on adrenal function and hair pigmentation further demonstrating the role of centrally synthesized POMC in the regulation of energy homeostasis (Smart and Low, 2003). In contrast, overexpression of POMC has been shown to prevent the development of obesity in mice (Mizuno et al., 2003). In the field of energy homeostasis, the most widely studied POMC derived peptide is α-MSH. Central administration of α-MSH decreases food intake and markedly stimulates energy expenditure (Murphy et al., 1998). α-MSH primarily exerts its central effects via two types of MCRs, the MC3R and the MC4R.

Similarly to the neuronal absence of POMC, the loss of MC4R leads to increased food intake, decreased energy expenditure and obesity in mice (Adan et al., 2006, Huszar et al., 1997). In humans, the mutations of *Pomc* and Mc4r genes also exist (Challis et al., 2002, Farooqi et al., 2006, Krude et al., 1998). These mutations can be detected in approximately 6-10% of the clinically obese patients (Farooqi et al., 2006). Similarly to rodents, POMC deficiency is characterized by adrenal deficiency, red-hair pigmentation and early onset obesity in humans (Farooqi et al., 2006, Krude et al., 1998). Mutations of the *Mc4r gene* result in increased food intake, decreased energy expenditure and obese phenotype in humans (Farooqi and O'Rahilly, 2008).

CART is also proteolitically processed in neurons (Douglass et al., 1995). The most abundant CART peptides in the brain are the CART 55-102 and CART 62-102 (Douglass and Daoud, 1996, Gautvik et al., 1996). Both intracerebroventricular administration and hypothalamic intranuclear injections of CART can cause inhibition of food intake (Abbott et al., 2001, Kristensen et al., 1998). Moreover, central administration of neutralizing CART antibodies leads to hyperphagic response, demonstrating that not only the exogenous, but also the endogenous CART inhibits food intake (Kristensen et al., 1998). Interestingly, overexpression of CART in different neuronal groups of the hypothalamus provided inconsistent data suggesting that in some neuronal connections CART may have rather orexigenic effect (Kong et al., 2003, Qing and Chen, 2007). In order to better understand the consequences of the absence of CART expression, several KO models have been generated, summarized in the work of Lau and Herzog (Lau and Herzog, 2014). CART KO mice have increased body weight only after 40 weeks of age when kept on standard chow (Wierup et al., 2005). These mice have, however, elevated blood insulin level with normal circulating glucose level suggesting that they develop insulin resistance (Wierup et al., 2005). However, when CART KO mice are fed with high-fat diet (HFD), they have significantly increased food intake and body weight and altered behavior (Asnicar et al., 2001). Surprisingly, CART is not expressed in the POMC neurons of the human infundibular nucleus, the homologue of the rodent ARC (Menyhert et al., 2007). CART is rather expressed in the orexigenic AGRP/NPY neurons of the human hypothalamus (Menyhert et al., 2007) raising the possibility that CART may have different role in humans. However, polymorphism of the CART gene is associated with reduced metabolic rate,

hyperphagia, obesity and increased chance to develop type II diabetes suggesting its anorexigenic effect even in the human hypothalamus (Banke et al., 2013).

In rodents, the unequivocal proof for the anorexigenic nature of the POMC/CART neurons is that ablation of these neurons in adult mice results in hyperphagia and weight gain (Gropp et al., 2005).

1.4.2. The orexigenic cell population of the ARC

The ventromedial part of the ARC contains the orexigenic neurons that express AgRP and NPY and utilize GABA as classical transmitter (Aponte et al., 2011, Krashes et al., 2011).

Shortly after the discovery of NPY, its orexigenic effect was also described (Clark et al., 1985, Levine and Morley, 1984). Intracerebroventricular administration of NPY stimulates food intake in a dosage dependent manner (Clark et al., 1985). Furthermore, chronic intrahypothalamic injection of NPY results in increased body weight (Beck et al., 1992). The NPY release from the terminals of the ARC neurons is regulated by the nutritional status. NPY release is the highest in the hypothalamic paraventricular nucleus (PVN) just before the time of the scheduled feeding and continuously decreases during feeding (Kalra et al., 1991). Animal models with obese phenotype caused for example by the loss of MCR or by leptin deficiency have elevated NPY levels (Kesterson et al., 1997). Surprisingly, NPY KO animals have normal body weight and respond to fasting with regular hyperphagia (Erickson et al., 1996a) suggesting that the lack of NPY can be compensated. However, if NPY KO mice are crossed with leptin-deficient mice, the lack of NPY attenuates the obesity of ob/ob mice by reducing the food intake and stimulating the energy expenditure emphasizing the importance of NPY in the leptin dependent energy balance pathway (Erickson et al., 1996b). Conversely, the viral overexpression of NPY causes a marked obesity syndrome with elevated adiposity and hyperinsulaemia (Lin et al., 2006), further demonstrating the orexigenic role of NPY.

A great majority of the ARC NPY neurons co-express AgRP, a second orexigenic peptide (Hahn et al., 1998). Central injection of AgRP increases food intake as an antagonist of the MC3R and MC4R (Ollmann et al., 1997). Both overexpression of

AgRP and the central administration of the peptide cause significant increase in food intake with simultaneous decrease in energy expenditure (Goto et al., 2003, Korner et al., 2003). The effect of AGRP on the energy expenditure is mediated at least partly via the hypothalamic-pituitary-thyroid axis as central administration of AGRP markedly inhibits the TRH expression of the hypophysiotropic neurons and results in a fall of peripheral thyroid hormone levels (Fekete et al., 2004). Rodents sensitive to diet-induced obesity show altered AgRP/NPY expression (Wang et al., 2002a) and similarly in humans, a strong correlation can be found between body mass index and hypothalamic AgRP/NPY expression (Alkemade et al., 2012). In spite of the clear correlation between obese phenotype and the elevated AgRP expression, the lack of *Agrp* gene does not induce an obvious phenotype. Similarly to those seen in the case of NPY KO animals, the inactivation of *Agrp* gene does not have any effect on the body weight regulation (Qian et al., 2002). Furthermore, even the NPY/AgRP double KO mice have normal body composition (Flier, 2006, Qian et al., 2002).

As slow, progressive post-embryonic ablation of the NPY/AgRP neurons results in moderate reduction of body weight of adult mice (Bewick et al., 2005), however, rapid ablation of the AgRP neurons in adult animals leads to life threatening anorexia and weight loss (Gropp et al., 2005), it is likely, that there are compensatory processes that can balance the absence of these neurons and their transmitters. This is further supported by the experiments that if the mice are treated for two weeks with $GABA_A$ agonist after the ablation of these neurons, their energy homeostasis can normalize (Wu and Palmiter, 2011).

1.4.3. Intra-ARC connections

During the last decades, several investigations have substantiated the existence of neuroanatomical connections between the orexigenic and anorexigenic cell populations of the ARC. These connections utilize GABA and melanocortin peptides (Bagnol et al., 1999, Cowley et al., 2001). GABA release from the NPY/AgRP/GABA-containing nerve terminals induces inhibitory currents and hyperpolarization of the innervated POMC/CART neurons (Cowley et al., 2001). This way GABA decreases the firing rate of the POMC/CART cells. On the other hand, POMC/CART neurons were shown to express MC3R, which specifically binds POMC derivates with high affinity. The

activation of POMC/CART neurons evokes elevated release of POMC-products forming a short autoinhibitory feedback loop through MC3R activation (Cowley et al., 2001).

1.4.4. The perception of the peripheral signals by the ARC neurons

A critical area of the brain that can sense the energy homeostasis-related hormones and circulating nutrients is the ARC (Schwartz et al., 2000). Neonatal ablation of ARC causes obesity and leptin resistance (Morris et al., 1998). Both the NPY/AGRP and the POMC/CART neurons can sense the peripheral energy homeostasis-related signals (Schwartz et al., 2000). These neuronal groups express leptin, insulin, ghrelin, PYY and glucocorticoid receptors and are sensitive to glucose, amino- and fatty acids (Blouet et al., 2009, Cheng et al., 1998, Corander and Coll, 2011, Hakansson et al., 1996, Havrankova et al., 1978, Ibrahim et al., 2003, Morton et al., 2006, Willesen et al., 1999). Thus, changes of the energy availability regulate both neuronal groups of the ARC. Fasting increases the firing of the NPY/AGRP neurons and stimulates the NPY and AGRP synthesis in these cells (Takahashi and Cone, 2005). In contrast, fasting inhibits the anorexigenic neurons and decreases the POMC and CART synthesis in these cells (Mizuno et al., 1998). Both central and peripheral administration of leptin to fasted animals completely reverse these fasting induced changes (Takahashi and Cone, 2005).

Leptin has both direct and indirect effects on the POMC neurons (Cowley et al., 2001, Elias et al., 1999). The POMC neurons express leptin receptors (LepRs) and leptin directly excites these cells, but the effect of the selective ablation of LepR from the POMC neurons is relatively modest compared to the effect of the deletion of POMC or the MC4R (Balthasar et al., 2004) suggesting that other neuronal populations also play role in the mediation of leptin's effect on the POMC neurons. As absence of lepR from glutamatergic neurons has also only mild phenotype, but the lack of this receptor from GABAergic neurons induces obesity, it was suggested that leptin induced inhibition of the GABAergic input of POMC neurons is important for the leptin induced activation of the POMC neurons (Cowley et al., 2001, Elias et al., 1999).

Similarly to leptin, glucose and insulin also stimulates the POMC/CART neurons (Ibrahim et al., 2003, Schwartz et al., 2000). Interestingly, however, these signals have

20

different effects on the synthesis of POMC and CART when administered to fasted animals. While leptin stimulates the synthesis of both peptides, glucose and insulin has stimulatory effect only on the POMC gene (Fekete et al., 2006). This would suggest that the activation of POMC/CART neurons by different peripheral signals may exert different effect on the second order neuronal groups.

GHRS1a is also present in a population of POMC neurons; however, data suggest that the effect of ghrelin on the POMC neurons may be primarily indirect via the NPY/AGRP neurons (Chen et al., 2004).

The NPY/AGRP neurons are oppositely regulated by peripheral signals compared to the POMC/CART neurons. Leptin administration hyperpolarizes these neurons and inhibits their NPY and AGRP synthesis (Vong et al., 2011). Glucose and insulin also inhibit these cells, but while insulin inhibits only the NPY synthesis in these cells, glucose influences neither the NPY nor the AGRP synthesis (Fekete et al., 2006). Ghrelin directly stimulates these neurons (Hewson and Dickson, 2000, Wang et al., 2002b).

The presence of Y_2 receptor in the NPY expressing neurons of the ARC suggest, that besides NPY, PYY can also act directly on these cells (Broberger et al., 1997). Injection of PYY into the ARC inhibits the nerve terminals of NPY/AGRP neurons (Batterham et al., 2002) (*Figure 2*).

The ARC can also sense and respond to the changes of the plasma levels of free fatty acids (FFAs) (Lam et al., 2005). Increased FFA levels of the plasma in the case of HFD were shown to be associated with higher levels of FFAs in the orexigenic and anorexigenic neurons of the ARC. Furthermore, both long-term diet rich in the saturated fatty acid palmitate or rapid enteral palmitate-rich milk injection leads to the elevation of FFA levels of ARC, suggesting, that not only prolonged HFD, but also postprandial elevations of the peripheral FFA levels can be sensed by hypothalamic neurons (Valdearcos et al., 2014). The sensation of FFAs and the induction of the adaptive inflammatory response by the ARC neurons can occur by the involvement of receptor- and metabolism-dependent mechanisms. As ARC neurons express toll-like receptor 2 (TLR2) (Shechter et al., 2013), it is likely, that these neurons are able to directly sense FFAs. On the other hand, as FFAs are normally unreactive, the esterification of FFAs is essential in order to initiate lipid signaling pathways (Schmelz and Naismith, 2009). It

21

has been shown, that NPY/AgRP neurons express a key enzyme of FFA metabolism further proving the involvement of ARC feeding-related neurons in the sensation of lipids (Andrews et al., 2008).
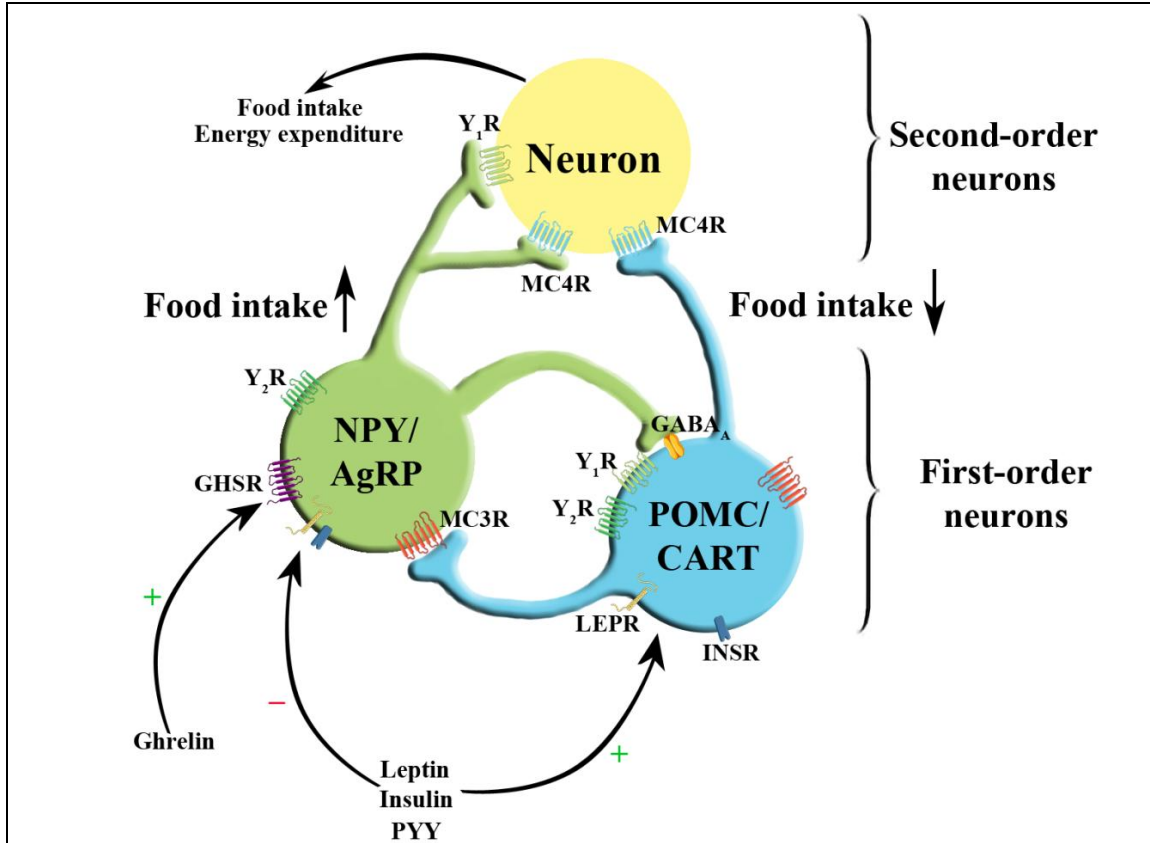
Figure 2: Schematic illustration of the perception of the peripheral signals by the ARC neurons, intra-ARC connections and transmission of the signals to second-order neurons.

The peripheral hormones regulate the activity of the feeding-related neurons by acting directly on their own receptors. The feeding-related neurons of the ARC, containing either orexigenic NPY and AgRP or anorexigenic POMC and CART form a well-organized autoregulatory network. NPY/AgRP neurons also co-express GABA, inhibiting POMC/CART neurons, while POMC/CART neurons inhibit NPY/AgRP neurons via MCRs. The signals from the ARC neurons are transmitted to second-order neurons by activating them via MCRs or Y receptors.

Abbreviations: GABA_A – gamma aminobutyric acid receptors A; GHSR – growth hormone secretagogue receptor; INSR – insulin receptor; LEPR – leptin receptor; MC3R, MC4R – melanocortin receptor 3 or 4; PYY – peptide YY; Y1R, Y2R – neuropeptide Y 1 or 2 receptor.

Based on (Cone, 2005) and (Schwartz et al., 2000) after modification.

1.4.5. Connections of the ARC neurons with second-order neurons of the energy homeostasis

The NPY/AGRP and the POMC/CART neurons of the ARC transmit the peripheral information toward the so-called second-order neurons. These neurons express melanocortin and NPY receptors. As both the NPY/AgRP and the POMC/CART neurons have widespread projections, the second order neurons are also found in many brain areas including the PVN, the hypothalamic dorsomedial nucleus (DMN) and cell groups of the lateral hypothalamic area (LH) which are also involved in the regulation of energy homeostasis (Elmquist et al., 1998).

The DMN receives very dense innervations from both AGRP and the POMC neurons (Gao and Horvath, 2007). In addition to this ARC inputs, de DMN also receives information from the circadian master regulator, the suprachiasmatic nucleus via relay neurons of the subparaventricular zone (Huang et al., 2011), thus this nucleus can integrate the energy homeostasis and circadian information. Besides its projections to other energy homeostasis related hypothalamic nuclei, like the PVN (Bernardis and Bellinger, 1998, Gao and Horvath, 2007), the DMN sends a multisynaptic descending pathway to the brown adipose tissue that has important role in the regulation of thermogenesis and energy expenditure (Bamshad et al., 1999, Chitravanshi et al., 2016).

The PVN also receives very dense innervations from the two feeding-related neuronal groups of the ARC and these inputs converge on the very same PVN neurons indicating that the two antagonistic ARC neuron populations together fine tune the activity of the PVN neurons (Cone, 2005, Fekete et al., 2000a, Schwartz et al., 2000). In accordance to the very dense AGRP and α-MSH-containing input of this nucleus, the PVN has the highest MC4R content among the hypothalamic nuclei (Shukla et al., 2012). The PVN has critical role in the regulation of energy homeostasis. Hypophysiotropic TRH, CRH and somatostatin neurons of the PVN regulate energy homeostasis by controlling the hypothalamic-pituitary-thyroid and adrenal axes and the hypothalamic-somatotrop axis (Fekete and Lechan, 2014). In addition, descending inputs from the PVN innervates important vegetative nuclei of the brainstem, thus PVN can also regulate food intake and energy expenditure via these brainstem connections.

The LH is also a target of the of the ARC neurons (Elias et al., 1999). In this hypothalamic region, the MCH, orexin and neurotensin neurons are the most well known energy homeostasis related neuronal groups (Schwartz et al., 2000). In addition to other hypothalamic nuclei, these LH neuronal groups are also interconnected with reward-related neuronal circuits suggesting their role in the integration of the energy homeostasis and reward related signals (Stuber and Wise, 2016).

1.5. The role of tanycytes in the regulation of feeding and energy metabolism

1.5.1. Tanycytes, a special glial cell type of the hypothalamus

Tanycytes are specialized glial cells that line the floor and the ventrolateral walls of the third ventricle between the rostral and caudal limits of the hypothalamic ME. Earlier, tanycytes were simply considered as supporting and barrier forming cells, but during the last years number of data was published demonstrating that tanycytes can actively regulate neuronal functions in the hypothalamus (Lechan and Fekete, 2007).

1.5.2. General features of tanycytes

A dominant feature of tanycytes is their obvious polarization (Bruni, 1974, Rodriguez et al., 2005). The small cell bodies of tanycytes are located in the ependymal layer of the third ventricle. Microvilli or bulbous protrusions project from their ventricular surface into the cerebrospinal fluid (CSF) (Firth and Bock, 1976), while a single, long process projects into the neuropil of the hypothalamus from their basal surface (Akmayev and Popov, 1977, Monroe and Paull, 1974).

According to the localization and anatomy of these cells, tanycytes can be classified into four subtypes (Akmayev and Fidelina, 1976, Akmayev et al., 1973, Akmayev and Popov, 1977, Rodriguez et al., 1979). The α1- and α2-tanycytes line the ventrolateral walls of the third ventricle (Akmayev et al., 1973, Rodriguez et al., 1979), β1-tanycytes line the lateral extensions of the infundibular recess of the third ventricle (Amat et al., 1999) and β2-tanycytes are situated in the floor of the ventricle. The projection field of the four subtypes differs. The basal process of α1-tanycytes projects to the DMN and ventromedial nuclei, the α2-tanycytes project to the ARC, the process of β1-tanycytes terminate on the surface of the tuberoinfundibular sulcus, while the basal process of β2-

tanycytes terminate around the portal capillaries of the ME (Flament-Durand and Brion, 1985, Kozlowski and Coates, 1985, Peruzzo et al., 2000).

By forming tight junctions in the wall of third ventricle, tanycytes are involved in the formation of the blood-brain barrier separating the CSF from the extracellular fluid of the BBB free ME (Mullier et al., 2010). Tanycytes are also involved in the formation of the BBB around the capillaries of the ARC. In addition, tanycytes actively regulate neuroendocrine functions including the hypothalamic-pituitary-gonadal (Prevot, 2002) and -thyroid axes (Fekete et al., 2000b, Tu et al., 1997), and play role in the control of physiological functions such as thermoregulation, feeding and energy balance (Bolborea and Dale, 2013).

1.5.3. Tanycytes as barrier forming cells

In most brain areas the molecular trafficking is restricted between the blood and the neuropil by the BBB, built up by tight junctions of the adjacent endothelial cells that line the capillaries and the surrounding glial end feet (Neuwelt et al., 2011). The exemptions are the so called circumventricular organs (CVOs) where the endothelium around microvessels is fenestrated, thus allowing the free passage of the blood-borne molecules (Ciofi, 2011).

The ME represents one of the CVOs, however, tight junctions among the cell bodies of β-tanycytes in the ventral wall of the third ventricle act as a shifted physical barrier between blood and CSF, preventing the uncontrolled diffusion of the blood-borne molecules to other brain areas. Indeed, β-tanycytes express elements of tight junctions like zonula occludens 1, occludin and claudin 1 and 5 (Mullier et al., 2010). In contrast, α-tanycytes do not express claudin 1 and form less organized tight junction pattern of zonula occludens 1, occluding and claudin 5, thus lack barrier properties (Rodriguez et al., 2005). On the other hand, tanycytes located on the border of ME and ARC; establish an interface between the CSF, blood and the ARC promoting the passage of peripheral signals to the energy homeostasis-related brain regions.

Changes of energy homeostasis are able to restructure the barrier composed of tanycytes between ME and ARC and thus change the permeability of this barrier (Prevot et al., 2013). Fasting increases the organization of tight junction proteins and also enhances

25

the fenestration of the capillary loops in the ME and ARC (Langlet et al., 2013). Thus the permeability of the ARC ME blood vessels increases, but the tanycytes prevent the leakage of blood born molecules to the CSF and other brain regions. Similarly to fasting, glucose deprivation and 2-deoxy-D-glucose (2-DG) treatment that inhibits glucose metabolism cause tight junction reorganization, while intravenous glucose administration prevents this process (Langlet et al., 2013). Both fasting and 2-DG treatment result in increased synthesis of vascular endothelial growth factor A (VEGF-A) in tanycytes. Selective ablation of *Vegfa* prevents the above mentioned structural reorganization of tight junctions and the increase of the permeability of microvessels (Langlet et al., 2013) indicating that VEGF-A is a crucial factor mediating the BBB rearrangement.

According to these data, the blood-hypothalamus barrier composed by tanycytes is changing its permeability in response to metabolic challenges, thus, tanycytes might act as the first line reached by peripheral signals and play a crucial role in the regulation of the availability of peripheral signals for the ARC neurons.

1.5.4. The role of tanycytes in the regulation of glucose homeostasis

The presence of tight junctions in tanycytes not only ensures the barrier properties for these special cells, but also regulates the polarity of the cell and the intracellular trafficking of the blood-borne molecules.

Tanycytes ability to respond to changes of glucose level is indicated by the expression of the elements of the glucose sensing molecular machinery in these cells (Rodriguez et al., 2005). α- and β1-tanycytes express glucose transporter 1 (GLUT1), that play a crucial role in the entry of glucose into the cells (Garcia et al., 2001, Peruzzo et al., 2000), while glucose transporter 2 (GLUT2) is present in the apical membranes of β1- and β2-tanycytes (Garcia et al., 2003), making them candidates for sensors of CSF glucose levels. Moreover, glucokinase (GK), an enzyme that catalyses the phosphorylation of glucose, was detected in β1-tanycytes by Western blot analysis and immunocytochemistry. The subcellular distribution of GK is altered depending on the glycemic status of the animal (Millan et al., 2010). Glucokinase regulatory protein (GKRP), another key enzyme of glucose metabolism, that controls both the intracellular localization and the activity of GK, is also present in tanycytes (Salgado et al., 2014).

The presence of the above mentioned glucose sensing molecular elements in tanycytes that are critical for the glucose-sensing in the pancreatic β-cells (Schuit et al., 2001), suggests that glucose is able to enter into tanycytes through glucose transporters, then it is phosphorylated by GK. The resultant glucose-6-phosphate enters the Krebs-cycle, resulting in ATP production and the alteration of ATP-ADP ratio, which leads to the closure of ATP-inhibited potassium channels (K_{ATP}) also present in tanycytes (Thomzig et al., 2005). The closing of this channels leads to membrane depolarization and the increase of the intracellular Ca^{2+} levels (*Figure 3A*).

Beside the above mentioned process, it is proved that tanycytes perform another, more complex response to external glucose. Tanycytes of acute brain slices were shown to respond to glucose and glucose analogue puffs on their cell bodies (Frayling et al., 2011). Essentially, tanycytes are able to respond to the increase of local glucose levels with elevated intracellular Ca^{2+} levels, triggering the release of ATP to their extracellular space. Tanycytes have the ability of perceiving ATP via purinoreceptor 1 (P2Y1) that supports the propagation of Ca^{2+} waves to the neighboring tanycytes. This process allows a rapid response to the changes of glucose levels (Frayling et al., 2011). This glucose induced ATP release occurs via connexin 43 (Cx43) hemichannels based on *in vitro* data of cell cultures derived from one day old rat pups (Orellana et al., 2012). However, it is currently unknown whether tanycytes of adult animals express Cx43 and whether this protein form hemichannels, gap junctions or both in tanycytes.

Tanycytes may also utilize other alternative mechanisms of glucose sensing. Glucose may be taken up by tanycytes via Na^+/glucose co-transporters (Bolborea and Dale, 2013). This way, entry of glucose into tanycytes results in an increase of the intracellular Na^+ levels, resulting in depolarization that may lead to the inversal of the Na^+/Ca^{2+} exchanger, transporting Na^+ to the extracellular and Ca^{2+} to the intracellular space (*Figure 3B*). The other proposed mechanism of tanycyte glucosensing is the activation of a G-protein coupled receptor. This mechanism is proved by the presence of the heterodimer sweet taste receptor Tas1r2/Tas1r3 in tanycytes (*Figure 3C*) (Benford et al., 2017).
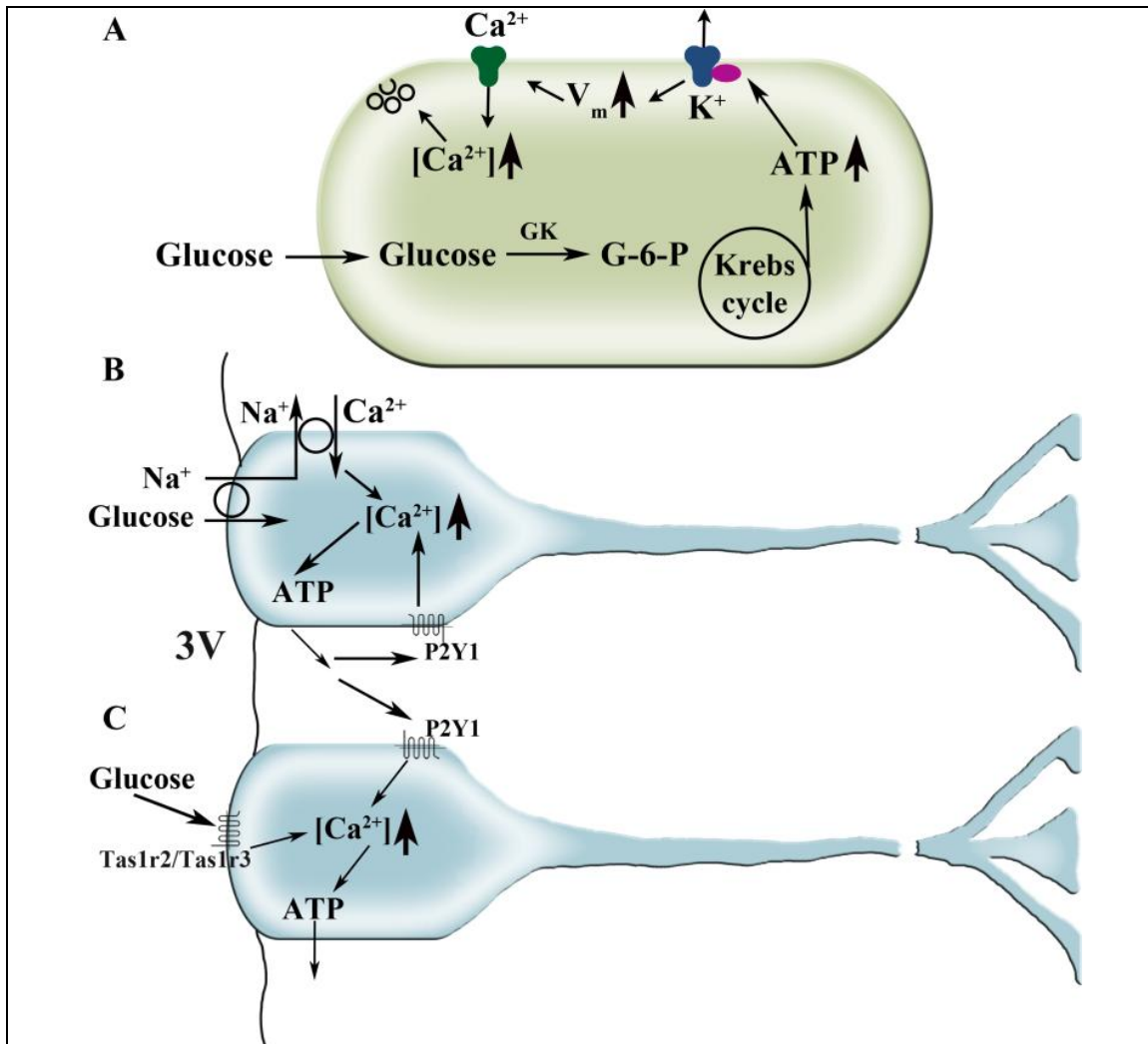
Figure 3: Schematic illustration of the glucose sensing mechanisms of tanycytes

According to the pancreatic β-cell paradigm (A), glucose is taken up into cells and converted to glucose-6-phosphate via glucokinases. G-6-P then enters the Krebs-cycle resulting in ATP production which causes the closure of the ATP-dependent K^+-channels and depolarization, opening the voltage-gated Ca^{2+} channels and increasing the intracellular calcium level. As tanycytes express all elements of this mechanism, it is likely, that tanycytes may sense glucose on the same way like pancreatic cells. B and C represent alternative mechanisms by which tanycytes may perform glucose sensation. On B, glucose enters into tanycytes via Na^+-linked glucose transporter. The increasing intracellular Na^+ level leads to the reversal of the Na^+-Ca^{2+} exchanger, which increases the intracellular Ca^{2+} level promoting the release of ATP which can act through P2Y1 receptors and modulate the mobilization of the intracellular Ca^{2+} stores in the neighboring tanycytes. C shows that glucose may act through G-protein coupled receptors like the Tas1r2/Tas1r3 heterodimer sweet taste receptor that leads to direct increase of intracellular Ca^{2+} level resulting in further ATP release.

Based on (Benford et al., 2017, Bolborea and Dale, 2013, Dale, 2011) after modification.

28

1.5.5. Tanycytes and leptin

Leptin regulates energy homeostasis and food intake and can act in the brain via activation of the LepR (Ahima et al., 2000) initiating several pathways, including the signal transducer and activator of transcription 3 (STAT3), extracellular regulated kinase (ERK) and the phosphatidylinositol-3-kinase (PI3K) pathways (Munzberg and Myers, 2005).

Peripheral administration of the adiposity signal leptin activates the feeding-related neurons in the ARC along a gradient moving from the ventral to the dorsal site of the hypothalamus. However, central injection of leptin can access all the hypothalamic nuclei within a few minutes (Faouzi et al., 2007). It has also been proved by using fluorescently labeled leptin that this adiposity signal is able to cross the wall of the fenestrated capillaries in the external zone of the ME (Vauthier et al., 2013) raising the possibility that tanycytes represent the first line reached by the peripheral leptin. Indeed, five-minutes after peripheral leptin administration phosphorylated STAT3 is already present in the tanycytes, but not in the neurons of the ARC (Balland et al., 2014). Similarly, the fluorescent leptin administered intravenously labeled tanycytes 5 minutes after injection. As a further proof of the involvement of tanycytes in the leptin signaling, all LepR isoforms, the a, b, c and e are expressed in the tanycytes, moreover, ERK and STAT3 phosphorylation have been shown after leptin treatment in tanycyte cell cultures (Balland et al., 2014) suggesting the presence of the functional LepR signaling in tanycytes. According to these data, tanycytes represent the first line reached by the adipostatic leptin, thus tanycytes my act as a conduit also between other peripheral signals and the brain.

1.5.6. Tanycytes and other metabolites

Besides exploring the role of tanycytes in the perception to leptin or glucose, a few researchers aimed to explore the potent ability of tanycytes to respond to other metabolites.

The above mentioned Tas1r2/Tas1r3 heterodimer G-protein coupled sweet-taste receptor shares a subunit with the special glutamate receptor which is responsible for the perception of umami taste and can be found in the tongue (Nelson et al., 2002). As

tanycytes express the Tas1r2/Tas1r3 receptor and the umami taste receptor differs from this only in one subunit, the hypothesis was that tanycytes might be able to sense and respond to amino acids via Tas1r1/Tas1r3 receptor similarly to those, seen in the case of glucose sensation. Indeed, it has been proved by calcium imaging and ATP biosensing, that tanycytes can represent the umami taste signaling pathway by expressing the Tas1r1/Tas1r3 receptor exhibiting the first non-neuronal mechanism of amino acid sensing (Lazutkaite et al., 2017). Another study points to the potential role of tanycytes in the sensation of lipids (Hofmann et al., 2017). Tanycytes of obese animals increase the size of their lipid droplets. In addition, tanycytes have different immune response for saturated or unsaturated lipids (Hofmann et al., 2017) raising the possibility, that tanycytes can sense the quality of fatty acids, as well.

1.5.7. Tanycytes as diet-responsive neurogenic niche

In the last years, several publications proved the neural stem cell (NSC) properties of tanycytes meaning their ability to generate new neurons in adult animals (Kriegstein and Gotz, 2003). Tanycytes express a series of NSC markers like vimentin, nestin, Sox2 and glial fibrillary acidic protein (GFAP) reviewed by Rodriguez (Rodriguez et al., 2005). Furthermore, tanycytes were also shown to retain the expression of progenitor markers Notch1 and 2 and Rax in the adult brain (Lee et al., 2012). Besides the self-renewing ability of α-tanycytes (Robins et al., 2013a), these cells also produce neurons that migrate to the ME, ARC and ventromedial nucleus (VMN) (Haan et al., 2013, Lee et al., 2012). As the ARC and the VMN are involved in the regulation of energy metabolism, and HFD regulates the number of the newborn neurons, it is likely, that tanycytes have the ability to renew neuronal populations involved in the regulation of energy homeostasis. As a further proof of the role of tanycytes in the renewal of energy homeostasis-related neuronal populations, tanycyte-derived neurons born from prepubertal period in the ARC respond to leptin with STAT3 phosphorylation (Haan et al., 2013), moreover, the blockade of tanycyte neurogenesis results in altered weight and metabolic activity in adult mice (Lee et al., 2012).

1.6. Diet-induced obesity and hypothalamic responses

1.6.1. Diet-induced peripheral and central responses

Obesity represents one of the major health problems in both industrialized and emerging nations. The main reasons that make obesity a worldwide problem can be traced back to the reduced physical activity partly due to sedentary lifestyle and to the increased consumption of dietary fats. Obesity can be characterized by the increase of excess body fat and associated with the elevated risk of type 2 diabetes, cardiovascular disease and atherosclerosis (Semenkovich, 2006). Previous investigations have shown that, diet-induced obesity (Thaler et al.) is linked to immune cell-mediated inflammatory responses initiating insulin resistance in several organs like liver, skeletal muscle and adipose tissue (Shoelson et al., 2006). Besides peripheral consequences of the HFD, it was also shown, that the hypothalamus is also affected by diet-induced inflammation, moreover, the central inflammatory response represents a more rapid process initiated by the activation of microglia (Thaler et al., 2012c, Tran et al., 2016).

1.6.2. Diet induced inflammation in the ARC

Long-term consumption of 60% fat containing chow can increase the expression of proinflammatory cytokines in the hypothalamic ARC (De Souza et al., 2005). However, recent studies demonstrated that the expression of proinflammatory cytokines is very quickly increased in the ARC by HFD (Thaler et al., 2012c). Only 3 days of HFD is sufficient to induce inflammation in this nucleus (Thaler et al., 2012c). The initiation of the inflammation in the ARC is triggered by FFAs resulting in endoplasmatic reticulum stress (Ozcan et al., 2009, Zhang et al., 2008). The increased production of reactive oxygen species, then, facilitates the induction of inflammation (Zhang and Kaufman, 2008). This inflammatory process plays important role in the development of the diet induced obesity. Indeed, specific ablation of the nuclear factor kappa B (NF-κB) signaling, a key second messenger of cytokine receptors, in the AgRP neurons, results in resistance to diet induced obesity (Zhang et al., 2008). Thaler and his colleagues reported the measurable level of markers of the inflammation within 24 hours of HFD and the neuronal injury associated with reactive gliosis in the first week of HFD (Thaler et al., 2012c). The expression levels of proinflammatory interleukin-6 (Il6,) tumor

necrosis factor alpha (Tnfa), suppressor of cytokine signaling 3 (Socs3), inhibitor of nuclear factor kappa-B kinase subunit beta (Ikbkb) and epsilon (Ikbke) are rising in the initiation of the HFD and then stagnating between the days 7 to 14 and elevating again suggesting the existence of an early adaptive response (Thaler et al., 2012c).

According to all of these data it is likely, that hypothalamic ARC neurons are able to sense and initiate the appropriate response to elevated levels of dietary fats, however, the role of other non-neuronal cell types, like glial cells cannot be excluded from the central inflammatory responses.

1.6.3. The role of glial cells in the development of the diet- induced inflammation

Glial cells, including microglia, astrocytes, NG2-positive glial cells and tanycytes play a pivotal role in the homeostatic regulation of the CNS (Jha and Suk, 2013). Moreover, these cells are also involved in the metabolic sensing within the hypothalamus (Freire-Regatillo et al., 2017). In physiological conditions, glial cells support the normal energy homeostasis of the ARC neurons, however, certain conditions, like HFD can lead to misregulation of this glia-neuron cooperation. HFD induces activation of both microglial cells and astrocytes in the ARC that is apparent from the morphological and gene expression changes (Hanisch and Kettenmann, 2007, Pekny and Nilsson, 2005). This glial activation is claimed to be important in the development of diet induced obesity and the associated metabolic changes (Horvath et al., 2010, Thaler et al., 2012c).

Microglia is a special neuroglial cell type located in the spinal cord and the brain and performs the task like the macrophage cells and monocytes in the peripheral tissues, namely, the main role of the microglia is to scavenge all the foreign materials and the damaged cells and to secrete immune factors (Graeber et al., 2011).

In response to HFD, the number of cells expressing the microglia-specific marker, the ionized calcium-binding adapter molecule 1 (Iba1) (Ito et al., 1998) increases accompanied by morphological changes of microglia (Thaler et al., 2012c) indicating that HFD induces microglial activation. The HFD induced microglial activation is further suggested by the increased expression of the EGF-like module-containing

mucin-like hormone receptor-like 1 (*Emr1*), a marker of activated microglia, in the ARC (Thaler et al., 2012c), however, the exact role of this process in the initiation of the central inflammatory process is still contentious (Thaler et al., 2012c, Valdearcos et al., 2014). According to Thaler (Thaler et al., 2012c), the microglia accumulation and activation only occurs, when the hypothalamic inflammation has developed, however the microglial response is still trackable, even when the inflammatory response has decayed. Based on this interpretation, microglia has neuroprotective effect during HFD (Thaler et al., 2012c). According to Valdearcos (Valdearcos et al., 2014), however, during HFD a rapid microglial activation can be observed and the depletion of microglia perfectly repressed the hypothalamic inflammation, therefore, microglia are responsible for the HFD-induced hypothalamic inflammation (Valdearcos et al., 2014). In spite of this, the long-term effect of microglia in the inflammatory process in both interpretations is similar: prolonged activation of microglial cells leads to high level of proinflammatory mediators like cytokines and chemokines.

Astroglia represent the other supporting glial cell type of the brain. Astrocytes are involved in many neuronal homeostatic functions, such as regulation of synaptic transmission, maintaining the BBB and the fluid and ion homeostasis by spatial buffering (Abbott et al., 2010, Kofuji and Newman, 2004). Astrocytes seem to be sensitive for leptin by expressing LepRs, moreover, leptin is essential for their proliferation (Rottkamp et al., 2015) raising the possibility of their involvement in the control of appetite. During obesity, astrocytes show significantly altered morphology in the ARC that is characteristic for astrocyte activation (Pekny and Nilsson, 2005, Thaler et al., 2012c). The alteration of astrocyte morphology may change the ensheatment of hypothalamic neurons (Horvath et al., 2010). Moreover, this reactive gliosis causes the release of proinflammatory cytokines from astrocytes resulting in local inflammation via IKKβ/NF-κB signaling (Douglass et al., 2017).

NG2-positive cells play a crucial role in the control of hypothalamic function by contacting neuronal processes (Robins et al., 2013b). A recent study has shown that, NG2-positive cells directly contact the ARC processes in the ME regulating their responsiveness to leptin (Djogo et al., 2016).

The effect of diet-induced obesity on the hypothalamic ARC and the involvement of glial cells in the inflammatory process seems to be evident, however, it is still unclear, which hypothalamic cell population is responsible for the initiation of the hypothalamic inflammatory response. As tanycytes represent the first line reached by peripheral signals, thus play a crucial role in the hypothalamic control of metabolism, moreover, tanycytes are proved to be able to respond to neurotransmitters, glucose and leptin, it is likely, that these special cells besides other glial cells also play a role in the regulation of the inflammatory processes in the case of HFD.

2. Aims

The neuronal networks involved in the central regulation of energy homeostasis were intensely studied during the last decades. Recently, however, more and more data accumulate suggesting that glial cells are also involved in the regulatory apparatus of energy homeostasis. Tanycytes, a special glial cell type of the hypothalamus represent a glucose- and leptin-sensitive, diet-responsive neurogenic niche and play an active role in the transportation of metabolic signals to the hypothalamic neurons involved in the regulation of food intake and energy balance. Microglia, the resident macrophage cells of the brain are also involved in the regulation of energy homeostasis, like via the HFD-related inflammatory processes. However, the exact role of these glial cell types in the central regulation of energy homeostasis is still unclear.

To better understand how tanycytes and microglia regulate energy metabolism- and feeding-related mechanisms, the aim of my PhD work was to investigate the communication and the POMC gene expression of tanycytes and the importance of microglia in the development of short-term HFD induced metabolic changes.

In order to achieve this, our specific aims were:

1. To investigate the localization of Cx43 gap junctions and hemichannels in tanycytes.

2. To characterize the POMC expression in tanycytes

3. To determine the importance of the microglia in the mediation of the HFD induced metabolic changes.

3. Materials and methods

3.1. Experimental animals

The experiments were carried out on adult male or female laboratory mice or rats. The animals used in each experiments and their sources and body weight are listed in *Table 1* and *Table 2*. The animals were housed under standard environmental conditions (lights on between 06.00 and 18.00 h, temperature 22±1 °C, chow and water *ad libitum*). All experimental protocols were reviewed and approved by the Animal Welfare Committee at the Institute of Experimental Medicine of the Hungarian Academy of Sciences.

Table 1: The strain, source, sex, body weight and age of animals used in each experiment.

For the characterization of POMC expression in tanycytes, rats with different age and body weight were used, see Table 2.Abbreviations: Cx43 - connexin 43, POMC – proopiomelanocortin, ISH – in situ hybridization, IHC – immunohistochemistry, HFD – high fat diet, M – male, F – female.

Experiment	Species	Strain	Source	Sex	Age	Body weight (g)
The localization of Cx43 gap junctions and hemichannels in tanycytes						
	mouse	CD1	Charles River	M	8 weeks	30-35
The characterization of POMC expression in tanycytes						
ISH, fluorescent IHC	rat	Sprague-Dawley	Taconic Farms	M/F	described in detail in *Table 2*	
Immuno-electron microscopy	rat	Wistar	ToxiCoop	M	8 weeks	250-275
Importance of microglia in the development of HFD induced metabolic changes						
	mice	C57Bl/6J	Charles River	M	8 weeks	20-25

Table 2: The sex, age and body weight of Sprague-Dawley rats used for the characterization of the POMC expression in tanycytes.

Abbreviations: POMC – proopiomelanocortin, ISH – in situ hybridization, M – male, F – female.

Experiment	Sex	Age	Body weight (g)	Number of the used Sprague-Dawley rats
Adult rats for *Pomc* ISH				
	M	8 weeks	240-260	4
	M	8-9 weeks	257-284	6
	F	9-10 weeks	224-245	6
	M	9-10 weeks	286-293	4
	M	15 weeks	413-436	6
Adult rats for POMC immunofluorescence				
	M	10 weeks	290-320	4
	M	10 weeks	290-320	4
	F	11 weeks	238-258	7
Adolescent rats for *Pomc* ISH				
	M	31 days	80-93	4
	F	31 days	67-81	4

GENERAL METHODS

3.2. Anesthesia

The anesthesia of the animals was performed either by using intraperitoneal injection of a mixture of ketamine (50 mg/kg body weight) and xylazine (10 mg/kg body weight) or by inhalation of isoflurane.

3.3. Transcardial perfusion with fixative

Animals processed for immunocytochemistry were deeply anesthetized by intraperitoneal ketamine-xylazine injection and transcardially perfused with 10 ml (mice) or 50 ml (rat) 0.01 M phosphate buffered saline (PBS, pH 7.4) followed by fixative.

For Cx43 immunocytochemistry, the mice were perfused with 50 ml 4% paraformaldehyde (PFA) in sodium-acetate buffer (pH 6.0) followed by 50 ml 4% PFA

in Borax buffer (pH 8.5). For Iba1 immunocytochemistry, the mice were perfused with 4% PFA in 0.1 M phosphate buffer (PB, pH 7.4). For rat immunofluorescent experiments, rats were transcardially perfused with 150 ml 4% PFA in 0.1M PB (pH 7.4). For the ultrastructural detection of POMC-immunoreactivity in tanycytes, rats were transcardially perfused with 150 ml fixative containing 4% acrolein and 2% PFA in 0.1 M PB, pH 7.4.

After transcardial perfusion, the brains were rapidly removed from the skull and postfixed.

3.4. Tissue preparation for light microscopic investigations

For light microscopic experiments, the brains were postfixed in 4% PFA for 2 hours. In order to ensure cryoprotection, the brains were incubated in 30% sucrose in 0.01 M PBS overnight. After that, the brains were frozen on powdered dry ice and 25 μm thick coronal sections were cut using a Leica SM2000 R freezing microtome (Leica Microsystems, Wetzlar, Germany). The sections were placed into antifreeze solution (30% ethylene glycol; 25% glycerol; 0.05 M PB) and stored at -20 °C until further processing. The sections were then placed into 0.5% Triton X-100 and 0.5% H_2O_2 in 0.01 M PBS for 20 min to improve penetration and block the endogenous peroxidase activity. To reduce non-specific antibody binding, the sections were incubated in 2% normal horse serum (NHS) in PBS for 10 min.

3.5. Tissue preparation for electron microscopic investigations

For electron microscopic investigations, the brains were postfixed in 4% PFA in 0.1 M PB, (pH 7.4), for 24 h at 4°C, then serial 25 μm thick coronal sections of the hypothalamus were cut on a Leica VT1000 S vibratome (Leica Microsystems, Wetzlar, Germany). When the fixative contained acrolein, the sections were incubated in 1% sodium-borohydride dissolved in 0.1 M PB (pH 7.4) for 30 min. In all cases, the sections were treated in 0.5% H_2O_2 in PBS for 15 min. After that, the sections were cryoprotected by incubation in 15% sucrose in 0.01 M PBS for 15 min at room temperature and in 30% sucrose in PBS overnight at 4°C. Thereafter, the sections were frozen over liquid nitrogen and thawed quickly three times to improve antibody

penetration. To reduce non-specific antibody binding, the sections were incubated in 2% NHS in PBS for 10 min.

3.6. Embedding for electron microscopic studies

The immunolabeled sections were osmicated using 1% osmium tetroxide in 0.1 M PB for 1 h. The sections were washed in 50 and 70% ethanol, sequentially, and incubated in 2% uranyl-acetate in 70% ethanol for 30 min. After dehydration of sections in ascending series of ethanol and in acetonitrile, respectively, sections were embedded in Durcupan ACM epoxy resin on liquid release agent (Electron Microscopy Sciences) coated slides and polymerized at 60°C for 48 h.

3.7. Tissue preparation for in situ hybridization (ISH)

Rats were deeply anesthetized with ketamine-xylazine (Section 3.2) and decapitated. The brains were removed and frozen on powdered dry ice. Coronal, 18 μm thick sections were cut through the entire extent of the ARC using a Leica CM3050 S cryostat (Leica Microsystems, Germany), thaw-mounted on Superfrost Plus glass slides (Fisher Scientific Co.) and air-dried. Sections were collected in 1-in-12 series on a total of 24 (2×12) slides per brain. With 6 hypothalamic sections on each slide, a series containing every 12th section fit on 2 slides, one containing the rostral, and another, containing the caudal part of the tanycyte region. The sections were stored at -80°C until processed for ISH.

3.8. Tissue preparation for laser capture microdissection (LCM)

In order to preserve the integrity of RNA for further gene expression investigations, the experimental animals were deeply anesthetized (Section 3.2) and transcardially perfused with ice-cold 10% RNAlater solution (Ambion) diluted in diethylpyrocarbonate (DEPC) treated 0.1 M PBS. The mice were perfused with 30 ml, while the rats were perfused with 70 ml 10% RNAlater solution. The brains were quickly removed from the skull and frozen in -40°C 2-methylbutane. The brains were stored at -80°C until sectioning. Coronal, 12 μm thick sections between the rostral and caudal limits of the ME were cut at -18°C using a Leica CM3050 S cryostat (Leica Microsystems, Wetzlar, Germany Sections were mounted on PEN-membrane covered slides (Zeiss, Germany), thawed

and counterstained with 0.6% cresyl violet dissolved in 70% ethanol and dehydrated with ascending series of ethanol. The slides were thoroughly dried on a 42°C hot plate and stored at -80°C until LCM.

3.9. Isolation of tanycytes and ARC using LCM

From the RNAlater perfused and preconditioned brain sections (Section 3.8), the tanycyte containing ventral and lateral walls of the third ventricle and the area of ARC were microdissected by using Zeiss Microbeam LCM system and PALM software. The ARC and the-tanycyte samples were pressure-catapulted with a single laser pulse into 0.5 ml tube adhesive caps (Carl Zeiss Microimaging) using a 10 or ×20 objective lenses.

3.10. RNA isolation and RNA concentration measurements

RNA was isolated from the microdissected samples by using Arcturus PicoPure RNA Isolation Kit (Applied Biosystems) according to the manufacturer's protocol. DNase treatment was carried out on the isolation column by using RNase-Free DNase Set (Qiagen) to digest the potential DNA contamination of the samples. The quality and the concentration of the isolated RNA samples were measured on Agilent 6000 RNA Pico chips with Agilent Bioanalyzer using 2100 Expert software (Agilent Technologies). Samples with RNA integrity number below 5.0 were excluded from further studies.

3.11. Statistical analysis

For the statistical analysis the Statistica 13.1 software was used. The data were described as mean+SEM. T-test was used for comparison of two groups. The statistical examination of three or more groups was performed using one-way or factorial ANOVA followed by Newman–Keuls or Tukey HSD post hoc, respectively.

DETAILED METHODS BY PROJECTS

3.12. The localization of Cx43 gap junctions and hemichannels in tanycytes

3.12.1. Loading the tanycytes with Lucifer yellow (LY) via patch pipette

To demonstrate that the tanycytes are connected via gap junctions, tanycytes were loaded with the gap junction permeable dye, LY via patch pipette and the spreading of the dye among tanycytes was studied. These experiments were performed with the help of Edina Varga.

CD1 mice were deeply anesthetized with isoflurane and decapitated. The brains were rapidly removed and immersed in ice cold slicing solution (containing 87 mM NaCl, 2.5 mM KCl, 0.5 mM $CaCl_2$, 7 mM $MgCl_2$, 25 mM $NaHCO_3$, 25 mM D-glucose, 1.25 mM NaH_2PO_4, 75 mM sucrose saturated with 95% O_2/5% CO_2 carbogen). Coronal 250 μm thick slices containing the ME were cut using a vibratome (Leica WT 1200S), then, the slices were transferred into a holding chamber containing artificial cerebrospinal fluid (aCSF, containing: 126 mM NaCl, 2.5 mM KCl, 26 mM $NaHCO_3$, 2 mM $CaCl_2$, 2 mM $MgCl_2$, 1.25 mM NaH_2PO_4, 10 mM glucose; pH 7.4; 280-300 mOsm/L) at 36°C. Before uploading tanycytes, the slices were allowed to cool down to room temperature for at least 1 h. Tanycytes were patched in aCSF at 30–32°C perfused at a rate of 2 ml/min via perfusion pump. The patch pipettes (OD = 1.5 mm, thin wall, Garner Borosilicate pipettes, 6–7 MΩ) were filled with intracellular recording solution (110 K-gluconate, 4 mM NaCl, 20 mM HEPES, 0.1 mM EGTA, 10 mM phosphocreatine di(tris) salt, 2 mM ATP, 0.3 mM GTP; pH 7.25; 280–300 mOsm/L) and 1 mg/ml LY. The tanycytes were loaded with LY for 20 min at -80–85 mV holding potential.

To demonstrate that the spreading of LY among tanycytes is due to the presence of gap junctions, tanycytes were loaded with LY in the presence of a gap junction inhibitor, carbenoxolone (200 μM), in the extracellular solution.

All studied slices were then fixed in 4% PFA dissolved in 0.1 M PB (pH 7.4). Z-stack images were taken using a Zeiss LSM 780 confocal laser scanning microscope (Carl Zeiss Microscopy GmbH) with Plan-Apochromat 40x/1.4 Oil DIC M27 objective (Carl

Zeiss AG). The sections were scanned for LY using laser excitation line 405 and emission filter wavelength 477-685 nm. Pinhole sizes were set to obtain the minimal thickness of optical slices.

3.12.2. Double-labeling immunofluorescence for Cx43 and vimentin

For immunohistochemical detection of Cx43, mice were deeply anaesthetized by intraperitoneal injection and perfused transcardially as described in sections 3.2 and 3.3, respectively. Then, the brain tissues were prepared according to section 3.4. and incubated in rabbit antiserum against Cx43 (1:400, Invitrogen) diluted in PBS containing 2% NHS and 0.2% sodium-azide (antibody diluent) overnight at room temperature. This step was followed by direct visualization of the immunoreaction with incubation in Alexa-488 conjugated donkey anti-rabbit IgG (1:250, Invitrogen). Vimentin was used as a marker of tanycytes. In order to make the tanycytes and their processes visible, the sections were transferred into sheep antiserum against vimentin (1:3000, Santa Cruz Biotech), followed by incubation in biotinylated donkey anti-sheep IgG (1:500, Jackson ImmunoResearch) for 2 h, then in avidin-biotin-peroxidase complex (1:000, Vectastain Elite ABC, Vector Laboratories) for 1 h. The immunoreaction product was amplified with biotinylated tyramide by using the TSA amplification kit (Perkin Elmer Life and Analytical Sciences, Waltham, MA) according to the manufacturer's description. Vimentin was visualized by incubating the sections in Alexa-594 conjugated Strepavidin (1:500, Invitrogen). The double-labeled immunofluorescent sections were mounted on glass slides and coverslipped with Vectashield mounting medium (Vector Laboratories) and examined with Zeiss LSM 780 confocal laser-scanning microscope (Carl Zeiss Microscopy GmbH) with Plan-Apochromat 10x0.45 M27, 20x 0.8 M27, 40x1.40 Oil DIC M27, 63x1.40 Oil DIC M27 objectives (Carl Zeiss AG). The sections were sequentially scanned for Alexa 488 and Alexa-594 using laser excitation lines 488 nm for Alexa-488 and 561 nm for Alexa 594 and emission filter wavelength 493–556 nm for Alexa-488 and 586-697 for Alexa 594. Pinhole sizes were set to obtain the minimal thickness of optical slices.

3.12.3. Ultrastructural detection of Cx43-immunoreactivity

For ultrastructural localization of Cx43 in tanycytes, mice were deeply anesthetized (Section 3.2) and perfused subsequently by 4% PFA at low and high pH (pH 7.4 and 6), respectively, as described above in Section 3.3. After preconditioning as described in Section 3.5, the sections were incubated in rabbit antiserum against Cx43 (1:2000) for 4 days, followed by overnight incubation in biotinylated donkey-anti-rabbit IgG (1:500, Jackson ImmunoResearch) and ABC (1:1000). The immunoreaction was visualized with nickel-diaminobenzidine developer (0.05% diaminobenzidine (DAB), 0.15% nickel ammonium sulfate, 0.005% H_2O_2 in 0.05 M Tris buffer at pH 7.6) and amplified by silver-intensification by using Gallyas method (Gallyas and Merchenthaler, 1988). After electron microscopic embedding as described in Section 3.6, 60–70 nm thick ultrasections were cut with Leica Ultracut UCT ultramicrotome (Leica Microsystems, Wetzlar, Germany). The ultrathin sections were mounted onto Formvar-coated single slot grids, contrasted with 2% lead citrate and examined with a Jeol-100 C transmission electron microscope. The tanycytes were identified based on their characteristic morphological features, while the tanycyte subtypes were distinguished based on their localization (Rodriguez et al., 2005).

3.13.   Characterization of the POMC expression in tanycytes

The ISH experiments and the immunofluorescent investigations were carried out by Gábor Wittmann.

3.13.1. Radioactive ISH

Radioactive ISH was performed on serial sections of rats (see Attachment 1 for sex/age/body weight). The Pomc riboprobe was synthesized in the presence of [35S]-uridine 5′-(alpha-thio) triphosphate (PerkinElmer), and purified with Mini Quick Spin RNA columns (Roche Applied Sciences, Basel, Switzerland). The riboprobe template was mouse cDNA corresponding to bases 532-1007 of mouse Pomc mRNA, GenBank Acc. No. NM_008895.3 (plasmid provided by Dr. Malcolm J. Low). This sequence is 93% homologous with the rat Pomc sequence (504-935 of NM_139326.2). ISH was performed on every 12th coronal section per brain, using 50,000 CPM/µl radiolabeled

probe concentration. Following stringency washes, sections were dehydrated in ascending series of ethanol, air-dried, and dipped into Kodak NTB autoradiography emulsion (Carestream Health Inc., Rochester, NY). The emulsion coated-slides were placed in light-tight boxes containing desiccant, and stored at 5°C for 8d, when the autoradiograms were developed using Kodak D19 developer (Eastman Kodak Company, Rochester, NY). Slides were immersed into 0.0005% Cresyl Violet acetate (Sigma-Aldrich) for 2 min for fluorescent counterstaining, then dehydrated in ascending series of ethanol followed by xylene (Sigma-Aldrich), and coverslipped with DPX mountant (Sigma-Aldrich).

3.13.2. Fluorescent ISH combined with immunofluorescence

Fluorescent ISH was performed on serial sections of 16 adult Sprague-Dawley rats. The Pomc riboprobe was labeled with digoxigenin-11-UTP (Roche) by in vitro transcription. ISH was performed on every 12th coronal section, as described previously for fresh frozen sections (Wittmann et al., 2013). Following the hybridization procedure, sections were treated with 0.5% Triton X-100/0.5% H_2O_2 in PBS (pH 7.4) for 15 min, rinsed in PBS, immersed in maleate buffer (0.1 M maleic acid, 0.15 M NaCl, pH 7.5; 10 min), and in 1% blocking reagent for nucleic acid hybridization (Roche). The sections were incubated overnight in Fab fragments of peroxidase-conjugated sheep anti-digoxigenin antibody (1:100 in 1% blocking reagent, Roche) using CoverWell incubation chambers (Grace Bio-Labs Inc., Bend, OR). After rinses in PBS, the hybridization signal was amplified using the TSA Biotin Tyramide system (Perkin Elmer) for 30 min, followed by Alexa Fluor 488-conjugated Streptavidin (Life Technologies, Grand Island, NY) for 2h, diluted at 1:500 in 1% blocking reagent. Then sections were then incubated in the mixture of a mouse antibody against the neuronal proteins HuC/HuD (Molecular Probes) and chicken vimentin antiserum (Millipore). The primary antibodies were detected with Alexa Fluor 647-conjugated donkey anti-mouse IgG (Jackson ImmunoResearch Labs) and Cy3-conjugated donkey anti-chicken IgG (Jackson ImmunoResearch Labs). The antibodies and the used concentrations are listed in *Table 3* and *Table 4*. Sections were coverslipped with Vectashield mounting medium containing 4',6-diamidino-2-phenylindole (DAPI).

3.13.3. Immunofluorescent detection of POMC, β-endorphin, α-MSH and adrenocorticotropic hormone (ACTH)

Adult Sprague-Dawley rats were deeply anesthetized with ketamine-xylazine (Section 3.2) and then perfused transcardially with 4% PFA (Section 3.3). The brains were removed and the tissues were preconditioned as described above (Section 3.4).

The following three immunofluorescent preparations were made from each brain, each on an individual, full series of 1-in-6 coronal sections: triple immunofluorescence for the N-terminal portion of POMC, vimentin and HuC/D; dual immunofluorescence for β-endorphin and α-MSH; and single immunofluorescence for ACTH. The antibodies and the used concentrations are listed in *Table 3* and *Table 4.* For triple-labeling immunofluorescence, the sections were first incubated in rabbit anti-POMC serum (Phoenix Pharmaceuticals) for 2d followed by Alexa 488-conjugated donkey anti-rabbit IgG (Jackson ImmunoResearch Labs) for 2h. Then, the sections were incubated in the cocktail of chicken anti-vimentin serum and mouse anti-HuC/D antibodies overnight and then in Cy3-conjugated donkey anti-mouse IgG (Jackson ImmunoResearch Labs) and Alexa 647-conjugated donkey anti-chicken IgG (Jackson ImmunoResearch Labs) for 2h. For dual immunofluorescence, sections were incubated in the cocktail of rabbit anti-β-endorphin (Phoenix Pharmaceuticals) and sheep anti-α-MSH antisera (Millipore) overnight followed by Cy3-conjugated donkey anti-rabbit IgG (Jackson ImmunoResearch Labs) and Alexa 488-conjugated donkey anti-sheep IgG (Jackson ImmunoResearch Labs) for 2h. For single-labeling immunofluorescence for ACTH, the sections were incubated in rabbit anti-ACTH serum (Phoenix Pharmaceuticals) for 2d and then in Cy3-conjugated donkey anti-rabbit IgG for 2h. The sections were mounted and coverslipped with DAPI-containing Vectashield mounting medium (Vector).

3.13.4. Ultrastructural detection of POMC-immunoreactivity in tanycytes

The immune-electron microscopic investigations were carried out with the help of Erzsébet Hakkel.

Adult male rats were deeply anesthetized with ketamine/xylazine (Section 3.2) and perfused transcardially as described in Section 3.3. The brains were rapidly removed and preconditioned for immune-electron microscopic investigation as described in

Section 3.5. The sections were incubated in 2% NHS in PBS for 10 min before placed in rabbit anti-POMC serum (1:15000, Phoenix Pharmaceuticals) diluted in 2% NHS in PBS for 4 days at 4°C followed by overnight incubation in biotinylated donkey anti-rabbit IgG (Jackson ImmunoResearch) and then in ABC (1:1000, Vector) for 2h. The POMC-immunoreactivity was detected with NiDAB developer and the immunoreaction was intensified by using Gallyas-method for 2 min (Gallyas and Merchenthaler, 1988). The sections were embedded in Durcupan resin as described in Section 3.6. After polymerization, 60–70 nm thick ultra-sections were cut with Leica Ultracut UCT ultramicrotome. The ultrathin sections were mounted onto Formvar-coated single slot grids, contrasted with 2% lead citrate and examined with a Jeol-100 C transmission electron microscope.

Table 3: The manufacturer and concentration of the primary antibodies used in the experiments.

Antibody	Immunogen	Manufacturer, species, clonality	Concentration
Cx43	C-terminal portion of rat connexin 43 peptide	Invitrogen, rabbit polyclonal	1:400 for immunofluorescence, 1:2K for immuno-electron microscopy
vimentin	C-terminus of vimentin of human origin	Santa Cruz Biotech, sheep monoclonal	1:3K
POMC	N-terminal 26 amino acids of porcine proopiomelanocortin peptide	Phoenix Pharmaceuticals, rabbit polyclonal	1:20K for immunofluorescence 1:15K for electron microscopy
β-endorphin	rat β-endorphin	Phoenix Pharmaceuticals, rabbit polyclonal	1:10K
ACTH	rat ACTH	Phoenix Pharmaceuticals, rabbit polyclonal	1:10K
α-MSH	α-MSH	Millipore, sheep polyclonal	1:10K
vimentin	recombinant vimentin	Millipore, chicken polyclonal	1:4K after ISH; 1:20K for immunofluorescence
HuC/HuD	human HuC/D	Life Technologies, mouse monoclonal	2 μg/ml after ISH; 1 μg/ml for immunofluorescence
digoxigenin,	digoxigenin, peroxidase conjugated	Roche, sheep	1:100
Iba1	C-terminus of Iba1	Wako, rabbit polyclonal	1:2K

Table 4: The manufacturer and the concentration of the secondary antibodies used in the experiments.

Antibody/fluorochrome	Immunogen	Manufacturer, clonality	Concentration
Alexa 488-conjugated donkey anti rabbit IgG	rabbit IgG	Invitrogen	1:250
Biotinylated donkey anti-sheep IgG	sheep IgG	Jackson ImmunoResearch polyclonal	1:500
Alexa 594-conjugated Streptavidin		Invitrogen	1:500
Alexa 647-conjugated donkey anti-mouse IgG	mouse IgG		1:200
Cy3-conjugated donkey anti-chicken IgG	chicken IgY		1:200
Alexa 488-conjugated donkey anti-rabbit IgG	rabbit IgG		1:400
Alexa 647-conjugated donkey anti-chicken IgG	chicken IgY	Jackson Immunoresearch, polyclonal	1:200
Cy3-conjugated donkey anti-mouse IgG	mouse IgG		1:200
Alexa 488-conjugated donkey anti-sheep IgG	sheep IgG		1:200
Cy3-conjugated donkey anti-rabbit IgG	rabbit IgG		1:200
Biotinylated donkey anti-rabbit IgG	rabbit IgG		1:500

3.13.5. RNA-seq analysis of tanycyte transcriptome

Male, 13 week old Wistar rats (n=5) were deeply anesthetized with ketamine-xylazine (Section 3.2) and transcardially perfused with 70 ml ice cold 10% RNAlater (Ambion) dissolved in 0.1 M PBS (Section 3.8). The brains were rapidly removed and preconditioned for LCM as described in Section 3.8. LCM, RNA isolation and RNA concentration measurements were carried out as described in Sections 3.8, 3.9, 3.10, respectively. Ovation RNA amplification system V2 was used to amplify the RNA and write cDNA. The library generation and the Illumina next generation sequencing and the bioinformatic analyses were performed by Eurofins. CPM values for each gene were compared between the tanycyte and ARC samples with Students' t-test.

3.14. Importance of microglia in the development of HFD induced metabolic changes

3.14.1. Microglia-ablation with PLX5622-pretreatment

In order to ablate microglia in the brain, half of the mice were fed with low fat (10%) chow containing 1200 mg/kg PLX5622, a specific colony stimulating factor 1 receptor (CSF1R) inhibitor in microglia for three weeks, while the other half of the mice, as control group consumed the same low fat (10%) chow without PLX5622. The special diets were formulated by the Research Diet INC (New Brunswick, NJ). The PLX5622 was kindly provided by Plexxikon Inc (Berkeley, CA).

To monitor the success of microglia ablation in treated mice, sentinel mice were maintained and treated with PLX5622-containing or PLX5622-free chows and sacrificed for immunocytochemistry using the microglial marker Iba1 (3.14.4). During the PLX pretreatment the consumption and the body weight of the experimental mice was measured every week.

3.14.2. Short-term HFD treatment

In order to investigate the effect of short-term HFD, the half of the mice pretreated with PLX5622 chow continued consuming the same low-fat (10%) chow containing PLX5622 (LF+PLX group), while the other half of these mice was switched to high fat (60%) chow containing 1200 mg/kg PLX5622 (HFD+PLX group) for three days.

Similarly, the half of the control group continued consuming low fat (10%) PLX5622-free chow (LF group), while the other half of these mice was switched to high fat (60%) PLX5622-free chow (HFD group). The HFDs were also formulated by the Research Diet INC (New Brunswick, NJ). *Figure 4* illustrates the experimental design.
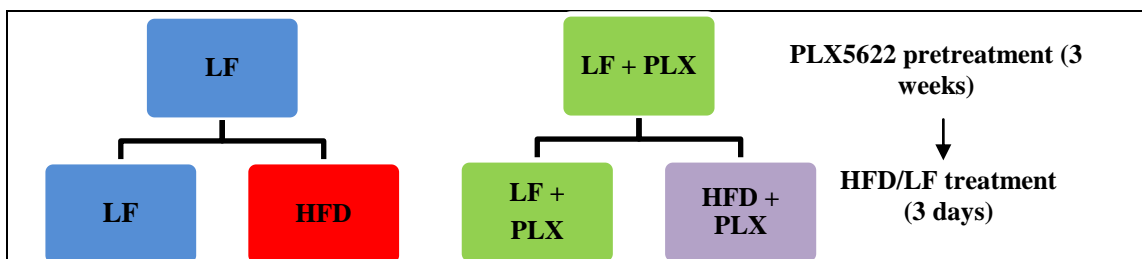
Figure 4: The experimental design of short-term HFD experiments.

In order to ablate microglia, half of the mice were fed with low fat (10%) chow-containing 1200 mg/kg PLX5622 for three weeks, while the other half of the mice, as control group consumed the same low fat (10%) chow without PLX5622. In order to investigate the effect of short-term HFD, the half of the mice pretreated with PLX5622 chow continued consuming the same low-fat (10%) chow containing PLX5622 (LF+PLX group), while the other half of these mice was switched to high fat (60%) chow-containing 1200 mg/kg PLX5622 (HFPLX group) for three days. Similarly, the half of the control group continued consuming low fat (10%) PLX5622-free chow (LF group), while the other half of these mice was switched to high fat (60%) PLX5622-free chow (HFD group). Abbreviations: LF – low fat diet, HFD – high fat diet.

3.14.3. Indirect calorimetric measurements and body composition analysis

After the PLX pretreatment the experimental animals were transferred to the Metabolic Phenotyping Center of the Institute of Experimental Medicine, Budapest, Hungary.

Three days before the beginning of the HFD, the mice were placed into training cages in order to let the animals habituate to the same metabolic cages and to learn the usage of the special drinking nipples and feeders. In order to evaluate the effect of short-term HFD on the metabolism of the PLX-treated and control mice, water and food intake, locomotor activity and indirect calorimetric measurements including oxygen consumption and carbon-dioxide production were performed with the TSE PhenoMaster System (TSE Systems GmbH, Bad Homburg, Germany) during the three days of the HFD. The metabolic data was analyzed with the TSE PhenoMaster software.

Before and after the metabolic measurements, body composition analysis (total body mass, lean body mass, total and free water content) was performed by using EchoMRI Whole Body Composition Analyzer (EchoMRI LLC, Houston, TX).

3.14.4. Iba1 immunocytochemistry

In order to verify the microglia ablation, immunocytochemistry against the microglial marker, Iba1 was performed. For immunohistochemical detection of Iba1, mice were

deeply anaesthetized by intraperitoneal injection and perfused transcardially as described in sections 3.2 and 3.3, respectively. The brain tissues were prepared according to section 3.4. After that, sections were incubated in rabbit antiserum against Iba1 (1:2000, Wako Laboratory Chemicals) diluted in PBS containing 2% NHS and 0.2% sodium-azide overnight at room temperature. On the next day, after washing in 0.01 M PBS, the sections were placed into biotinylated donkey anti-rabbit IgG for 2 hours and then incubated in ABC for 1 hour. The immunoreaction was visualized with NiDAB developer. The sections were mounted on glass slides dehydrated in ascending series of ethanol and xylene and coverslipped with DPX. The sections were examined with a Zeiss Axioimager M2 fluorescent microscope.

3.14.5. cDNA synthesis and preamplification from the LCM samples

The RNA samples prepared as described in Sections 3.8 3.9 and 3.10 were reverse transcribed by using ViLO Superscript III cDNA Reverse Transcription Kit (Invitrogen) according to the manufacturer's protocol. The cDNA concentration was measured with Qubit® Fluorometer by using Qubit® ssDNA Assay Kit (Invitrogen). The cDNA product served as a template for preamplification by using Preamp Master Mix Kit (Applied Biosystems) and the double-stranded DNA concentration was measured with Qubit® Fluorometer by using Qubit® dsDNA BR Kit.

3.14.6. Quantitative TaqMan PCR

In order to verify the inflammatory process in the ARC, the expression of genes involved in inflammatory processes were elucidated by MicroAmp Fast Optical 96-Well Reaction Plates with Barcode and TaqMan® Gene Expression Assays (Applied Biosystems). See the list of the investigated genes in *Table 5*. The expression of the genes of our interest was determined by qPCR. ViiA 7 real-time PCR platform (Life Technologies) was used for thermal cycles of the qPCR with the usage of Fast-96 well block and comparative CT method.

Table 5: The list of the investigated genes to verify the microglia ablation in the ARC.

MicroAmp Fast Optical 96-Well Reaction Plates with Barcode and TaqMan® Gene Expression Assays were used to determine the expression of the genes of our interest by qPCR with ViiA 7 real-time PCR platform. In this experiment Gapdh served as housekeeping gene.

Assay ID	Symbol	Gene name
Mm00802529_m1	*Emr1*	EGF-like module-containing mucin-like hormone receptor-like 1
Mm00479862_g1	*Iba1*	ionized calcium-binding adapter molecule 1
Mm99999915_g1	*Gapdh*	glyceraldehydes-3-phosphate dehydrogenase

4. Results

4.1. The localization of Cx43 gap junctions and hemichannels in tanycytes

4.1.1. Presence of functional gap junctions between tanycytes

The fluorescent dye LY loaded into a single β-tanycyte via patch pipette was able to spread into a larger group of the adjacent tanycytes and labeled both cell bodies and the basal processes of these cells. The expansion of the dye was not only apparent by movement between adjacent tanycyte cell bodies, but it also transported among contiguous tanycyte end feet process. LY also appeared around blood vessels contacted by tanycyte processes (*Figure 5A-B*). To determine whether LY spread through Cx43 gap junctions, the experiment was repeated in the presence of the gap junction inhibitor, carbenoxolone. The inhibitor completely prevented the spreading of LY from the patched cell and the fluorescent labeling was only present in the patched cell (*Figure 5C*).
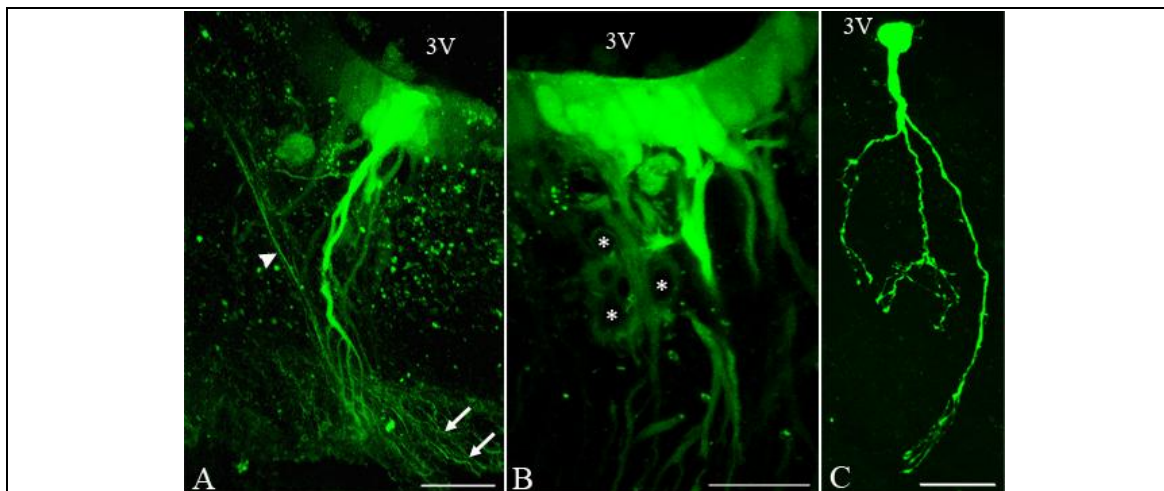

Figure 5: Presence of functional gap junctions among tanycytes.

Fluorescent microscopic images illustrate the spreading of Lucifer yellow (LY) among cells in the ME after loading a single β-tanycyte via patch pipette. Note that LY fills a larger group of neighboring tanycytes (A, B). In addition, LY filled tanycytes through contacts of their end feet processes in the external zone of median eminence (A). This phenomenon is illustrated by a backfilled tanycyte process labeled by an arrowhead. LY also labeled capillaries contacted by tanycyte processes (B, *). The gap junction inhibitor, carbenoxolone, blocked the spreading of LY from the patched tanycyte to neighboring cells, resulting in the labeling of only the patched tanycyte (C).

Scale bars = 20 μm. Abbreviations: 3V – third ventricle, ME – median eminence

4.1.2. Detection of Cx43-immunoreactivity in tanycytes

Double-labeling immunocytochemistry for Cx43 and vimentin, the latter a molecular marker of glial cells including tanycytes, demonstrated an abundance of Cx43 in tanycytes (*Figure 6A-C*). The highest density of Cx43-immunoreactive puncta was observed in the cell bodies of α–tanycytes (*Figure 6D*), although Cx43 was also present, but in lower density, in β-tanycyte cell bodies lining the floor of the third ventricle (*Figure 6F*). The location of Cx43-immunoreactivity in tanycyte cell bodies appeared to be polarized (*Figure 6E-G; I*), as the greatest density concentrated primarily on the ventricular surface of tanycytes, but was also present in lower density on the lateral surfaces of adjacent tanycyte cell bodies. Cx43-immunoreactivity was also observed in basal processes of both α- and β-tanycytes and particularly apparent in the external zone of the ME (*Figure 6G*) and ARC where the processes were in close proximity to small capillaries (*Figure 6H*).
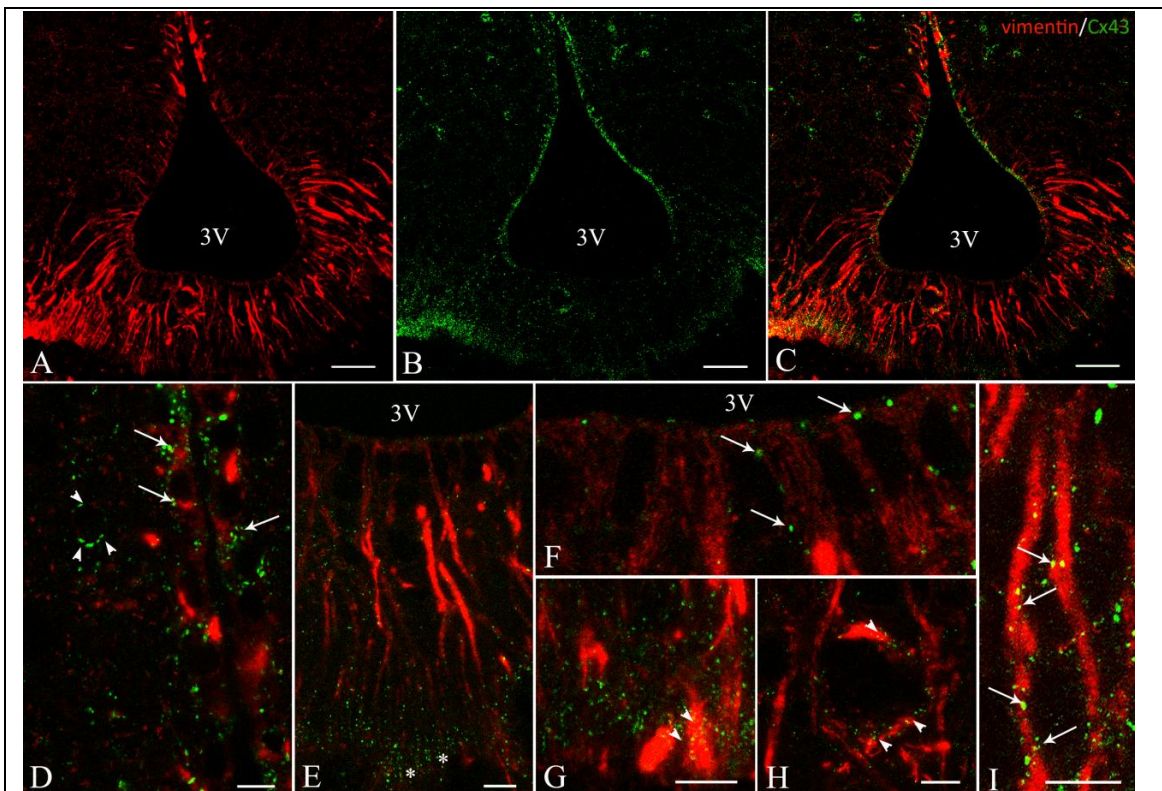

Figure 6: Distribution of Cx43-immunoreactivity in tanycytes.

Confocal microscopic images (A–C) of sections labeled for Connexin 43 (Cx43, green) and the tanycyte marker, vimentin (Redecker), illustrate that distribution of Cx43-immunoreactivity in the different types of tanycytes. (A) shows the vimentin-immunoreactive tanycytes, while the Cx43-immunoreactivity is illustrated in (B). The

4.1.3. Ultrastructural localization of Cx43-immunoreactivity in tanycytes

Ultrastructural examination of tanycytes demonstrated that Cx43-immunoreactivity was confined to the outer cell membranes (*Figure 7).* In instances where the lateral surface of tanycyte cell bodies was adjacent to each other, Cx43-immunoreactivity was present in the contacting cytoplasmic membranes of both cells, supporting the existence of gap junctions (*Figure 7D*). As observed by confocal microscopy, the ventricular surface of tanycytes, including their protrusions projecting into the third ventricle, were densely labeled with silver grains denoting Cx43-immunoreactivity *(Figure 8),* particularly in more dorsal portions of the third ventricular wall where both tanycytes and ependymal cells are found (*Figure 8A*). Cx43-immunoreactivity was also present in the cytoplasmic membrane of tanycyte end feet processes, terminating on capillaries both in the ARC and in the external zone of the ME (*Figure 9A*). In addition, Cx43 was concentrated in cytoplasmic membrane of tanycyte end feet processes where the end feet processes were juxtaposed to another tanycyte process or to axon varicosities (*Figure 9B*).

Figure 7: Ultrastructural localization of Connexin 43-immunoreactivity on the contact surface of tanycytes.

Electron microscopic images demonstrate Connexin 43 (Cx43) immunoreactivity in the cytoplasmic membrane along the lateral surfaces of α-tanycytes (A, arrows) and β1-tanycytes in the lateral evagination of the third ventricle (B, arrows). Inset of B shows interwoven β1-tanycytes in higher magnification. Cx43-immunoreactivity is associated with the contacting surfaces of β-tanycyte cell bodies (C) and processes (D). The presence of silver grains on both contacting surfaces raises the possibility of the existence of functional gap junctions (arrowheads in C and D). Insets of C and D demonstrate contacting surfaces of tanycyte cell bodies and processes in higher magnification.

Scale bars: 500 nm and 200 nm on the insets. Abbreviations: 3v – third ventricle; nu – nucleus of a tanycyte; p – basal process of a tanycyte.
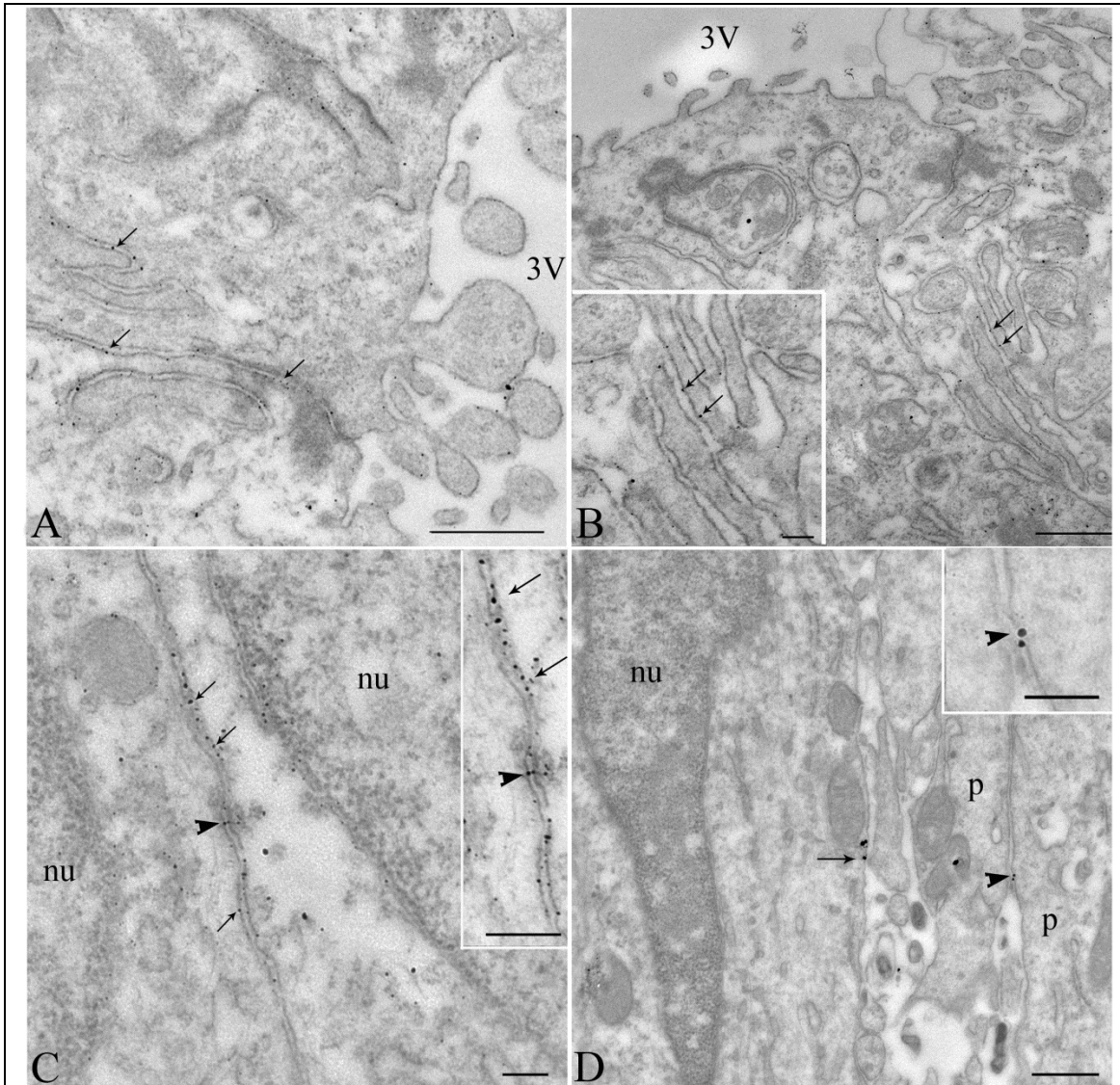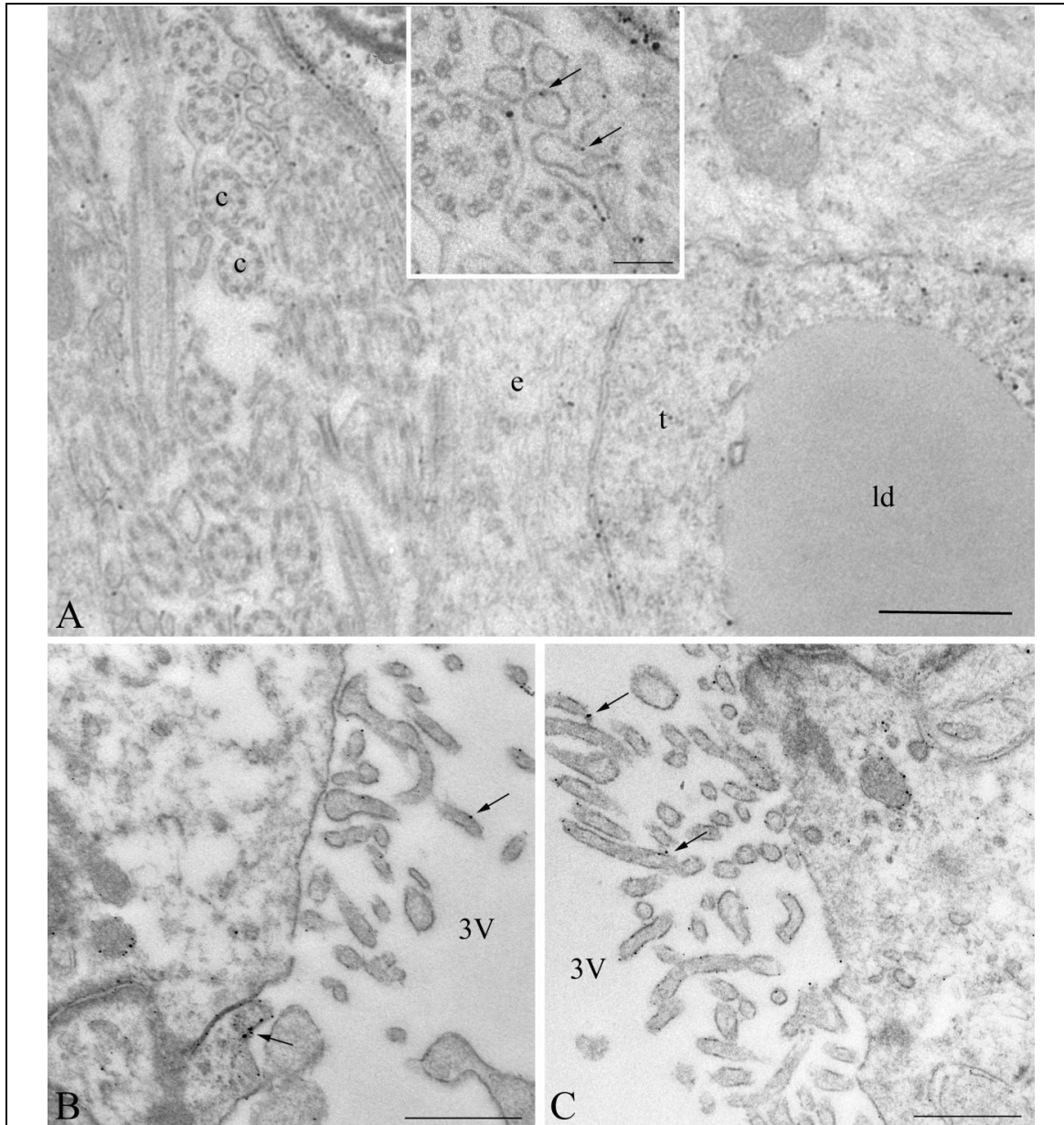
Figure 8: Ultrastructural localization of Connexin 43 (Cx43) -immunoreactivity on the ventricular surface of tanycytes.

Electron microscopic images illustrate α-tanycytes in the wall of the ventral and dorsal parts of the third ventricle. In the dorsal part of the ventricle (A), ciliated ependymal cells (marked by e) alternate with tanycytes (marked by t). The latter cell type is identified by the presence of lipid droplets (marked by ld) in their cytoplasm. The cilia of the ependymal cells are marked by (c). Cx43-immunoreactivity is labeled by silver grains. The inset shows higher magnification of Cx43-immunoreactivity in the cytoplasmic membrane of the ventricular surface of tanycytes and in the cytoplasmic membrane of their protrusions (arrows). In the ventral part of the ventricle (B, C), protrusions of the tanycytes show dense Cx43-immunoreactivity (arrows).

Scale bars: 500 nm and 100 nm on the inset. Abbreviations: 3V – third ventricle; c – cilia; e – ependymal cell; ld – lipid droplet; t – tanycyte.
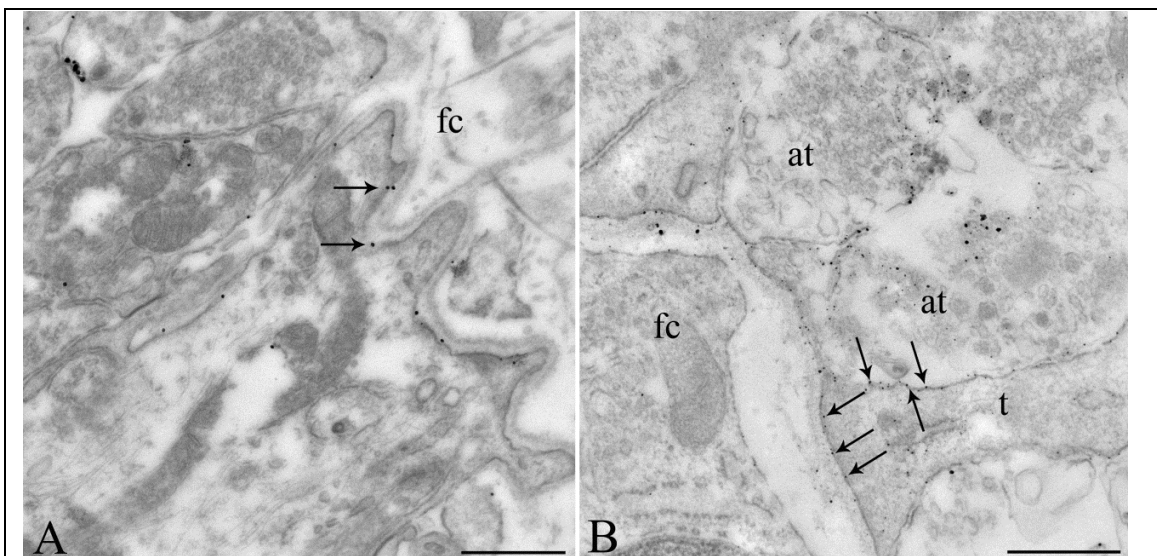
Figure 9: Ultrastructural localization of Connexin 43 (Cx43) -immunoreactivity on tanycyte end feet processes in the external zone of the median eminence.

Electron micrographs illustrate the localization of Cx43-immunoreactivity (silver grains, arrows) in the cytoplasmic membrane of a tanycyte end foot contacting a portal capillary (A). Cx43-immunoreactivity (arrows) is also present in the cytoplasmic membrane of the tanycyte end foot (marked by t) contacting a hypophysiotropic axon terminals (marked by at) in the external zone of the ME in the proximity of a fenestrated capillary (B).

Abbreviations: at – axon terminal, fc – fenestrated capillary, ME – median eminence; t – tanycyte end foot. Scale bars: 500 nm.

4.2. Characterization of the POMC expression in tanycytes

4.2.1. *Pomc* mRNA expression in non-neuronal cells

By radioactive and fluorescent ISH on serial coronal sections of rats covering the entire rostrocaudal extent of the tanycyte region and ARC, a large variability between brains was observed as to the extent and abundance of *Pomc* expression in tanycytes and similar non-neuronal cells of the ME and pituitary stalk. Therefore, we categorized the brains according to the POMC mRNA content of tanycytes: low-, intermediate- or high-level of non-neuronal *Pomc* mRNA (*Figure 10, Figure 11*).

In brains with low-level of non-neuronal *Pomc* mRNA, the *Pomc* signal was largely confined to a population of cells in the pituitary stalk and a caudal subset of β- and the most ventral α-tanycytes, located between Bregma levels -3.1 and -3.8 mm. Hybridization signal was also present in several non-neuronal cells in the caudal ME (*Figure 11A, B*). Rostral to Bregma level -3.1 mm, only few β tanycytes and non-neuronal ME cells contained hybridization signal (*Figure 10A, B*). In these brains, the hybridization signal in tanycytes was generally much lower than in POMC neurons. In brains with high-level of non-neuronal *Pomc* mRNA, the hybridization signal extended rostro-caudally to virtually the entire β-tanycyte population (between Bregma -1.7 to -4.0 mm), dorsally to a large portion of α2-tanycytes, and to more non-neuronal cells in the ME and pituitary stalk (*Figure 10D, E, Figure 11D, E*). *Pomc* mRNA was never observed, however, in the most dorsal tanycyte population, the α1-subtype. In these "high-level" brains, the intensity of tanycyte hybridization signal approximated that of POMC neurons. In brains with "intermediate-level" of non-neuronal *Pomc* mRNA, the general pattern was similar to "high-level" brains, but the intensity of tanycyte hybridization signal remained well below that of POMC neurons, particularly in the rostral half of the tanycyte region (*Figure 10C, Figure 11C*).
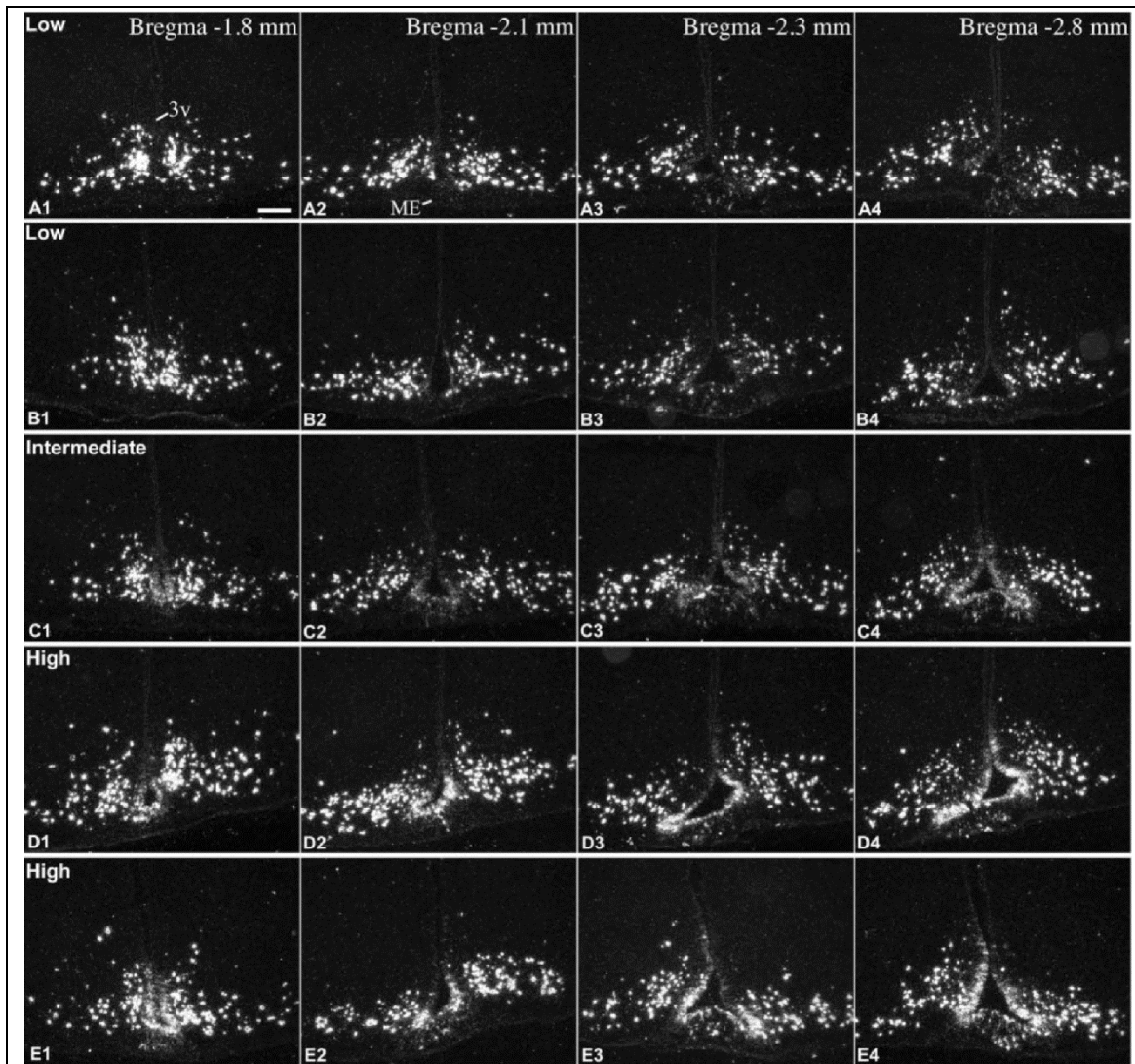
Figure 10: Radioactive in situ hybridization of POMC mRNA in the rostral part of the tanycyte region of 5 adult rats.

Radioactive ISH demonstrates different expression levels of Pomc mRNA in the rostral part of the tanycyte region in 5 adult rats with different expression levels in tanycytes of the third ventricle and non-neuronal cells of the ME. A and B show low, C shows intermediate, while D and E show high Pomc mRNA expression in tanycytes. A, B and D are male, C and E are female rats, between 8-10 weeks of age. Images from the caudal part of the tanycyte region from the same brains are presented in Figure 11.

Abbreviation: ME – median eminence. Scale bar: 200 µm.
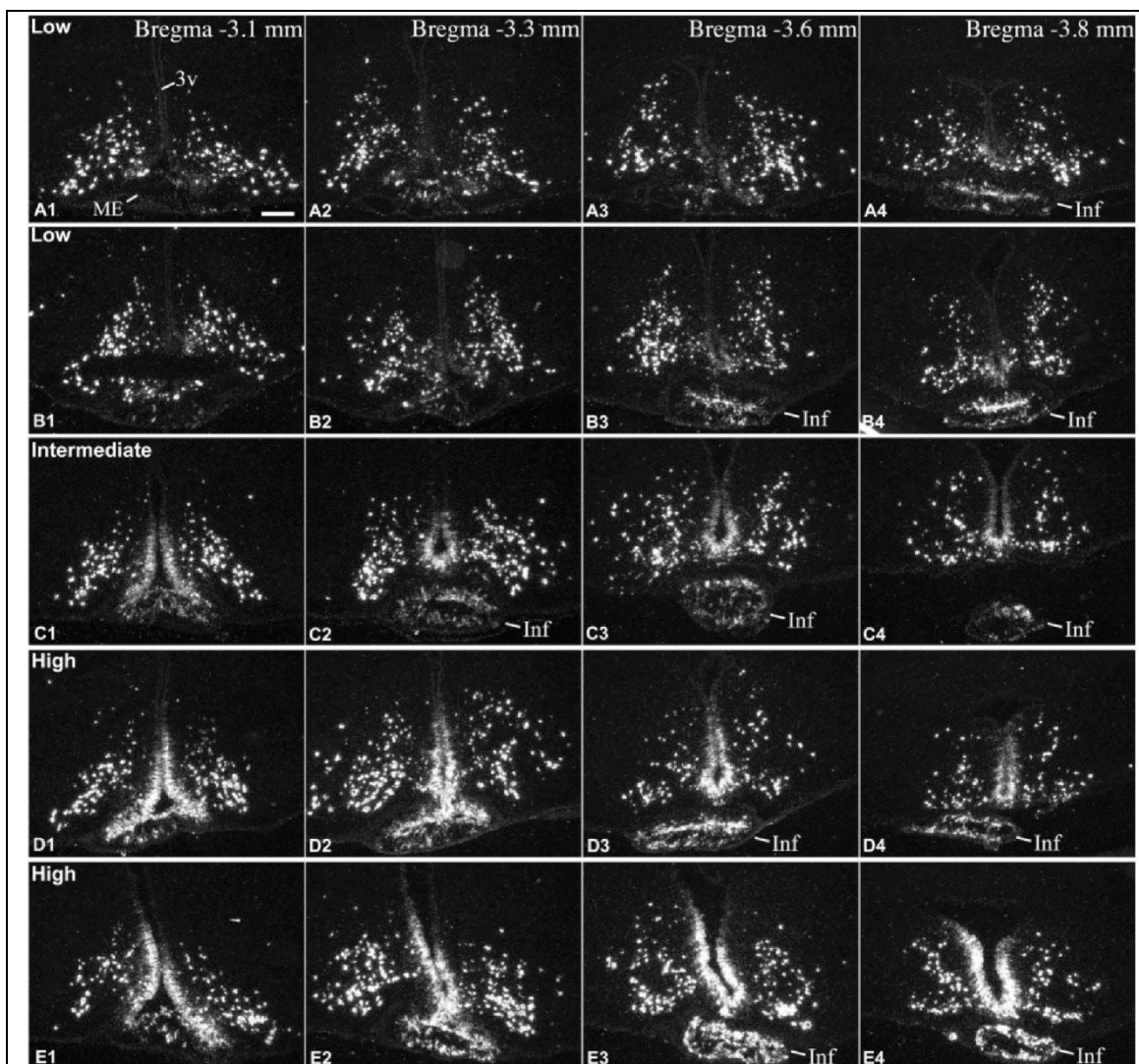
Figure 11: Radioactive in situ hybridization of POMC mRNA in the caudal part of the tanycyte region of 5 adult rats.

As a continuation of Figure 10., radioactive ISH demonstrates Pomc mRNA in the caudal part of the tanycyte region in 5 adult rats with different expression levels in tanycytes of the third ventricle and non-neuronal cells of the ME and infundibular (pituitary) stalk. A and B show low, C shows intermediate, while D and E show high Pomc mRNA expression in tanycytes. A, B and D are male, C and E are female rats, between 8-10 weeks of age. The infundibular stalk appears at different rostro-caudal levels due to differences in the plane of sectioning.

Abbreviations: ME – median eminence; 3V – third ventricle; Inf – infundibular stalk. Scale bar: 200μm.

This variability was observed in both adult males and females, with similar age and body weight, which were euthanized together within 2 h of the mid-day period. Among the total 26 rat brains we analyzed with ISH, 10 brains had low, 5 intermediate and 11 high Pomc mRNA levels in tanycytes. Importantly, variability was observed in both young adult rats, between ages 8-10 weeks, and in fully adult, 15 week-old rats *(Table 6)*

Table 6: Number of rats with low-, intermediate- and high-level Pomc mRNA in tanycytes in the different experiments.

In each experiment rats were euthanized within 2h of the mid-day period.

Experiment	Sex	Age	*Pomc* mRNA levels		
			Low	**Intermediate**	**High**
Adult rats for *Pomc* ISH	M	8 weeks	3	1	0
	M	8-9 weeks	4	0	2
	F	9-10 weeks	1	2	3
	M	9-10 weeks	0	0	4
	M	15 weeks	2	2	2
Adolescent rats for *Pomc* ISH	M	31 days	4	0	0
	F	31 days	4	0	0

To examine whether variability in non-neuronal Pomc mRNA is present before adulthood, ISH was performed in adolescent, 31 day old male (n=4; BW 80-93g) and female (n=4; BW 67-81g) rats. Hybridization pattern in all of the 8 young rats was highly similar to that observed in "low-level" adult rats *(Table 6)*. Moderate signal was present in the pituitary stalk, as well as in a portion of β1-, β2-, α2- and in tanycytes in mid and caudal levels of the third ventricle and ME. Signal in the rostral half of the tanycyte region was occasional and very light *(Figure 12)*. Neuronal *Pomc* hybridization signal was also less intense than in adults.
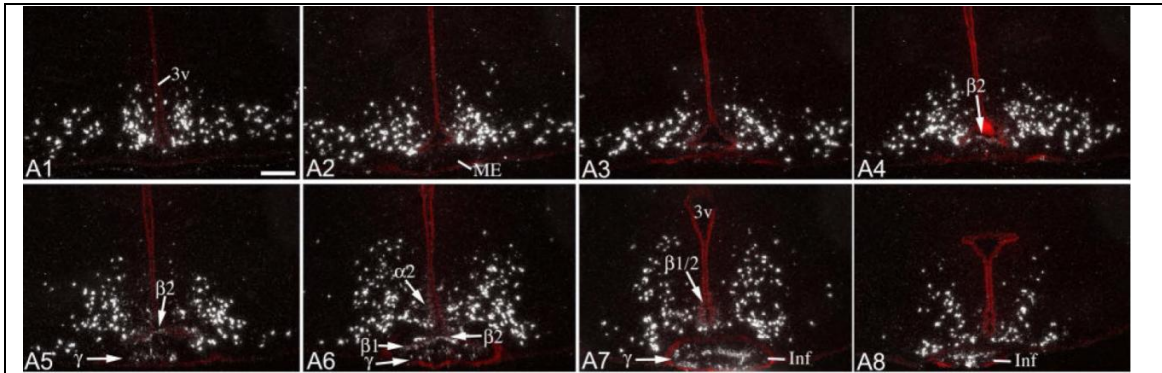
Figure 12: Radioactive ISH demonstrates Pomc mRNA distribution in a 31 day-old, adolescent male rat.

Sections are arranged in rostro-caudal order (A1: most rostral; A8: most caudal), with ~200 μm distance between consecutive sections. Fluorescent cresyl-violet staining (Redecker) is overlaid to help identify the location of the third ventricle, ME and infundibular stalk. Arrows point to non-neuronal signal in α2-, β1-, β2- and tanycytes in the mid and caudal levels of the ME.

Abbreviations: 3V- third ventricle; ME – median eminence; Inf – infundibular stalk. Scale bar: 200μm.

4.2.2. Non-neuronal *Pomc* mRNA-expressing cells are vimentin-positive tanycytes

To ascertain the identity of non-neuronal cells that express *Pomc* mRNA and to unambiguously distinguish them from POMC neurons, we combined fluorescent ISH with immunofluorescence for the tanycyte/ependymal marker, vimentin, and the neuronal marker, HuC/D. In general, non-neuronal *Pomc* mRNA-expressing cells could be easily distinguished from neurons based solely on different morphology and appearance of the hybridization signal (*Figure 13A, B*). In some cases, however, smaller POMC neurons with less intense signal could be unambiguously identified only by their HuC/D content (data not shown). While few POMC neurons were regularly found in the ME and pituitary stalk, occasionally even within the β-tanycyte layer, we did not observe *Pomc* mRNA-expressing cells that contained both vimentin and HuC/D (data not shown). Pomc mRNA-expressing cells in the ventricular wall, corresponding to the location of β1-, β2- and α2-tanycytes always contained vimentin (*Figure 13D, E*). The vast majority of non-neuronal *Pomc* mRNA-expressing cells that are located below the β-tanycyte layer throughout the external zone of the ME also contained vimentin (*Figure 13C, D*).

62
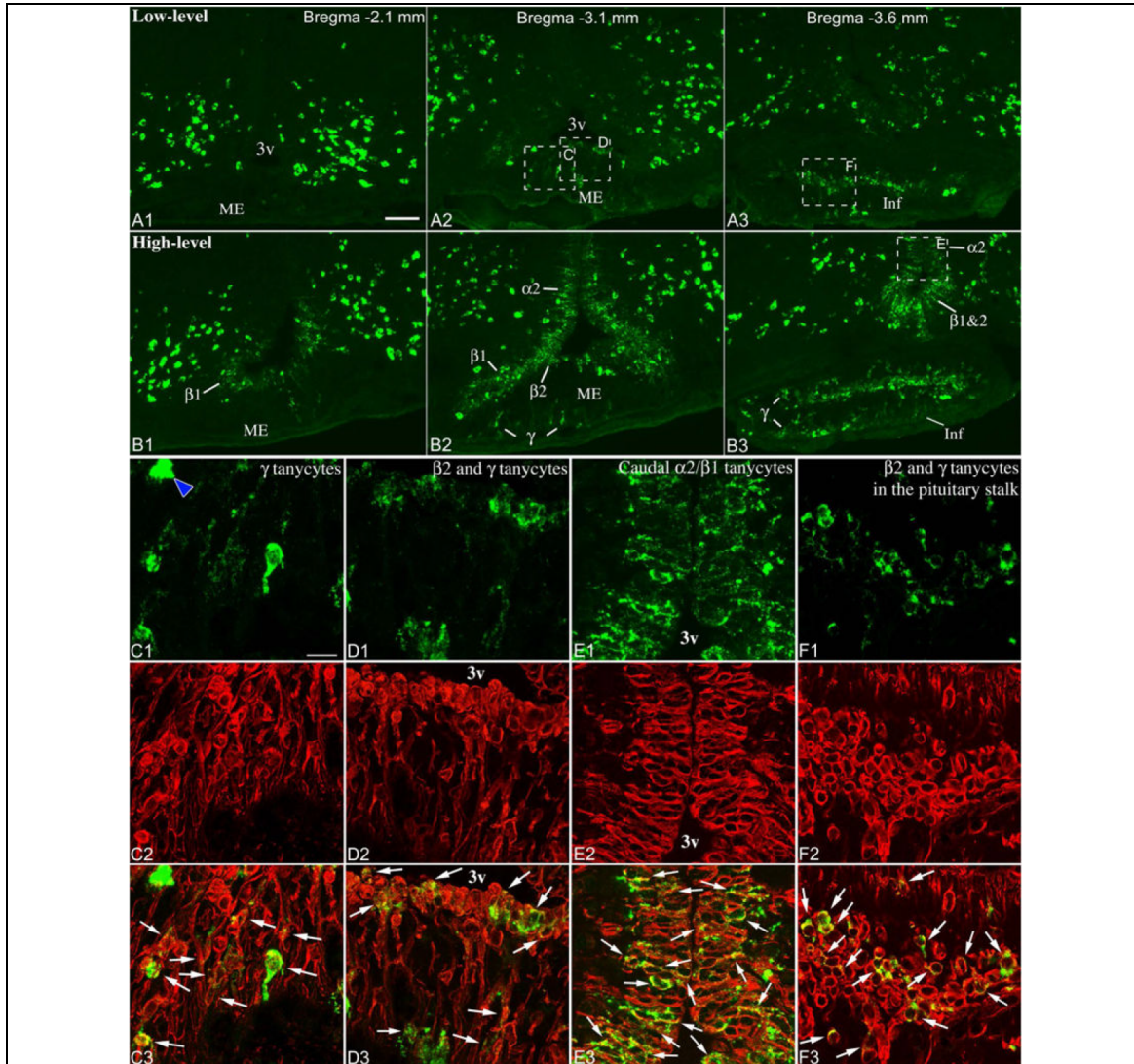
Figure 13: Pomc mRNA expression in tanycytes demonstrated by fluorescent in situ hybridization and fluorescent in situ hybridization combined with immunofluorescence.

A1-3 show low-level, while B1-3 show high-level of Pomc mRNA expression in tanycytes, demonstrated by fluorescent ISH. A1-3 is the same brain as in Figure 10A and Figure 11A and B1-3 is the same brain as in Figure 10D and Figure 11D.

Abbreviations: 3v - third ventricle; Inf, infundibular stalk; ME, median eminence. Scale bar: 100μm.

C-F represent confocal images of boxed areas from A2, A3 and B3 show combined Pomc ISH (green) and vimentin immunofluorescence (Redecker). Virtually all non-neuronal Pomc mRNA-expressing cells contain the tanycyte marker vimentin (arrows). Blue arrowhead on C1 points to a Pomc neuron in the ME. HuC/D immunofluorescence (not shown) allowed unambiguous identification of Pomc neurons. C, D and E are projections of multiple confocal planes; F shows a single confocal plane. Scale bar: 25μm.

These cells were apparently tanycyte-type cells often with an elongated shape perpendicular to the ventricular floor, or with a small, round-shaped cell body with multiple processes. *Pomc* mRNA-expressing cells in the pituitary stalk had round or elongated shape with apparent processes and virtually always contained vimentin (*Figure 13A, B, F*). Many of these cells were non-ependymal tanycyte-type cells, while others in the rostral part of the stalk were β-tanycytes bordering the third ventricular recess. To easily identify and distinguish these cells from the other tanycyte subtypes, we decided to integrate them into the tanycyte nomenclature and refer to them as gamma- (γ) tanycytes.

4.2.3. Variable POMC protein expression in tanycytes of adult rats

Immunofluorescence using an antibody against the N-terminal portion of POMC yielded the same pattern of cellular expression and variability as *Pomc* ISH experiments. In "low-level" brains, POMC was present in tanycytes of the pituitary stalk and a subset of β- and γ-tanycytes between Bregma levels -3.1 and -3.8 mm. Rostral to this level, POMC was present in some β-tanycyte processes and γ-tanycytes in the ME, the number of which varied among "low-level" brains (*Figure 14*).

In "high-level" brains, POMC was present in the vast majority of β- and α2-tanycytes, and a large number of γ-tanycytes, essentially mirroring *Pomc* mRNA distribution in "high-level" brains (*Figure 15*).

Of 8 adult male brains, 3 had low, 2 intermediate and 3 high POMC levels in tanycytes; of 7 female brains, 5 had low, 1 intermediate and 1 high POMC levels (*Table 7:*).
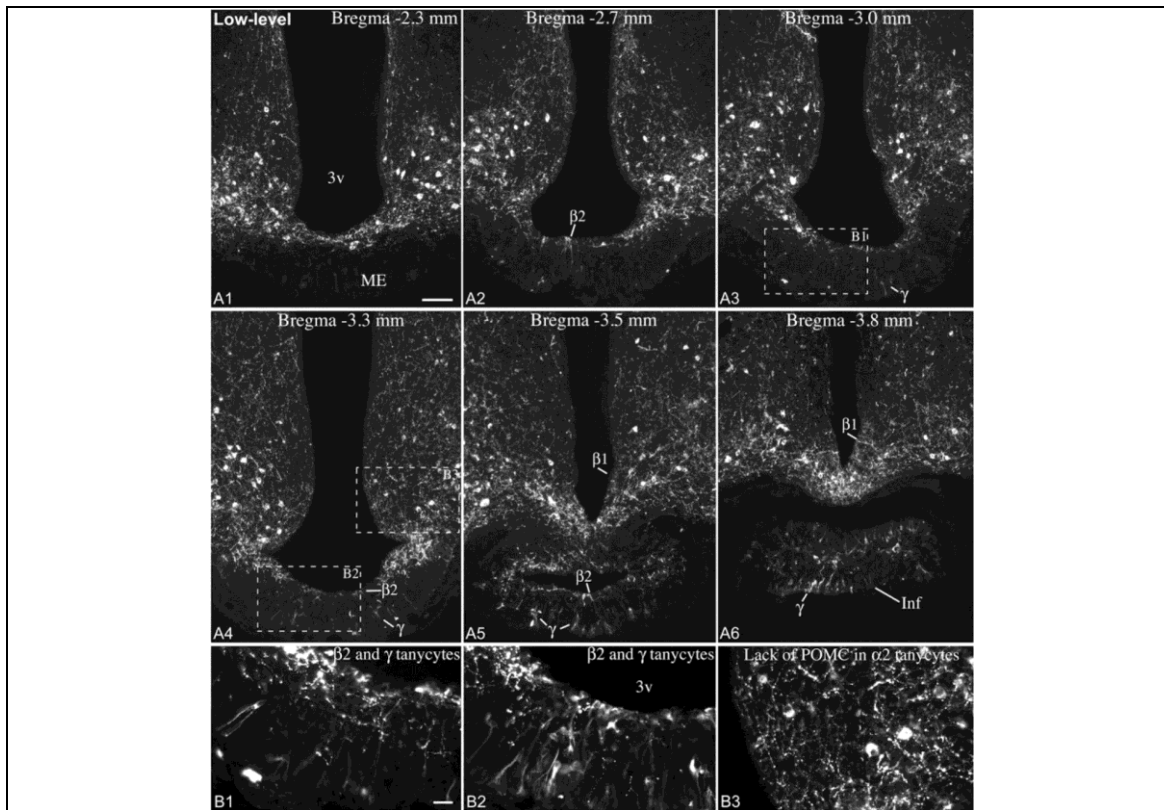
Figure 14: POMC immunofluorescence from an adult male rat with low POMC levels in tanycytes.

POMC is expressed in a small subset of β2- and β1-tanycytes in the wall of the third ventricle, as well as in γ-tanycytes in the ME and infundibular stalk (A). B1 and B2 show boxed areas in A3 and A4 in higher magnification and show POMC-expressing β2-tanycytes and γ-tanycytes in the ME. B3 shows boxed area from A4 in higher magnification and shows the lack of POMC in α2-tanycytes.

Abbreviations: 3V – third ventricle, Inf – infundibular stalk, ME – median eminence. Scale bar: 100 μm on A and 25μm on B.
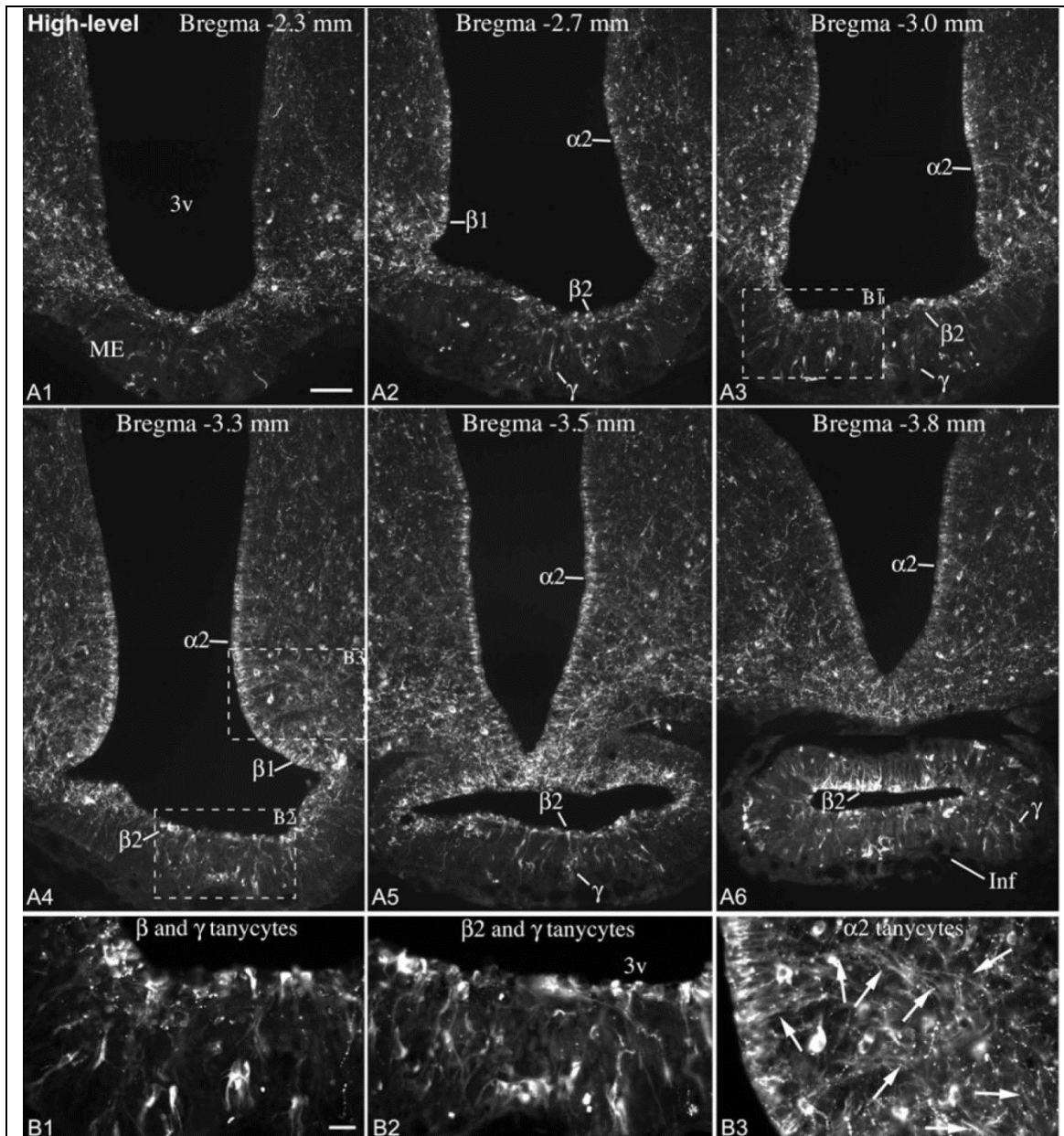
Figure 15: POMC immunofluorescence from an adult male rat with high POMC levels in tanycytes.

The majority of α2-, β1- and β2-tanycytes lining the third ventricle and a large number of γ-tanycytes in the ME and infundibular stalk express POMC (A). B1-B3 show higher magnification of boxed areas in A3 and A4 and represent POMC-expressing β--, γ- and α2-tanycytes. Arrows on B3 point to the POMC-positive processes of α2-tanycytes.

Abbreviations: 3V – third ventricle, Inf – infundibular stalk, ME – median eminence. Scale bar: 100 μm on A and 25 μm on B.

Table 7: Number of rats with low-, intermediate- and high-level POMC protein level in tanycytes in the different experiments.

In each experiment rats were euthanized within 2h of the mid-day period.

Experiment	Sex	Age	POMC protein levels		
			Low	Intermediate	High
Adult rats for POMC immunofluorescence	M	10 weeks	1	1	2
	M	10 weeks	2	1	1
	F	11 weeks	5	1	1

The varying shapes and morphological characteristics of POMC-positive γ-tanycytes (*Figure 14*, *Figure 15*), clearly delineated by the POMC immunofluorescent signal, were essentially identical to the original descriptions of these cells (Bitsch and Schiebler, 1979, Zaborszky and Schiebler, 1978). Triple immunofluorescence studies confirmed our combined ISH/immunofluorescence findings that POMC-positive γ-tanycytes were virtually always vimentin positive and comprised separate population from POMC neurons that were vimentin-negative but HuC/D-positive (*Figure 16*). By location, POMC neurons of the ME were found exclusively in the internal zone, close to and occasionally within the β-tanycyte-layer. POMC-positive γ-tanycytes, however, extended from the subependymal zone to the external zone (*Figure 12-14*).
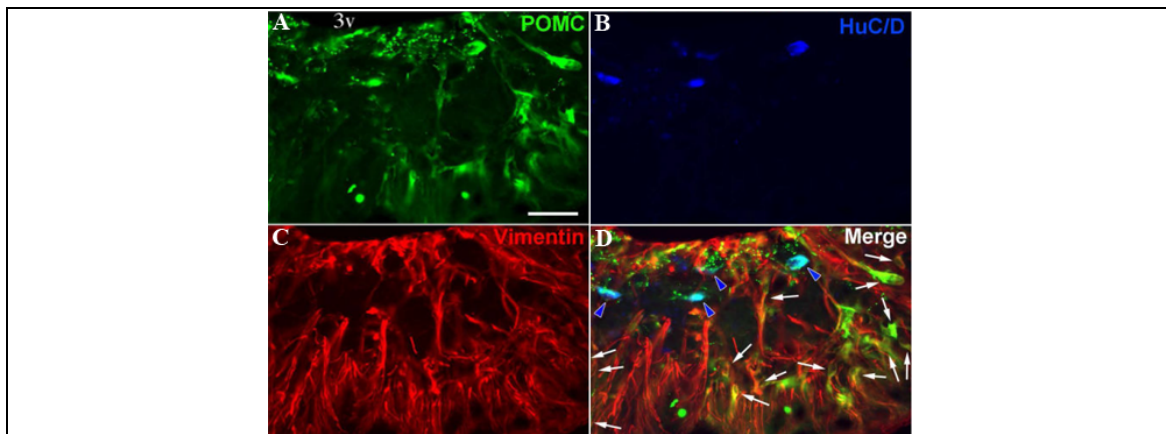
Figure 16: Triple immunofluorescence from the rostral median eminence of a brain with high-level of POMC in tanycytes.

POMC (A, green) is present in both HuC/D-positive (B, blue) neurons (blue arrowheads on D), and vimentin-positive (C, red) γ-tanycytes (arrows on D) but these two cell types form separate populations.

Abbreviations: 3v - third ventricle. Scale bar: 50 µm.

4.2.4. Ultrastructural examination of POMC-immunoreactive cells in the ME

By electron microscopic examination of the ME, POMC-immunoreactivity was detected in cell bodies and processes of β-tanycytes as well as in γ-tanycytes *(Figure 17)*. γ-tanycytes in the ME had ultrastructural characteristics similar to β-tanycytes, including numerous elongated mitochondria in their processes, and several large lipid drops (Akmayev and Fidelina, 1976, Brawer, 1972, Rodriguez et al., 2005, Zaborszky and Schiebler, 1978). Their processes often terminated on capillaries.
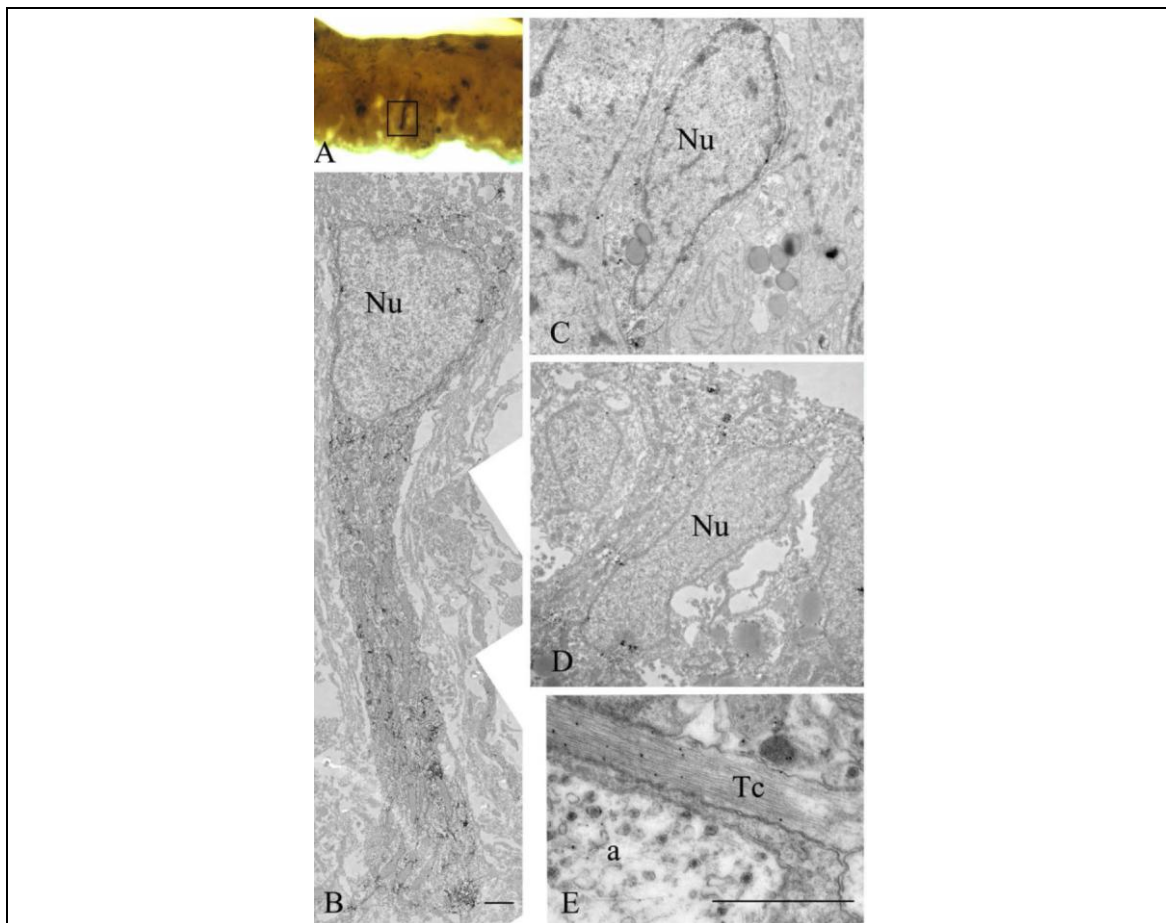
Figure 17: Immuno-electron microscopic detection of POMC in tanycytes.

The ultrastructure of a POMC-immunoreactive γ-tanycyte in the external zone of the ME (boxed area of A) is shown in B. POMC-immunoreaction is labeled by silver grains. Note the high concentration of mitochondria in the highly immunolabeled short process of the γ-tanycyte. C and D illustrate cell bodies of POMC-immunoreactive β-tanycytes lining the floor of the third ventricle. On E silver grains denoting POMC-immunoreactivity are associated with microfilaments in a tanycyte process.

Abbreviations: N - nucleus; a - axon varicosity; Tc - tanycyte process. Scale bar: 2 μm.

4.2.5. Detection of POMC-derived peptides in tanycytes

β-endorphin immunofluorescence resulted in highly similar patterns and variability as the POMC staining, but labeled substantially fewer tanycytes in the same brains (*Figure 18*). Namely, in "low-level" brains, non-neuronal β-endorphin staining was confined to some γ-tanycytes in the pituitary stalk and ME, as well as few β-tanycyte cell bodies and processes (*Figure 18A, B*). In "high-level" brains, β-endorphin staining labeled many more β- and γ-tanycytes, as well as α2-tanycytes and their processes (*Figure 18C, D*). Immunofluorescence using anti-ACTH serum labeled only occasional γ-tanycytes in the ME and the pituitary stalk (*Figure 19A, B*). Their number was independent on whether the brain had low- or high- POMC level in tanycytes; in some brains there were 1-2 cells in each section, while in others there were no clear ACTH-positive γ-tanycytes. The signal in γ-tanycytes was always much lighter than in neurons or axons (*Figure 19A, B*). In addition, in brains with high POMC levels in tanycytes we noted a very light ACTH-immunoreactivity primarily in α2-tanycyte cell bodies (*Figure 19C, D*).

α-MSH immunoreactivity that was clearly above background level was very rare in tanycytes. Very light signal was observed occasionally in γ-tanycytes in the ME and pituitary stalk, and in a few tanycyte-processes in brains with high-level POMC in tanycytes (*Figure 19E, F*).
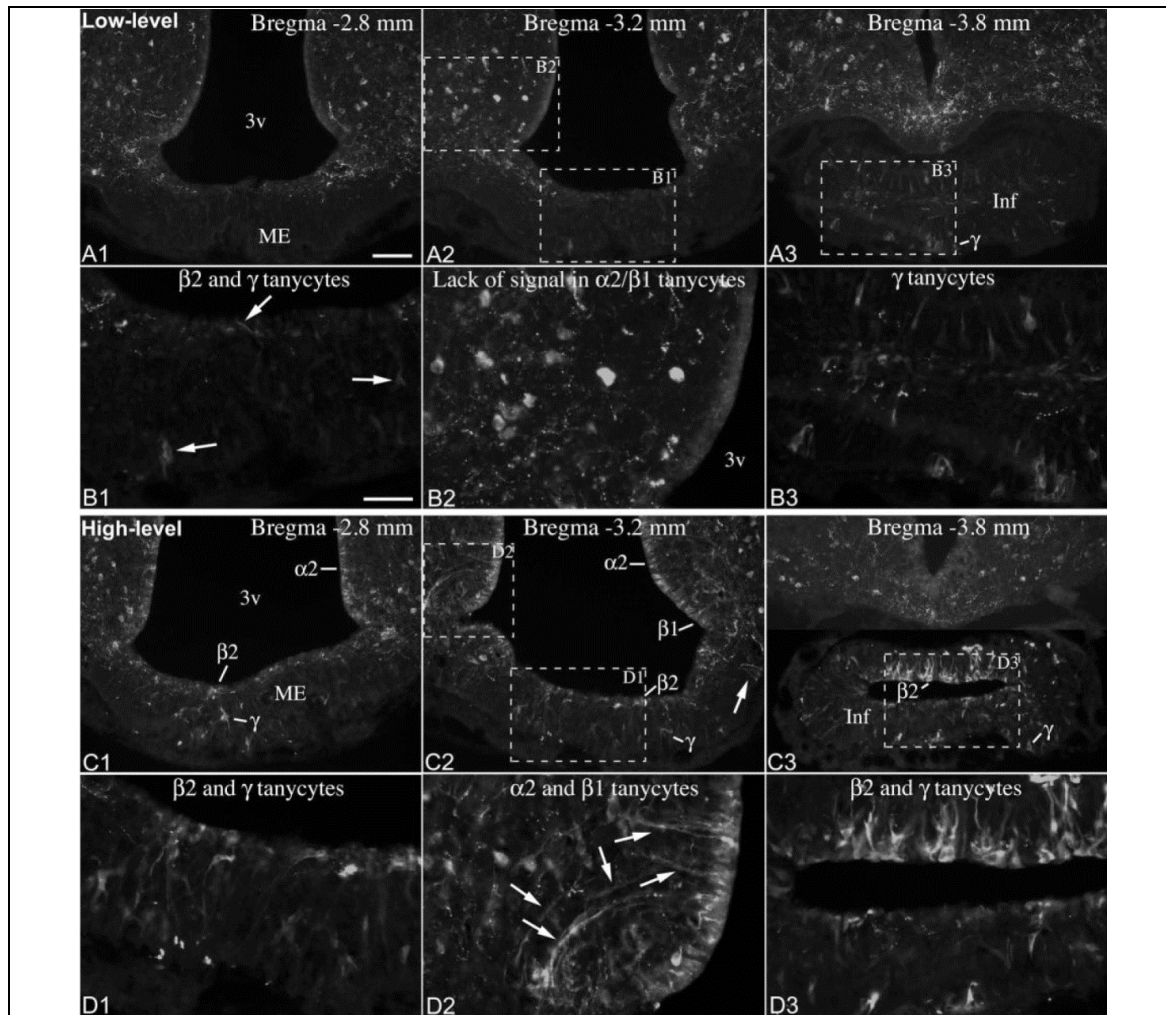
Figure 18: β-endorphin-immunofluorescence in brains with low-and high-level POMC in tanycytes

A1-A3 show a β-endorphin-immunoreactivity in a brain with low-level POMC in tanycytes (the same brain as in Figure 14). B1-B3 show A1-A3 boxed areas with higher magnification. Arrows in B1 represents β-endorphin immunoreactive β2- tanycyte and γ-tanycytes in the ME, B2 represents the lack of signal in α2- and β1-tanycytes, B3 shows numerous immunopositive γ-tanycytes in the pituitary stalk.

C1-C3 show β-endorphin-immunofluorescence in a brain with high-level POMC in tanycytes (same brain as in Figure 15). Arrow on C2 indicates intensely labeled tanycyte end feet in the lateral ME. D1-D3 show higher magnification of boxed areas in C1-C3 with β-endorphin-immunoreactive β2-tanycytes and γ-tanycytes in the ME on D1 α2- and β1-tanycyte cell bodies and processes (arrows on D2) and intensively labeled β2- and γ-tanycytes of the pituitary stalk on D3.

Abbreviations: 3v - third ventricle; Inf - infundibular stalk; ME - median eminence. Scale bar: 100 μm on A (for A and C); 50 μm on B (for B, D).
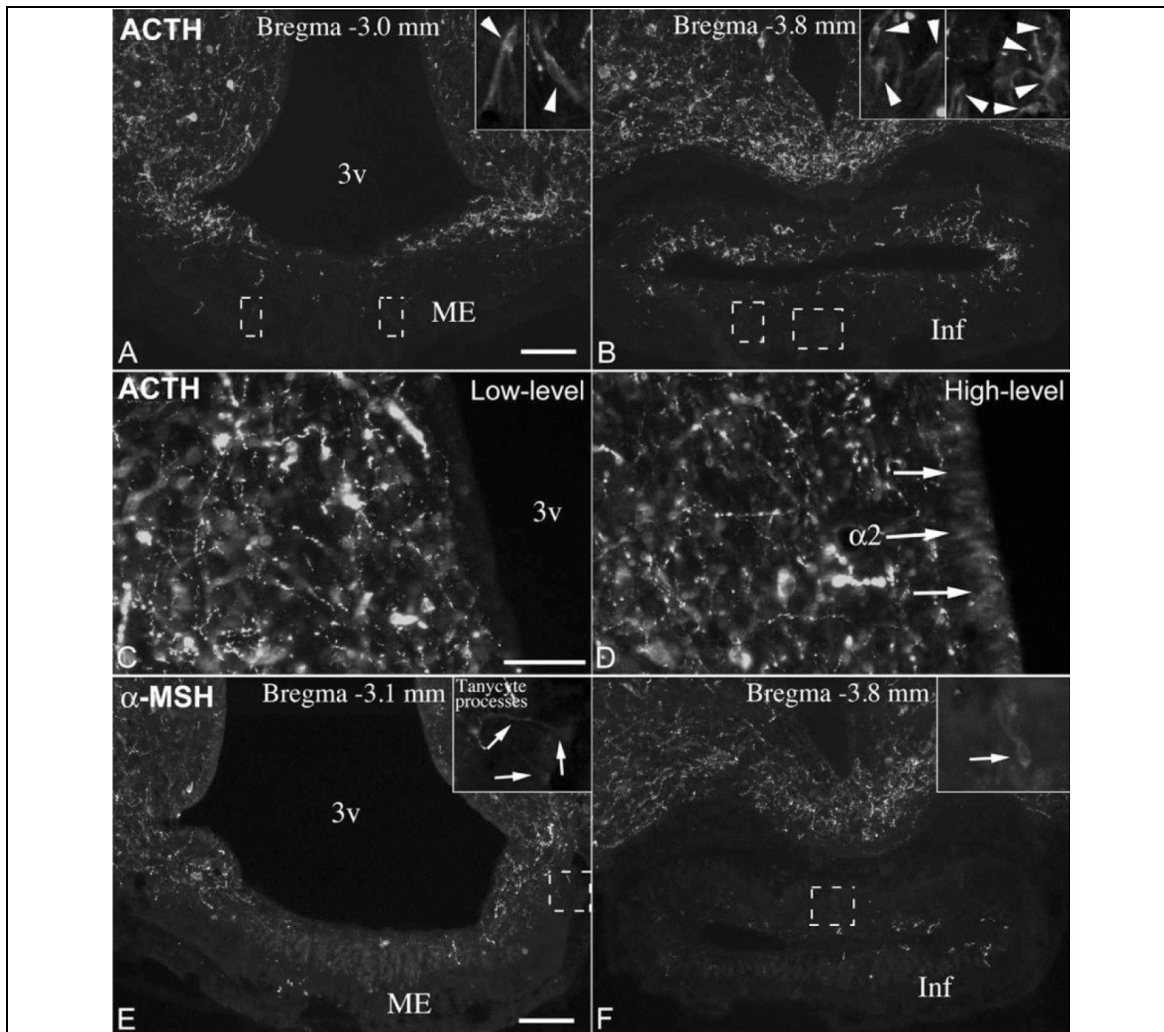
Figure 19: ACTH and α-MSH immunofluorescence in an adult male rat brain.

A and B show adult male rat brain with few ACTH-immunoreactive γ-tanycytes in the ME and pituitary stalk. Insets show ACTH-positive γ-tanycytes in boxed areas. (C, D) The cell body layer of α2-tanycytes lacks ACTH-immunofluorescence in a brain with low-level POMC in tanycytes (C), but a low-level signal (arrows) can be detected in a brain with high-level POMC in tanycytes (D).

E, F show α-MSH immunofluorescence in tanycyte processes and in a γ-tanycyte in the pituitary stalk. Insets show boxed areas in higher magnification.

Abbreviations: 3v – third ventricle, ME – median eminence, Inf – infundibular stalk. Scale bar: 100 μm on A and E (for A, B, E, F); 50 μm on C (for C, D).

4.2.6. Expression of POMC-processing enzymes in tanycytes

The scarce ACTH and α-MSH immunoreactivity in tanycytes suggested that there may be little processing of the POMC precursor in these cells. This would be in agreement with previous ISH studies that show no positive signal in tanycytes for the prohormone-convertase 1 and 2 (PC1, PC2) that cleave the POMC precursor to generate ACTH, and

71

further to α-MSH, respectively (Cawley et al., 2016). To further examine whether genes involved in POMC-processing are expressed in tanycytes, we used RNA-Seq analysis on the transcriptome of rat tanycytes (α1, α2, β1, β2) that were isolated by LCM. Expression levels were compared to samples obtained by the same method from the adjacent ARC. Expression values for PC1, PC2, carboxypeptidase E, peptidylglycine alpha-amidating monooxygenase and secretogranin V (or 7B2) mRNAs were significantly lower in tanycyte samples than in the ARC (*Table 8*), in agreement with ISH studies that show predominantly neuronal expression patterns for these genes in the hypothalamus (Cullinan et al., 1991, Schafer et al., 1993). PC2 mRNA had the lowest value in tanycytes, 7.4 ± 0.4, which was below the cutoff value of 10.0 considered for positive expression. The second lowest expression, *PC1* mRNA with 16.2 ± 0.8, was only slightly above the cutoff value. Pomc mRNA levels were similar in the tanycyte sample and the ARC sample (347.2 ± 36.2 in tanycytes *vs*. 397.2 ± 37.0 in the ARC).

Table 8: Next-Generation sequencing expression values of Pomc and genes involved in POMC-processing in tanycytes and neighboring ARC.

The samples were collected by laser capture microdissection from 5 male Wistar rats, statistical comparison was made by Student's t-test.

Description	Tanycytes Mean ± SEM (normalized CPM)	Arcuate nucleus Mean ± SEM (normalized CPM)	P value
Pomc - proopiomelanocortin	347.2 ± 36.2	397.2 ± 37.0	0.4921
Cpe - carboxypeptidase E	529.8 ± 33.5	1331.6 ± 44.2	< 0.0001
Pcsk1 - proprotein convertase substilin/kexin type 1	16.2 ± 0.8	51.7 ± 1.5	< 0.0001
Pcsk2 - proprotein convertase substilin/kexin type 1	7.4 ± 0.4	50.2 ± 4.9	0.0002
Pam - peptydilglicine alpha-amidating monooxygenase	204.8 ± 9.5	306.1 ± 6.3	0.0002
Scg5 - secretogranin V (7B2 protein)	36.3 ± 9.1	184.0 ± 46.0	< 0.0001

4.3. Importance of microglia in the development of HFD induced metabolic changes

4.3.1. Effect of HFD and microglia ablation on the body composition and metabolic parameters

After 3 weeks of pretreatment with PLX-containing LF diet to ablate the microglia or with PLX-free LF chow, half of the animals of each group were switched to a diet with 60% high-fat content, while the other half continued to consume the diet with low-fat content. This arrangement resulted in four treatment groups: LF, HFD, LF+PLX and HFD+PLX. At the start of the special diet, there was no significant difference in the body composition of the animal groups.

During the three days of diet, the change of the lean body mass was influenced by both the diet (P=0.001) and the PLX treatment (P=0.025), but there was no interaction between the two factors (P=0.241) by factorial ANOVA. The PLX treatment caused significant decrease (P=0.02) of the lean body mass of the LF mice (-0.078 ± 0.154 g) compared to the elevation of the lean body mass of mice on LF without PLX (0.616 ± 0.239). Moreover, significant difference was found between the lean body mass change of the LF+PLX and HFD+PLX animals (-0.078 ± 0.154 g *vs.* 0.883 ± 0.134 g; P=0.004).

The change of the total water content and body weight of the mice was influenced only by the diet (P=0.002 and 0.003 by factorial ANOVA, respectively), however, it was independent of the PLX treatment (P=0.157 and 0.307 by factorial ANOVA respectively). The total water content of the HFD+PLX mice had higher increase than that in the LF+PLX mice *vs.* (0.821 ± 0.120 *vs.* -0.109 g ± 0.113 g; P=0.008). Similarly, the HFD+PLX mice had significantly higher body weight change than the LF+PLX mice (1.819 ± 0.267 *vs.*0.436 ± 0.240 g; P=0.03) *(Figure 20)*. HFD had a tendency to increase the change of the water content and body weight in animals without PLX treatment, but this change did not reach the level of significance.
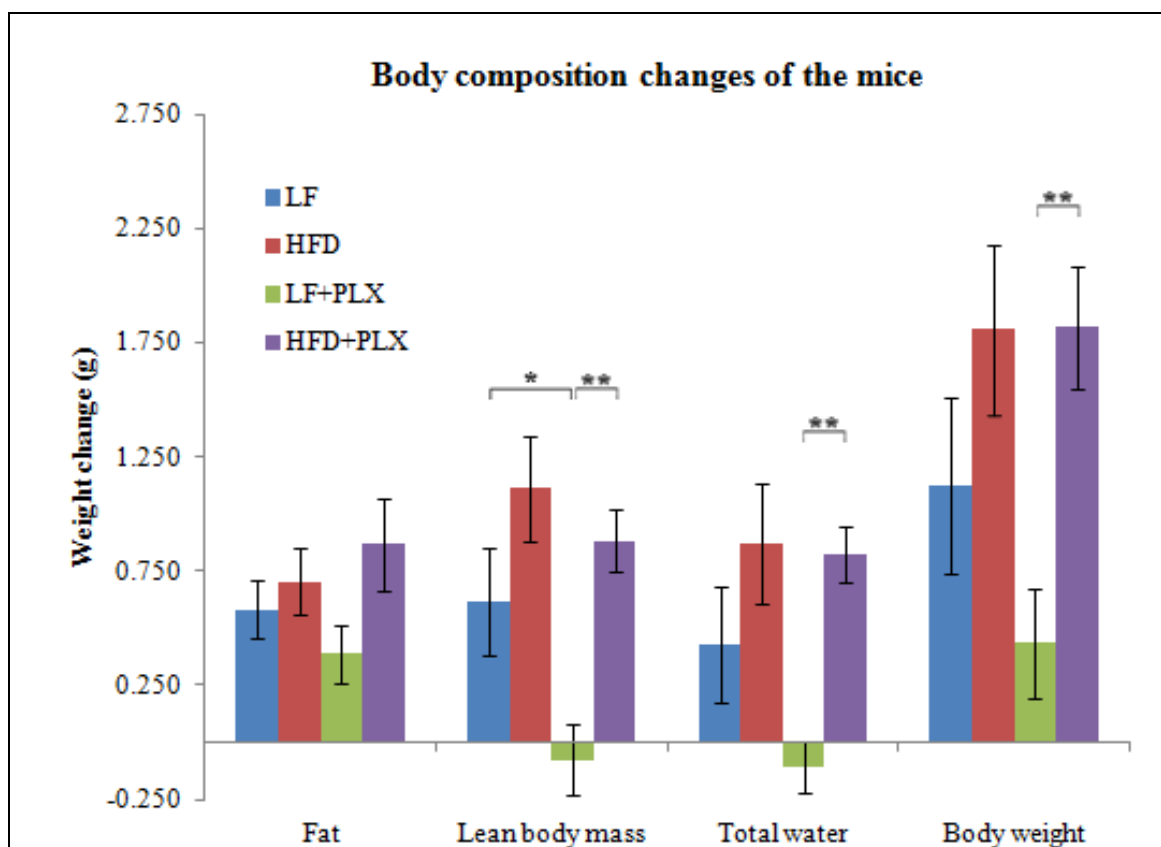
Figure 20: The changes of the body composition during the short-term LF or HFD combined with PLX treatment.

The body composition of the mice was measured with EchoMRI after 3 weeks of normal chow (Kristensen et al.) or normal chow with PLX pretreatment (LF+PLX) and after switching the half of both groups to HFD for 3 days. The average changes of the body components of the 4 groups (LF, HFD, LF+PLX, HFD+PLX) were analyzed. Significant differences were observed between the average change of the lean body mass of LF and LF+PLX animals and between the changes of lean body mass, total water and body weight of the LF+PLX and HFD+PLX animals. Data are shown as Mean ± SEM

*$p<0.05$; **$p<0.01$, by one-way ANOVA followed by Newman-Keuls post-hoc test.*

The total activity of mice was influenced by both the diet (P=0.00048) and the PLX treatment (P=0.0004), but there was no interaction between the two factors (P=0.948) by factorial ANOVA (*Figure 21*).

During the 3 days of the diet, the mice of the HFD groups had markedly increased activity compared to the LF groups. The average total activity of the LF *vs.* HFD mice was 2405.98 ± 234.68 *vs.* 3170.24 ± 552.18 beambreaks/h (P=0.013), while the total

locomotor activity of the LF+PLX *vs*. HFD+PLX was 1432.23 ± 244.57 *vs*. 2246.73 ± 567.09 beambreaks/hour (P=0.01).

The PLX treatment significantly decreased the locomotor activity both in LF+PLX and HFD+PLX groups compared to groups without PLX. The average total activity of LF *vs*. LF+PLX mice was 2405.98 ± 234.68 *vs*. 1432.23 ± 244.57 beambreaks/hour (P=0.007), while the average total activity of the HFD *vs*. HFD+PLX was 3170.24 ± 552.18 vs. 2246.73 ± 567.09 (P=0.009) (*Figure 21*).

The difference between LF and LF+PLX groups was significant both in the daylight period and at night, with 1652.92 ± 257.72 *vs*. 914.79 ± 161.74 (P=0.02) and 3136.05 ± 267.14 *vs*. 1949.66 ± 347.06 beambreaks/hour, respectively, (P=0.02). However, the difference between HFD and HFD+PLX was only significant at night (4027.00 ± 435.52 *vs*. 2668.54 ± 662.20 beambreaks/hour, P=0.009). The HFD significantly increased the activity of the HFD+PLX mice compared to LF+PLX mice in the daylight period (P=0.01), while significantly increased the activity of HFD mice compared to LF mice (P=0.047) at night (*Figure 21*).

Figure 21. The total activity of mice during the short-term LF or HFD combined with PLX treatment in the X, Y and Z dimensions

The upper part of the figure shows the average total activity pattern per hour. Data are shown as Mean ± SEM and the purple stripe represents the dark period. On the lower part, total activity of the mice divided to daylight, night and average components can be found. Data are shown as Mean+SEM on the bar graphs.

*p<0.05; **p<0.01 by one-way ANOVA followed by Newman-Keuls post-hoc test.

Similar differences between mice on PLX-free and PLX-containing chow groups were found when the ambulatory and fine activity componen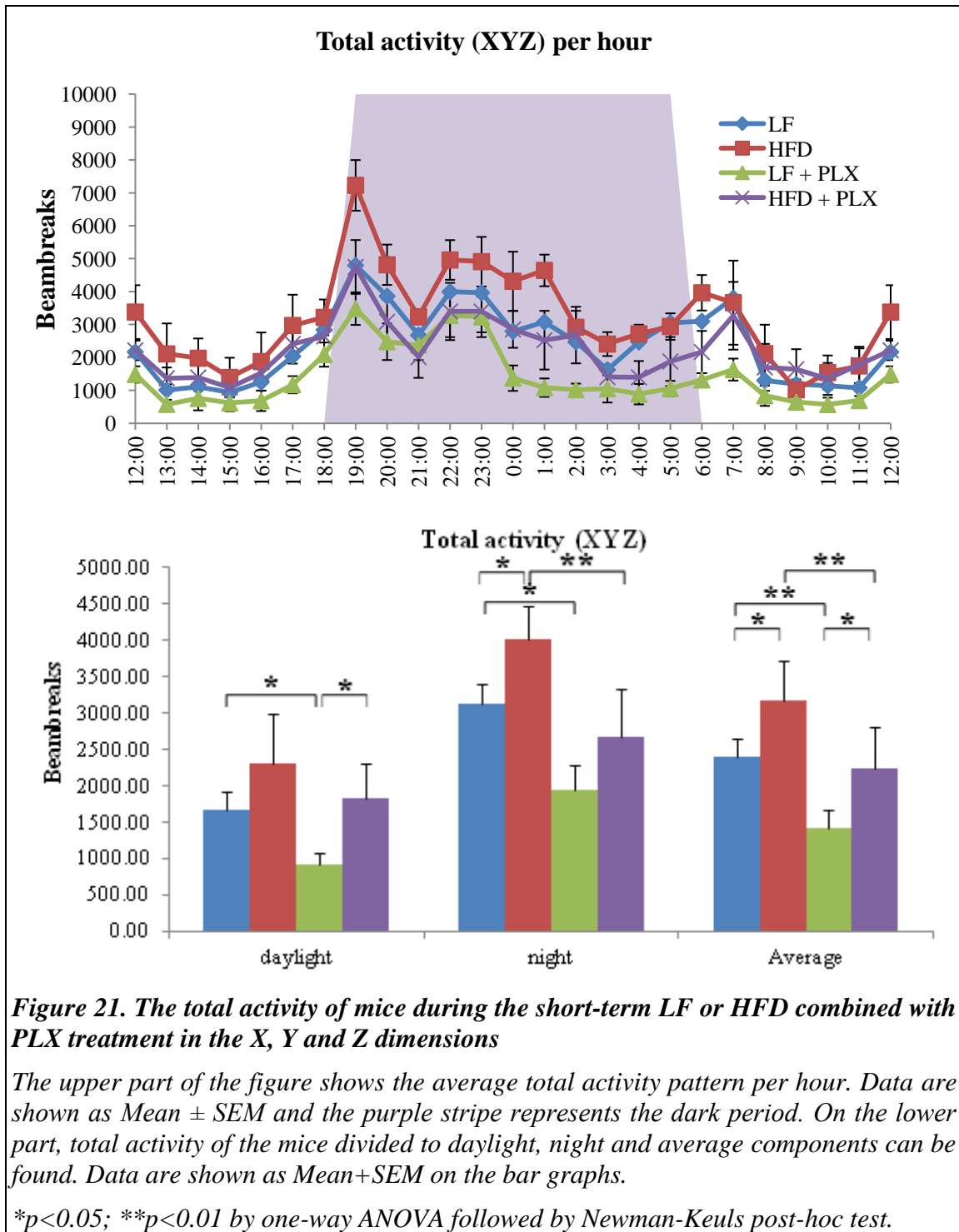ts of the total locomotor activity were analyzed. The average ambulatory activity of the mice was influenced by both the diet (P=0.0004) and the PLX treatment (P=0.011), but there was no interaction between the two factors (P=0.529) by factorial ANOVA. The average fine activity of mice was

only influenced by the PLX-treatment (P=0.0002), but not by the diet (P=0.427) and there was no interaction between the two factors (P=0.363) by factorial ANOVA. During the dark period, the PLX treatment significantly reduced the ambulatory activities in both LF- and HFD-consuming groups compared to PLX-free groups (*Figure 22*, *upper part).* The ambulatory activity in the case of LF *vs.* LF+PLX (in beambreaks/hour) was 1157.71 ± 74.55 *vs.* 662.54 ± 97.10 (P=0.03) at night, while in the case of HFD *vs.* HFD+PLX was (in beambreaks/hour) 679.05 ± 91.17 *vs.* 403.83 ± 61.42 (P=0.03) in the daylight and 1382.43 ± 126.43 *vs.* 791.92 ± 123.57 (P=0.008) at night. The difference between the average ambulatory activity of the HFD and HFD+PLX mice was also significant (P=0.02) and the diet-induced increase of the average ambulatory activity was also observed when LF vs. HFD (P=0.009) and LF+PLX and HFD+PLX (P=0.08) were analyzed.

The fine activity was similarly reduced by PLX-treatment (*Figure 22, lower part).* During the daylight the HFD-PLX mice moved less compared to HFD mice (HFD *vs.* HFD+PLX (in beambreaks/hour) 245.50 ± 34.25 *vs.* 148.68 ± 22.06; P=0.02). During night, both PLX-treated groups moved less compared to the corresponding PLX-free group: (LF *vs.* LF+PLX in beambreaks/hour 411.82 ± 22.12 *vs.*289.46 ± 42.81 (P=0.03) and HFD *vs.* HFD+PLX in beambreaks/hour 434.16 ± 57.79 *vs.* 272.06 ± 38.90 (P=0.03). The average difference between the fine activity of HFD and HFD+PLX mice was also significant (P=0.004).

Figure 22: The ambulatory and fine activity of the mice during the short-term LF or HFD combined with PLX treatment.

The upper part of the figure shows the ambulatory activity of the mice divided to daylight, night and average components. Ambulatory activity represents all movement with greater locomotions. On the lower part, fine activity of the mice divided to daylight, night and average components can be found. Fine activity represents the small movements without greater amount of locomotion, including grooming or movements while standing still. Data are shown as Mean + SEM.

*$p<0.05$; **$p<0.01$ by one-way ANOVA followed by Newman-Keuls post-hoc test.*

The food intake of the HFD group had a tendency to increase during the first day compared to LF group (P=0.06), however, this difference did not reach the level of significance and seemed to disappear in later time points. The cumulative food intake of HFD treated mice was above the consumption of the LF mice independently of the presence or absence of microglia until the second day of the experiment however, at the end of the experiment, the cumulative food intake of all four groups was similar (*Figure 23*).
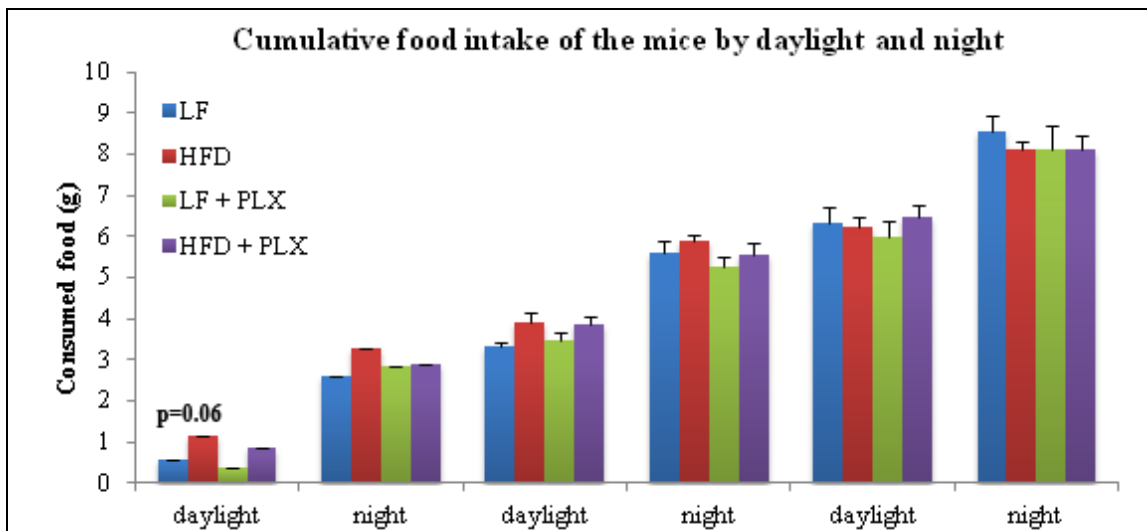
Figure 23: The cumulative food intake of the mice in grams during the short-term LF or HFD combined with PLX treatment.

The figure shows the cumulative food intake of the mice divided to 3 daylight and 3 night components. Data are shown as Mean + SEM. No significant difference, only a tendency was observed by the analysis of the consumed food in g.

P=0.06 by one-way ANOVA followed by Newman-Keuls post-hoc test.

As the energy content of the LF chow was 3.85 Kcal/g and the HFD chow was 5.24 Kcal/g, the HFD groups consumed significantly more calories compared to the calorie consumption of LF groups (P=0.0000 by factorial ANOVA). This was not influenced by the PLX treatment (P=0.637) and there was no interaction between the two factors (P=0.567) by factorial ANOVA). (*Figure 24*, upper part). The cumulative food intake in Kcal of the HFD animals were significantly higher compared to LF animals (LF *vs.* HFD p<0.01 and LF+PLX *vs.* HFD+PLX p<0.05) (*Figure 24, lower part*).

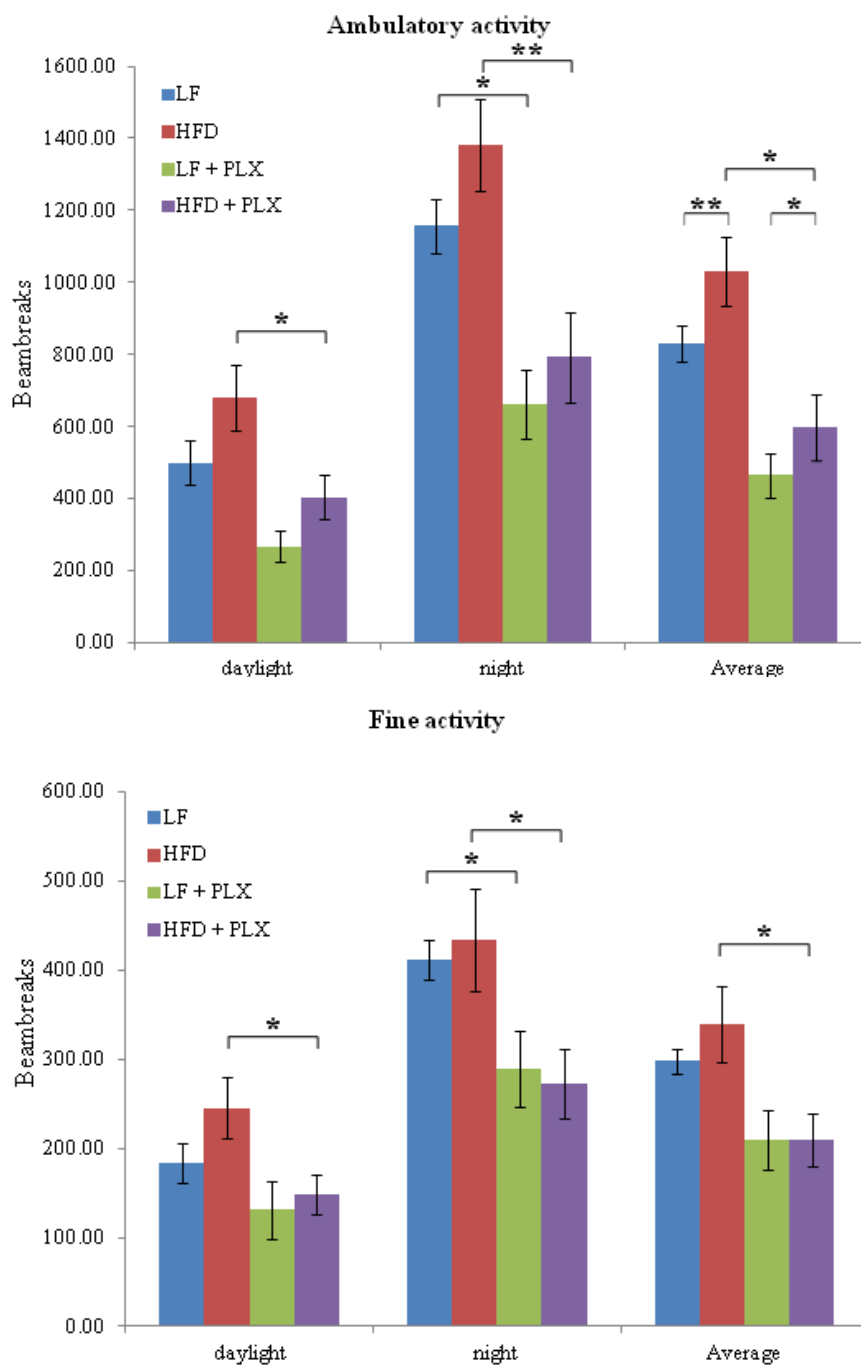***Figure 24: Calorie intake of mice during the short-term LF or HFD combined with PLX treatment***

The upper part of the figure shows the cumulative food intake pattern in Kcal. Data are shown in 9 minutes intervals and the purple stripes represent the dark periods. On the lower part, the cumulative energy intake of the mice divided to 3 daylight and 3 night phases can be found. Data are shown as Mean ± SEM on the bar graphs.

*$p<0.05$; **$p<0.01$ ***$p<0.001$ by one-way ANOVA followed by Newman-Keuls post-hoc test.*

The energy expenditure of the mice was normalized to the lean body mass of each animal (*Figure 25, upper part*). The average total energy expenditure of mice was influenced by the diet (P=0.0003), but not by the PLX treatment (P=0.162) and no interaction between the two factors was observed (P=0.917). There was no difference among the nighttime energy expenditure of the groups (P=0.066 and P=0.073). The daytime and the whole day energy expenditure were, however, significantly influenced by the diet. During daytime, the HFD significantly increased the energy expenditure (P=0.0002) that was not influenced by the PLX-treatment (P=0.162) with no interaction between the two factors (P=0.647) by factorial ANOVA. Similar differences were observed in the whole day energy expenditure data. The average energy expenditure of LF *vs*. HFD mice was 23.15 ± 1.51 *vs*. 25.15 ± 0.37 Kcal/kg lean body mass/hour (P=0.02), while of LF+PLX *vs*. HFD+PLX animals were 22.34 ± 0.63 *vs*. 24.25 ± 0.33 Kcal/kg lean body mass/hour (P=0.03) *(Figure 25, lower part)*.

As resting energy metabolism cannot be measured, it was estimated from the energy expenditure of the time points when the animal eats less than 0.1 g and moves less than 1% of the maximum ambulatory value in the preceding 30 minutes. Similarly to energy expenditure data, the calculated values were normalized to the lean body mass of the mice.

The HFD had significant effect on the resting energy expenditure (P=0.0000), while PLX treatment did not influence it (P=0.903). The two factor had no interaction (P=0.934) by factorial ANOVA. (*Figure 26, upper part*). The high-fat content of the diet caused significant increase in the resting metabolism in both PLX and PLX-free mice during the daylight, at night and in their average values (*Figure 26, lower part*). The average resting metabolism of LF *vs*. HFD mice was 19.56 ± 1.07 *vs*. 22.08 ± 0.51 Kcal/kg lean body mass/hour (P=0.0001) and the resting metabolism of LF+PLX *vs*. HFD+PLX mice was 19.46 ± 0.65 *vs*. 22.30 ± 0.43 Kcal/kg lean body mass/hour (P=0.0001).

Figure 25: The energy expenditure of the mice normalized to lean body mass during the short-term LF or HFD combined with PLX treatment

The upper part of the figure shows the average energy expenditure pattern per hour normalized to lean body mass. Data are shown as Mean ± SEM and the purple stripe represents the dark period. On the lower part, energy expenditure of mice, normalized to their lean body mass divided to daylight, night and average components can be found. Data are shown as Mean+SEM on the bar graphs.

*$p < 0.05$; **$p < 0.01$ ***$p < 0,001$ by one-way ANOVA followed by Newman-Keuls post-hoc test.*

Figure 26: The estimated resting metabolism of the mice normalized to lean body mass during the short-term LF or HFD combined with PLX treatment

The upper part of the figure shows the average estimated resting metabolism pattern per hour. Data are shown as Mean ± SEM and the purple stripe represents the dark period. On the lower part, estimated resting metabolism of the mice divided to daylight, night and average components can be found. Data are shown as Mean+SEM.

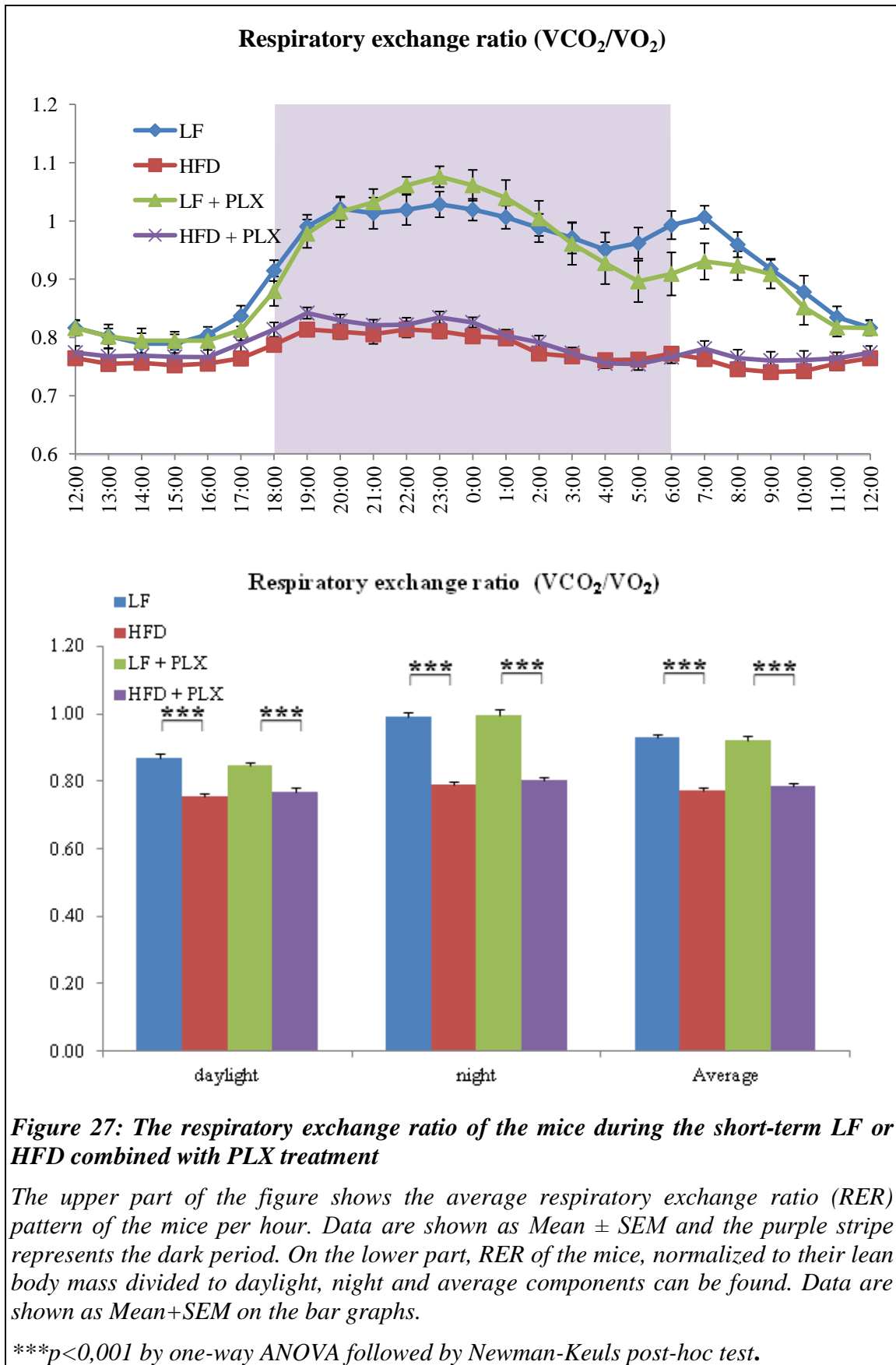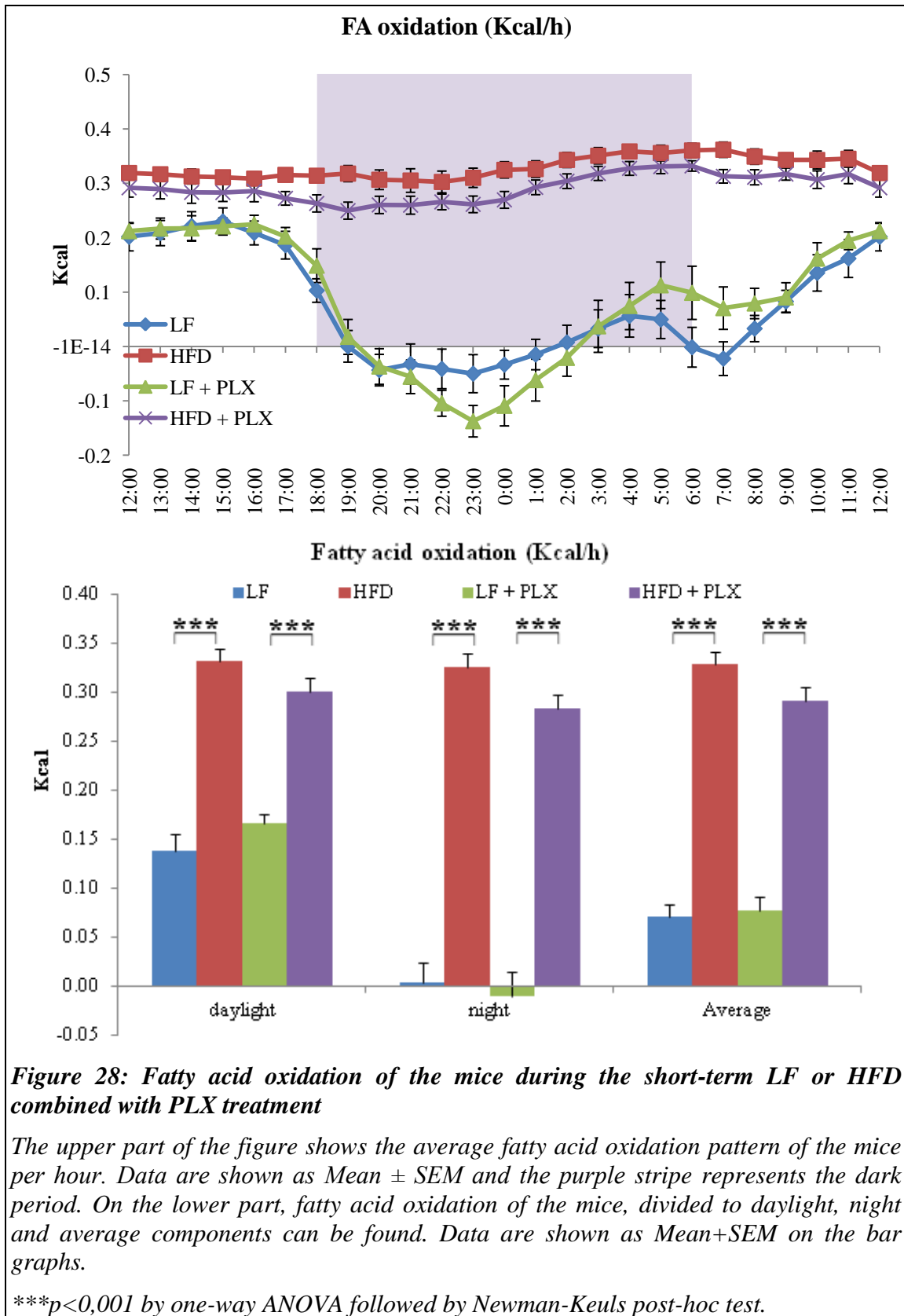****p<0.001 by one-way ANOVA followed by Newman-Keuls post-hoc test.*

The respiratory exchange ratio (RER) is a ratio calculated from volume of the produced CO_2 and the consumed O_2, which gives further information about the substrate utilization of the animals. The diet has significant effect on the RER of the animals, however, the PLX treatment had not (P=0.0000 and P=0.872, respectively) and there was no interaction between the two factors (P=0.410) by factorial ANOVA (*Figure 27, upper part*).

The RER of the HFD-consuming mice was significantly higher compared to LF-consuming groups during the 3 days of the experiment. The greatest differences were observed during the nighttime periods, when the RER of LF *vs*. HFD mice was 0.99 ± 0.02 *vs*. 0.79 ± 0.02 (P=0.0001), while the RER of LF+PLX *vs*. HFD+PLX mice was 0.99 ± 0.02 *vs*. 0.81 ± 0.01 (P=0.0001). This significance was present in the average values as well, when both night and daylight data was taken into consideration. The average RER of LF *vs*. HFD mice was 0.93 ± 0.01 *vs*. 0.77 ± 0.01 and the average RER of LF+PLX *vs*. HFD+PLX mice was 0.92 ± 0.01 *vs*. 0.79 ± 0.01(*Figure 27, lower part*).

As the HFD groups' fat consumption was far above the LF groups', not surprisingly their fatty acid oxidation was significantly higher, as well (P=0.00001), however, the PLX-treatment did not affect the fatty acid oxidation of the mice (P=0.353) during the experiment and there was no interaction between the two factors (P=0.167) by factorial ANOVA (*Figure 28, upper part*). The average fatty acid oxidation of the HFD animals was almost four times higher, than in the LF animals: in the LF *vs*. HFD mice 0.07 ± 0.01 *vs*. 0.33 ± 0.01 Kcal/hour and in the LF+PLX *vs*. HFD+PLX mice 0.08 ± 0.01 *vs*. 0.29 ± 0.01 Kcal/hour (*Figure 28. lower part*).

Respiratory exchange ratio (VCO_2/VO_2)

Figure 27: The respiratory exchange ratio of the mice during the short-term LF or HFD combined with PLX treatment

The upper part of the figure shows the average respiratory exchange ratio (RER) pattern of the mice per hour. Data are shown as Mean ± SEM and the purple stripe represents the dark period. On the lower part, RER of the mice, normalized to their lean body mass divided to daylight, night and average components can be found. Data are shown as Mean+SEM on the bar graphs.

***p<0,001 by one-way ANOVA followed by Newman-Keuls post-hoc test.

Figure 28: Fatty acid oxidation of the mice during the short-term LF or HFD combined with PLX treatment

The upper part of the figure shows the average fatty acid oxidation pattern of the mice per hour. Data are shown as Mean ± SEM and the purple stripe represents the dark period. On the lower part, fatty acid oxidation of the mice, divided to daylight, night and average components can be found. Data are shown as Mean+SEM on the bar graphs.

***p<0,001 by one-way ANOVA followed by Newman-Keuls post-hoc test.

4.3.2. Verification of the microglia-ablation by Iba1 immunocytochemistry and PCR

After only 1 week after the start of the PLX treatment, the 95-100% of the microglia was ablated in the PLX-treated sentinel mice, according to Iba1 immunolabeling, proving the effectiveness of the ablation (*Figure: 29*).
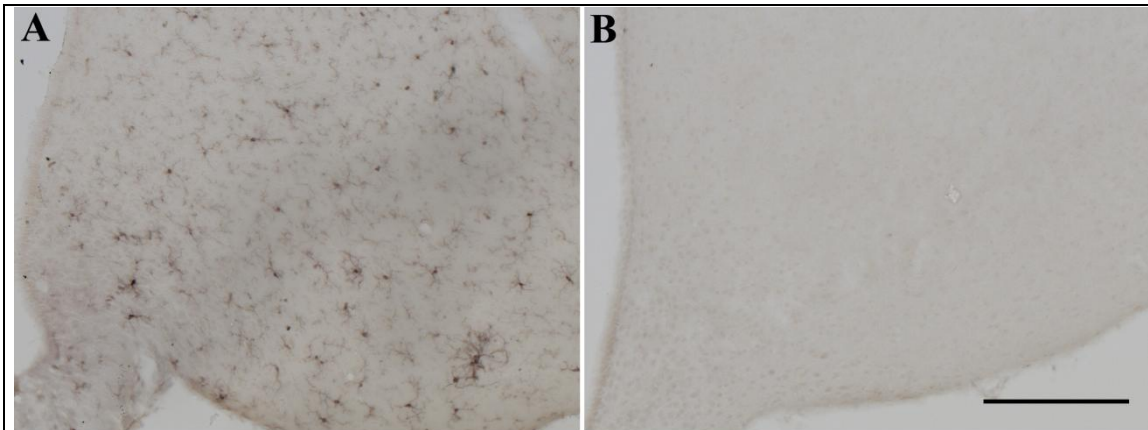

Figure: 29: The effectiveness of the microglia ablation by the Iba1 immunoreactivity in the ARC of the PLX-free and PLX-treated sentinel mice

The 1 week of PLX-treatment resulted in almost 95% loss of microglia (B) compared to intact mice (A).

Scale bar: 200 μm. Abrreviations: ARC – arcuate nucleus, Iba1- ionized calcium-binding adapter molecule 1

Similarly to those observed in the sentinel animals, the microglia ablation of the PLX pretreated mice was effective, independently from the fat content of the later consumed food. However, in the case of mice on diet without PLX, where the microglia were not affected by ablation, difference between the Iba1 immunoreactivity of the low fat and high fat diet fed mice were experienced.

PLX treatment markedly decreased the expression of microglial marker Emr1 and Iba1 in the ARC independently of the fat content of the diet. The Emr1 expression level of the PLX-treated animals decreased to approximately 20% of the LF group (0.209 ± 0.04; P=0.0001 and 0.223 ± 0.08; P=0.0003; in the LF+PLX and HFD+PLX mice, respectively), while Iba1 expression fell to 10% of the LF group (0.114 ± 0.01; P=0.0001 and 0.152 ± 0.06; P=0.0002, in the LF+PLX and HFD+PLX mice, respectively) *(Figure 30)*.
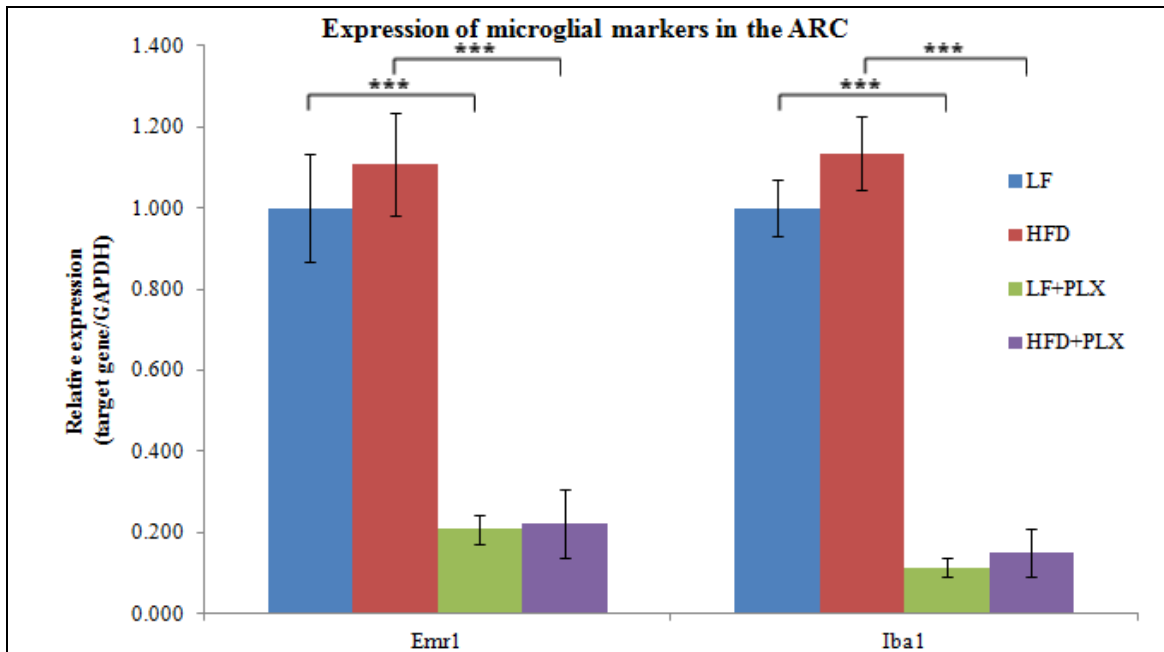

Figure 30: The relative expression of Emr1 and Iba1 in the ARC of the mice after the short-term LF or HFD combined with PLX treatment.

*The PLX pretreatment was effective as it significantly decreased the expression of the macrophage marker Emr1 and microglial marker Iba1 in the ARC of the PLX-treated mice. The expression of both genes was elevated in the case of HFD; however, this difference did not reach the level of significance. ***p<0.001 by one-way ANOVA followed by Newman-Keuls post-hoc test, data are shown as Mean ± SEM.*

5. Discussion

5.1. The localization of Cx43 gap junctions and hemichannels in tanycytes

Tanycytes integrate features of radial glia (Levitt and Rakic, 1980, Redecker, 1989) and astrocytes (Berger and Hediger, 2001), although also have distinguishing features. They have long been recognized to be involved in the formation of the BBB and blood-CSF barriers around the BBB-free ME (Smith and Shine, 1992). The apical surfaces of β-tanycytes are tightly bound by zonula occludens and tight junctions to form the barrier between the extracellular space of the ME and the CSF (Rodriguez et al., 2005) such that proteins cannot pass this barrier (Peruzzo et al., 2000, Rethelyi, 1984). In contrast, α-tanycytes lining the wall of the third ventricle are joined together by zonula occludens without the presence of tight junctions, allowing free transport of materials between the CSF and the neuropil (Akmayev and Popov, 1977). Besides the principal, barrier-forming function of tanycytes, studies also emphasize their potential role in the communication between different cell types and different fluid compartments of the brain (Peruzzo et al., 2004), allowing them to contribute to the regulation of neuroendocrine systems such as the thyroid and reproductive axes (Bolborea and Dale, 2013, Fekete et al., 2000b, Prevot, 2002, Tu et al., 1997). Gap junctions and connexin hemichannels may provide the mechanism for this communication.

5.1.1. The presence of functional gap junctions in tanycytes

In astrocytes, oligodendrocytes and microglia, the main gap junction-forming connexin subtype is Cx43 (Giaume and Theis, 2010). We have also identified Cx43 in our next-generation sequencing study as the main gap junction protein in the tanycytes. Furthermore, studies using cell cultures derived from 1 day old rats have shown the presence of Cx43 in hypothalamic tanycytes using Ethidium uptake, and that Cx43 is involved in their glucose sensing ability (Orellana et al., 2012).

To further characterize Cx43 in tanycytes, we performed a series of morphological studies using immunofluorescent and immune-electron microscopic techniques. As a first step, we demonstrated the existence of functional gap junctions among tanycytes in adult mice, taking advantage of the fluorescent dye, LY that can be loaded into a single

tanycyte *via* a patch pipette. As gap junctions are permeable in a size-dependent manner up to a 1 kDa (Saez et al., 2003), and the molecular weight of LY is 457 Da, the dye readily passes through gap junctions (Stewart, 1981). LY loaded into a single tanycyte always spread into a larger group of tanycytes. However, when tanycytes were loaded with LY in the presence of the gap junction inhibitor carbenoxolone, in all cases, carbenoxolone prevented the spreading of LY among tanycytes, and LY only filled the patched cell. These data demonstrate that intercellular spreading of LY is indeed facilitated by gap junctions,

In further support of gap junctions in tanycytes are the immunofluorescent and immune-electron microscopic studies demonstrating the presence of Cx43 immunoreactivity in the cytoplasmic membrane of tanycytes, particularly their lateral surfaces where tanycytes are closely opposed to each other. Interestingly, the density of Cx43-IR puncta was different among the different tanycyte subtypes, with a much higher density of Cx43-IR puncta in the cell bodies of α-tanycytes compared to the β-tanycytes. The basal processes of β-tanycytes were also strongly immunoreactive against Cx43, raising the possibility that gap junctions may also be located on their juxtaposed end feet processes, providing an alternative way tanycytes could communicate with each other. Indeed, in some cases, we observed the retrograde filling of tanycyte basal processes. Altogether, these data suggest that relatively large groups of tanycytes are interconnected *via* gap junctions, indicating that this communication may serve to coordinate the functioning of these tanycyte networks.

Tanycyte interconnections *via* gap junctions may enable the intercellular trafficking of a wide range of small molecules including ions, amino acids and metabolites. As glial cells contacted by gap junctions have been shown to have similar intracellular Na^+ concentrations (Rose and Ransom, 1997), it is possible that coupled tanycytes may also have a similar intracellular composition, hence forming groups that operate as a single unit. For example, the synchronized activity of tanycyte groups may contribute to the pulsatile release of the hypophysiotropic hormones into the portal circulation (Fekete and Lechan, 2014). This hypothesis is based on the observation that there is a close anatomical and physiological interaction between hypophysiotropic thyrotropin releasing hormone (TRH) axon terminals in the ME and tanycyte end foot processes (Lechan and Fekete, 2007, Rodriguez et al., 2005). Furthermore, since the unimpeded

transcellular transport of glucose and lactate *via* gap junctions in astrocyte networks ensures an energy source for neurons (Blomstrand and Giaume, 2006, Rouach et al., 2008) and the release of hormones from hypophysiotropic terminals is an energy dependent process, tanycyte networks may also be important to provide uniform energy supply to the large number of hypophysiotropic terminals in the external zone of the ME. In addition, it is possible that tanycytes are involved in spatial buffering of potassium ions in the region, similar to those has been described for astrocytes (Rose and Ransom, 1996). Activation of hypophysiotropic axon terminals would be expected to result in outward K^+ current, increasing the extracellular potassium concentration. Due to the interconnections among tanycytes, a large reservoir is created by the tanycyte "syncytium" providing an effective mechanism by which a single tanycyte can remove K^+ from the extracellular space around an activated axon. This may ensure that potassium can be rapidly removed from the extracellular space without causing significant changes in the intracellular potassium concentration of tanycytes located close to the neuronal activity.

5.1.2. The presence of Cx43 hemichannels in tanycytes

Cx43-immunoreactivity was also observed in the external membrane of the ventricular surface of both α- and β-tanycytes where gap junctions are not established. The presence of Cx43 in this location suggests that Cx43 may also form hemichannels, providing a route for the transport of small molecules between the CSF and the cytoplasm of tanycytes. Hemichannels may facilitate sensing of the CSF composition. Since Cx43 hemichannels are glucose permeable, the presence of Cx43 hemichannels on the ventricular surface of tanycytes may facilitate sensing of CSF glucose levels. Tanycytes are glucosensitive cells (Rodriguez et al., 2005) , and express K_{ATP} channels (Thomzig et al., 2001) and GLUT2 (Garcia et al., 2003). Glucose increases intracellular Ca^{++} concentration in α-tanycytes *ex vivo*, mediated by ATP via purinergic G-protein coupled receptor type 1 (P2Y1) (Frayling et al., 2011, Orellana et al., 2012). For this effect of glucose, the transport of intracellularly generated ATP via Cx43 hemichannels to the extracellular space where the P2Y1 is located is a critical step (Orellana et al., 2012).

Cx43 immunoreactive puncta were also observed in α-tanycyte end feet where they terminate on the capillaries of the ARC, and β tanycyte end feet where they terminate on fenestrated capillaries of the ME. The presence of hemichannels in this area would enable tanycytes to sense the composition of blood. Furthermore, the presence of Cx43 hemichannels on both the ventricular surface of tanycytes and their end feet processes may enable a bi-directional communication pathway between the CSF and the circulation. Presumably, regulation of the opening or closing of the hemichannels on the tanycyte end feet in the ARC may establish a filter zone in the BBB by allowing or preventing the passage of molecules from the blood to the neuropil.

Cx43 immunoreactivity was also found where tanycyte end feet processes were juxtaposed to axon varicosities, indicating that tanycytes might be able to perceive and/or induce microenvironmental changes of neurons derived from hypothalamic areas. Astrocytes were shown to exhibit Ca^{++} waves after glutamate stimuli that activates PLC-IP$_3$ dependent Ca^{++} release from intracellular Ca^{++} stores (Finkbeiner, 1992). Both Ca^{++} and IP$_3$ can pass through the cells via gap junctions, while astrocytes also release ATP to the extracellular space, likely through hemichannels, activating purinergic receptors and evoking additional Ca^{++} waves. The increasing Ca^{++} level can cause glutamate release and this way, astrocytes are able to modulate the excitability of the circumjacent neurons. Tanycytes might participate in similar way to astrocytes and secrete ATP, other small molecules and second messengers to their microenvironment, influencing the secretion of hypophysiotropic neurons.

5.2. Characterization of the POMC expression in tanycytes

It has been well known that POMC, rather uniquely among hormones/peptide transmitters, is expressed by two, very different cell types in the hypothalamic-pituitary complex: hormone-producing cells of the pituitary and neurons of the ARC. The findings of this study demonstrate that in rats there is yet a third, POMC-expressing cell-type in the hypothalamus-pituitary complex, which is the tanycyte. In fact, POMC-expressing tanycytes in the pituitary stalk effectively bridge the anatomical gap between pituitary cells and ARC POMC neurons, thus POMC expression from the pituitary to the hypothalamus is anatomically continuous but distributed in three different cell types.

5.2.1. Tanycyte *Pomc* ISH signal in previous studies

In preparation for this study we reviewed a wide range of the available literature that includes *Pomc* ISH in the rat hypothalamus. The list of these over 200 studies is reviewed in the Appendix of our study (Wittmann et al., 2017). Of these, 15 papers had images with very clear *Pomc* hybridization signal in tanycytes, but this was not mentioned in the text of most of the papers. The images of these papers collectively confirm that *Pomc* mRNA is expressed in tanycytes of different rat strains, both males and females, and under standard housing conditions. However, in the vast majority of the papers, *Pomc* hybridization signal could not be unambiguously identified in tanycytes. This included cases where tanycytes were clearly negative or the signal was too light to be considered positive; where background levels were too high, the image resolution too low, or too little portion of the ventricular wall was included in the image. It is important to note, however, that in the majority of these papers, the radioactive or alkaline phosphatase *Pomc* hybridization signal was light or moderate at best in POMC neurons. Therefore, tanycytes that generally express less *Pomc* mRNA than neurons may appear negative due to the low sensitivity of the detection.

We believe that the varying labeling of tanycytes seen in published papers at least in part reflects the natural variability of *Pomc* mRNA levels, which probably contributed the fact that only few researchers have recognized *Pomc* mRNA expression by tanycytes.

5.2.2. Diversity of POMC expression by tanycyte-subtypes

The present study reveals an unexpected diversity among tanycytes with respect to their capacity to express POMC. First, POMC expression was observed in every tanycyte subtype, except the α1 in which we never observed POMC mRNA or protein. Second, consistent POMC expression in tanycytes was restricted to a core region that included the pituitary stalk and the nearby mid-caudal region of the ME and third ventricle. Here we always observed a substantial population of POMC-expressing tanycytes, mostly from the β- and γ-subtypes. Outside this region, POMC expression varied among adult brains from only a few β- and γ-tanycytes to the vast majority of α2- β- and γ-tanycytes. Therefore, POMC expression in most α2-, β- and γ-tanycytes is conditional and driven by a yet undetermined factor.

Our results shed new light on a tanycyte-subtype that has received little attention since its first description. Gamma-tanycytes, described originally as astrocytic tanycytes, represent the most numerous non-ependymal cell type in the rat ME (Zaborszky and Schiebler, 1978). As defined by (Rutzel and Schiebler, 1980), these cells belong to the tanycyte series developmentally, but do not come into contact with the ventricular surface and morphologically somewhat differ from ventricular tanycytes. Their gene expression profile, however, is apparently very similar to α- and/or β-tanycytes, including vimentin, dopamine- and cyclic adenosine-3′:5′-monophosphate- regulated phosphoprotein (DARPP-32) (Hokfelt et al., 1988), type 2 deiodinase (Tu et al., 1997), organic anion-transporting polypeptide 1c1 (Wittmann et al., 2015) kainite-preferring glutamate receptor subunit GluR7 (Eyigor and Jennes, 1998), and POMC, among others.

5.2.3. Variable POMC levels in tanycytes

To the best of our knowledge, the natural variability of tanycyte POMC mRNA and protein levels among adult rat brains is a unique phenomenon among most genes expressed in the hypothalamus. We found that low- and high-level POMC expression in tanycytes occur with about equal frequency between ages 8 and 15 weeks, ~40% each, whereas the incidence of intermediate-level expression was lower, ~20%. Interestingly, *Pomc* mRNA levels were uniformly low in 8 adolescent rats, suggesting that higher

POMC levels in tanycytes may appear only after reaching adulthood. Theoretically, two possibilities could explain the variation in adult rats. One possibility is that the level of POMC expression in tanycytes remains constant in a given adult brain, but can markedly vary from one animal to another. A more intriguing possibility, however, is that POMC expression in tanycytes is dynamic, with high to low expression levels occurring periodically in each adult brain. This explanation would imply that *Pomc* gene expression in tanycytes is activity dependent, and may be induced by one or more specific signals that act periodically upon tanycytes. In this regard, it is important to consider that POMC expression levels in the tanycyte population follow a gradient pattern. This is especially apparent in intermediate-level brains, where the high mRNA levels present in the caudal core region decrease gradually in the rostral direction. Based on this pattern, we can speculate that upon some initiation signal, POMC expression may "spread" from core region tanycytes to adjacent tanycytes, and ultimately to most of the tanycyte population. The transmitting signal between tanycytes may be POMC itself, or it may spread via gap junctions and other cell-cell contacts, which are known to heavily interconnect tanycytes (Brawer, 1972, Hatton and Ellisman, 1982, Orellana et al., 2012, Szilvasy-Szabo et al., 2017). Future studies will be necessary to examine these possibilities. However, we believe that the present results favor the hypothesis of a spatio-temporally dynamic POMC expression pattern over a constant expression pattern with marked interindividual differences.

5.2.4. POMC processing in tanycytes

Another interesting feature of tanycyte POMC expression is the very low levels of ACTH and α-MSH-immunoreactivity that indicates little processing of POMC to these peptides. This is probably explained by the very low level of PC1 in tanycytes, according to our RNA-Seq analysis and previous ISH studies (Cullinan et al., 1991, Schafer et al., 1993). The lack of a substantial amount of ACTH in tanycytes may be of importance, as its secretion into the portal blood could potentially disrupt the normal feedback mechanism of cortisol on the hypothalamic-pituitary-adrenocortical axis. Interestingly, β-endorphin immunoreactivity was substantial in tanycytes, but we did not detect PC2, which is the primary enzyme that cleaves β-endorphin from POMC (Cawley et al., 2016). Thus, it is possible that β-endorphin immunoreactivity in

tanycytes mostly if not entirely represents the POMC precursor and/or the intermediate β lipotropin, both of which can be recognized by β-endorphin antibodies (Laurent et al., 2004, Miller et al., 2003). Alternatively, there may be a PC2-independent mechanism to produce β-endorphin in tanycytes, the existence of which was suggested by residual β-endorphin production in the hypothalamus of PC2 knockout mice (Allen et al., 2001). Future studies are required to determine the full extent of proteolytic POMC processing in tanycytes.

5.2.5. Potential functional implications

The physiological significance of POMC in rat tanycytes remains to be determined and at present remains highly speculative. Depending on the potential target cells of tanycyte-derived POMC, we suggest three potential roles for POMC in tanycytes. One is regulating the release of hypophysiotropic hormones via acting on hypophysiotropic axons in the ME. Hypophysiotropic axons in the rat ME contain large amounts of μ opioid receptors (Abbadie et al., 2000) that bind β-endorphin, and tanycyte-derived β-endorphin would be the best-positioned ligand to access these receptors. In addition, radioligand binding studies demonstrated that hypophysiotropic axons in the ME bind ACTH with high affinity (van Houten et al., 1981, Van Houten et al., 1985). This is probably due to the presence of MC4R that hypophysiotropic neurons express (Kishi et al., 2003, Tatro, 1990), although the presence of these receptor proteins on their axons remains to be determined. Therefore, it is possible that a low amount of ACTH and α-MSH released from tanycytes may also modulate the activity of hypophysiotropic axons. A second possible function is that tanycyte-derived POMC, acting in a paracrine/autocrine manner, may be involved in the proliferative/neurogenic functions of tanycytes themselves. Recent studies in mice demonstrated that tanycytes have stem cell properties and are capable of producing new neurons and glial cells during adulthood (Haan et al., 2013, Lee et al., 2012, Robins et al., 2013a). Studies in rats suggest a similar neural progenitor function for tanycytes in adulthood (Perez-Martin et al., 2010, Xu et al., 2005). Interestingly, N-terminal POMC peptides, such as pro-gamma-MSH, have mitogenic effects on the rat adrenal cortex (Bicknell, 2016), raising the possibility that N-terminal POMC peptides released from tanycytes may promote hypothalamic neurogenesis by increasing the proliferation of tanycytes. Lastly, N-

terminal POMC peptides secreted by tanycytes into the portal capillaries of the ME may regulate pituitary functions.

5.3. Importance of microglia in the development of HFD induced metabolic changes

5.3.1. The metabolic effects of short-term HFD

The effect of chronic consumption of HFD results in significant weight gain, hypothalamic injury and further consequences like cardiovascular diseases and diabetes type 2 (Fang et al., 2008, Muoio and Newgard, 2008). In the present study, however, the effect of short-term, 3 day long HFD was investigated on the body composition and metabolic parameters when the effect of the food composition can be studied without the influence of the HFD induced obesity. The cumulative food intake of the HFD mice was similar to the LF mice; however, due to the different energy content of the chows, the cumulative energy intake of HFD mice was significantly higher compared to LF mice during the whole experiment. However, the higher fat consumption did not cause significant body composition changes of the HFD-consuming mice, suggesting that, indeed, the short-time HFD cannot cause diet induced obesity. The average locomotor activity of the HFD mice, primarily its nighttime component exceeded the total activity of LF mice that might correlate to the higher energy intake of these animals. However, as the resting energy expenditure was also higher is mice with HFD, it suggests, that both the increased locomotor activity and the higher resting energy expenditure are responsible for the higher energy expenditure of the HFD animals. The largest difference between HFD- and LF-consuming groups was observed in their respiratory exchange ratio. The RER is the ratio of the produced CO_2 and the consumed O_2 and gives information about that type of macronutrient preferentially oxidized by the animal. If RER is close to 1, it indicates that the main energy source is carbohydrates, while if the value is close to 0.7, it suggests that lipids are the main utilized substrate. The RER of HFD animals showed low levels, around 0.7, suggesting, that HFD animals utilized fat as substrate compared to the higher RER values of LF animals, suggesting their protein and carbohydrate oxidation. Furthermore, the diurnal/nocturnal fluctuations of RER observed under physiological conditions seemed to be eliminated by HFD. These data were strengthened by the fat oxidation data. These data indicate

that even the short-time HFD can cause marked changes in the metabolic parameters that are in agreement with the data published in the literature (Tschop et al., 2011).

5.3.2. The metabolic effects of the absence of microglia

In our experiment, we used PLX5622, a selective CSF1R inhibitor (Elmore et al., 2014). CSF1R is selectively expressed in microglia and has essential role in the regulation of survival, proliferation and differentiation of the microglia (Gomez-Nicola et al., 2013). PLX5622 containing diet was shown to result in an almost complete disappearance of the microglia specific markers indicating the ablation of this cell type (Elmore et al., 2014). This treatment has no effect on peripheral macrophages and on any other studied cell types (Dagher et al., 2015, Elmore et al., 2014). This effect of the CSF1R inhibition is reversible, thus continuous PLX5622 treatment is necessary to maintain the absence of microglia (Elmore et al., 2014). Currently, the CSF1R inhibitors are the most widely used compounds to study the role of microglia (Coniglio et al., 2012, Dagher et al., 2015).

In our experiment, PLX5622-containing diet already induced microglia depletion after 1 week of treatment and it resulted in an almost complete absence of the microglia at the end of the experiment as shown by the absence of Iba1-immunoreactivity in the brain. Despite the remarkable effect of the PLX562 treatment on the number of microglia, it did not influence the HFD induced changes of metabolic parameters. The treatment decreased the lean body mass of the LF group without influencing the HFD induced increase of this parameter. The PLX5622 treatment had also effect on the locomotor activity. This treatment caused a decrease of the total locomotor activity in both the LF and HFD groups without preventing the HFD induced increase of this parameter. These data suggest that the microglia plays role in the regulation of locomotor activity, but the HFD induced effect is independent from this cell type.

The literature is currently inconsistent regarding the role of microglia in the regulation of the HFD induced metabolic changes.

Generally, the role of microglia seems to be diverse (Graeber, 2010). Microglia can be involved in the initiation of local inflammation, thus microglia activation can cause tissue damage (Dheen et al., 2007). There is, however, a growing amount of evidence,

that microglia is a potent regulator and supporter of the normal neuronal functions (Paolicelli et al., 2011). The neuroprotective role of microglia during demyelinating and after hypoxic conditions, where neurons are directly affected was also described (Hanisch and Kettenmann, 2007, Szalay et al., 2016). During the initial phase of the HFD, the early hypothalamic inflammation was suggested to be independent of the effect of microglia. It is more likely, that this time microglia have a neuroprotective role, as the activation of microglia only occurs, when there is detectable inflammation in the ARC, moreover, the microglial response is persistent even when the local inflammation is decreased (Thaler et al., 2012b). However, this hypothesis was not proved by experiments.

Valdearcos et al. (Valdearcos et al., 2017) however, has reported the effects of the inhibition of microglial function either by pharmacological microglia ablation or by microglia selective inhibition of the inflammatory NF-κB pathway on the hypothalamic inflammation and the accompanying changes in the metabolism. According to these data, after 4 weeks of HFD, the above mentioned PLX-treatment significantly reduces the body weight of the PLX-treated animals on HFD, compared to control mice. However, the PLX-treatment has no effect on the body weight of mice on normal chow. These findings indicate the role of microglia in maintenance of higher caloric intake in even after longer term HFD. Similar effects were observed when the NF-κB pathway was selectively silenced in microglia (Valdearcos et al., 2017). It is important to note, that these measurements were performed a longer period of HFD. Conversely, microglia activation by microglia specific deletion of the NF-κB regulator tumor necrosis factor alpha-induced protein 3 (A20) causes diet-independent metabolic dysfunction with significant increase in the food intake and reduced VCO_2 and VO_2, further suggesting the importance of microglia in the metabolic regulation (Valdearcos et al., 2017).

Our data, however, indicate that the metabolic effects of short-term HFD are independent from the microglia, thus the early microgliosis is rather the consequence than the cause of these early changes.

6. Conclusions

The present Ph.D. work provides an overview how tanycytes and microglial cells are involved in the regulation of energy homeostasis under physiological conditions and during short-term HFD.

Our data indicate that tanycytes are interconnected with each other via functional, Cx43-containing gap junctions, ensuring an effective communication among these cells. The presence of Cx43 immunoreactivity on the ventricular surface of tanycytes and on end feet processes terminating on capillaries or axon terminals further suggest that there could be an active transport of small molecules between tanycytes and different compartments of extracellular space through Cx43-containing hemichannels. These findings indicate that tanycytes have far more complicated functions than simply serving as barrier cells, and support their importance in neuroendocrine regulation by monitoring the extracellular environment in the ME-ARC region.

The present study also reveals a novel, unique type of POMC expression in tanycytes in the adult rat hypothalamus and pituitary stalk. Depending on the potential target cells of tanycyte-derived POMC, we suggest three potential roles for POMC in tanycytes. One is regulating the release of hypophysiotropic hormones via acting on hypophysiotropic axons in the ME. A second possible function is that tanycyte-derived POMC, acting in a paracrine/autocrine manner, may be involved in the proliferative/neurogenic functions of tanycytes themselves. Lastly, N-terminal POMC peptides secreted by tanycytes into the portal capillaries of the ME may regulate pituitary functions. However, future studies will be necessary to investigate the cause of variability, the exact nature of POMC-processing, the functional significance, and the potential existence of tanycyte POMC expression in other species.

The effectiveness of microglia ablation via consuming PLX-containing chow was supported by immunocytochemistry and PCR data, however, the recent work suggest that the loss of microglia does not influence the majority of the metabolic parameters of the mice during the short-term HFD. However, even the short time HFD causes marked metabolic changes in mice, including change of energy expenditure, RER and fat oxidation and also the elimination of diurnal-nocturnal changes of the metabolic parameters observed in control animals. As the presence of ARC inflammatory process

100

was not clearly justified, further experiments are needed to evaluate the role of tanycytes in this process.

7. Summary

The perception of the status of energy stores and the quality and quantity of the consumed food by the central nervous system plays a crucial role in the regulation of energy homeostasis. This regulation is guided by the communication between the peripheral organs and the brain. The primary central targets of peripheral, blood-derived energy homeostasis-related hormones are the orexigenic and anorexigenic cell populations of the hypothalamic ARC. The mechanisms related to the central regulation of energy homeostasis are intensively studied; however, the role of glial cell types in these processes is far less understood.

Thus, the aim of my Ph.D. thesis is to better understand how the special neuroglial cells of the hypothalamus, tanycytes and the resident macrophages of the brain, the microglial cells are involved in the regulation of homeostatic processes under physiological and HFD conditions. To achieve this goal, morphological, functional, ISH, gene expression and *in vivo* metabolic experiments were carried out.

According to our data, tanycytes are interconnected via Cx43 gap junctions and the formed tanycyte syncytium ensures effective communication among these cells. Furthermore, tanycytes also establish Cx43 hemichannels, by which tanycytes are able to monitor their extracellular environment that may facilitate the regulation of the neuroendocrine axes. We also observed non-neuronal expression of the anorexigenic *Pomc* gene was in tanycytes. The expression of *Pomc* gene and the presence of POMC protein were also detected in non-ependymal tanycyte-types in the external zone of the ME. We proposed this tanycyte subgroup should be added to the nomenclature of tanycytes as gamma-tanycytes. The tanycyte-derived POMC might participate in the modulation of the release of hypophysiotropic hormones, in the regulation of the pituitary functions and in the autocrine regulation of the proliferative function of tanycytes. According to our *in vivo* data, the ablation of the microglia cannot lead to significant changes of the metabolic parameters during a short-term HFD.

8. Összefoglalás

Az energia homeosztázis szabályozásában kritikus szerepet játszik az energiaraktárak állapotának és a felvett táplálék mennyiségének, minőségének központi idegrendszeri érzékelése, amit a perifériás szervek és az agy közti kommunikáció biztosít. Az agy egyik fő energiaháztartással kapcsolatos szenzor területe a hipotalamusz arcuatus magja. A perifériás, energiaháztartással kapcsolatos hormonok centrális hatásukat elsősorban az arcuatus mag orexigén és anorexigén idegsejtjeinek közvetítésével fejtik ki. Habár a centrális energiaháztartást szabályozó neuronhálózatok szerepét igen részletesen vizsgálják, kevéssé kutatott, hogy az agy glia sejttípusai miként vesznek részt e folyamatokban.

Doktori értekezésem célja ezért annak morfológiai, funkcionális, *in situ* hibridizációs, génexpressziós és *in vivo* metabolikus vizsgálatokkal történő megértése, hogy a hipotalamusz speciális glia sejtjei, a taniciták, valamint az agyi makrofágként működő mikroglia sejtek miként vesznek részt a homeosztatikus folyamatok szabályozásában fiziológiai és ettől eltérő állapotokban.

Kísérleteink igazolták, hogy a taniciták között Cx43 tartalmú gap junction kapcsolatok vannak. Az taniciták így funkcionális szincíciumot alkotnak, ami hatékony kommunikációt biztosít e sejtek között, összehangolva működésüket. A gap junction kapcsolatok mellett a taniciták felszínén Cx43 *hemichannel*-ek is találhatók, ami lehetővé teszi az extracelluláris környezetük állandó monitorozását elősegítve a neuroendokrin folyamatok szabályozását. További vizsgálatainkkal kimutattuk az anorexigén *Pomc* gén expresszióját a tanicitákban, illetve az eminencia mediána külső zónájában lokalizálódó nem ependimális, tanicita-szerű sejttípusban. Igazoltuk-e sejtek tanicita jellegét és az nevezéktanához illeszkedően a gamma-tanicita nevet javasoltunk számukra. A tanicita-eredetű POMC részt vehet a hipofízeotróp hormonok felszabadulásának modulálásában, a hipofízis funkciójának, valamint új taniciták proliferációjának szabályozásában. *In vivo* kísérleteink alapján megállapítottuk, hogy a mikroglia nem befolyásolja a rövid távú, magas zsírtartalmú diéta metabolikus hatásait.

9. References

Abbadie, C., Pan, Y.X., and Pasternak, G.W. (2000) Differential distribution in rat brain of mu opioid receptor carboxy terminal splice variants MOR-1C-like and MOR-1-like immunoreactivity: evidence for region-specific processing. J Comp Neurol 419, 244-256.

Abbott, C.R., Rossi, M., Wren, A.M., Murphy, K.G., Kennedy, A.R., Stanley, S.A., Zollner, A.N., Morgan, D.G., Morgan, I., Ghatei, M.A., Small, C.J., and Bloom, S.R. (2001) Evidence of an orexigenic role for cocaine- and amphetamine-regulated transcript after administration into discrete hypothalamic nuclei. Endocrinology 142, 3457-3463.

Abbott, N.J., Patabendige, A.A., Dolman, D.E., Yusof, S.R., and Begley, D.J. (2010) Structure and function of the blood-brain barrier. Neurobiol Dis 37, 13-25.

Adan, R.A., Tiesjema, B., Hillebrand, J.J., la Fleur, S.E., Kas, M.J., and de Krom, M. (2006) The MC4 receptor and control of appetite. Br J Pharmacol 149, 815-827.

Adrian, T.E., Long, R.G., Fuessl, H.S., and Bloom, S.R. (1985) Plasma peptide YY (PYY) in dumping syndrome. Dig Dis Sci 30, 1145-1148.

Ahima, R.S., Saper, C.B., Flier, J.S., and Elmquist, J.K. (2000) Leptin regulation of neuroendocrine systems. Front Neuroendocrinol 21, 263-307.

Akmayev, I.G. and Fidelina, O.V. (1976) Morphological aspects of the hypothalamic-hypophyseal system. VI. The tanycytes: their relation to the sexual differentiation of the hypothalamus. An enzyme-histochemical study. Cell Tissue Res 173, 407-416.

Akmayev, I.G., Fidelina, O.V., Kabolova, Z.A., Popov, A.P., and Schitkova, T.A. (1973) Morphological aspects of the hypothalamic-hypophyseal system. IV. Medial basal hypothalamus. An experimental morphological study. Z Zellforsch Mikrosk Anat 137, 493-512.

Akmayev, I.G. and Popov, A.P. (1977) Morphological aspects of the hypothalamic-hypophyseal system. VII. The tanycytes: Their relation to the hypophyseal adrenocorticotrophic function. An ultrastructural study. Cell Tissue Res 180, 263-282.

Alkemade, A., Yi, C.X., Pei, L., Harakalova, M., Swaab, D.F., la Fleur, S.E., Fliers, E., and Kalsbeek, A. (2012) AgRP and NPY expression in the human hypothalamic infundibular nucleus correlate with body mass index, whereas changes in alphaMSH are related to type 2 diabetes. J Clin Endocrinol Metab 97, E925-933.

Allen, R.G., Peng, B., Pellegrino, M.J., Miller, E.D., Grandy, D.K., Lundblad, J.R., Washburn, C.L., and Pintar, J.E. (2001) Altered processing of pro-orphanin FQ/nociceptin and pro-opiomelanocortin-derived peptides in the brains of mice expressing defective prohormone convertase 2. J Neurosci 21, 5864-5870.

Amat, P., Pastor, F.E., Blazquez, J.L., Pelaez, B., Sanchez, A., Alvarez-Morujo, A.J., Toranzo, D., and Amat-Peral, G. (1999) Lateral evaginations from the third ventricle into the rat mediobasal hypothalamus: An amplification of the ventricular route. Neuroscience 88, 673-677.

Andrews, Z.B., Liu, Z.W., Walllingford, N., Erion, D.M., Borok, E., Friedman, J.M., Tschop, M.H., Shanabrough, M., Cline, G., Shulman, G.I., Coppola, A., Gao, X.B., Horvath, T.L., and Diano, S. (2008) UCP2 mediates ghrelin's action on NPY/AgRP neurons by lowering free radicals. Nature 454, 846-851.

Aponte, Y., Atasoy, D., and Sternson, S.M. (2011) AGRP neurons are sufficient to orchestrate feeding behavior rapidly and without training. Nat Neurosci 14, 351-355.

Asnicar, M.A., Smith, D.P., Yang, D.D., Heiman, M.L., Fox, N., Chen, Y.F., Hsiung, H.M., and Koster, A. (2001) Absence of cocaine- and amphetamine-regulated transcript results in obesity in mice fed a high caloric diet. Endocrinology 142, 4394-4400.

Bagnol, D., Lu, X.Y., Kaelin, C.B., Day, H.E., Ollmann, M., Gantz, I., Akil, H., Barsh, G.S., and Watson, S.J. (1999) Anatomy of an endogenous antagonist: relationship between Agouti-related protein and proopiomelanocortin in brain. J Neurosci 19, RC26.

Balland, E., Dam, J., Langlet, F., Caron, E., Steculorum, S., Messina, A., Rasika, S., Falluel-Morel, A., Anouar, Y., Dehouck, B., Trinquet, E., Jockers, R., Bouret, S.G., and Prevot, V. (2014) Hypothalamic tanycytes are an ERK-gated conduit for leptin into the brain. Cell Metab 19, 293-301.

Balthasar, N., Coppari, R., McMinn, J., Liu, S.M., Lee, C.E., Tang, V., Kenny, C.D., McGovern, R.A., Chua, S.C., Jr., Elmquist, J.K., and Lowell, B.B. (2004) Leptin receptor signaling in POMC neurons is required for normal body weight homeostasis. Neuron 42, 983-991.

Bamshad, M., Song, C.K., and Bartness, T.J. (1999) CNS origins of the sympathetic nervous system outflow to brown adipose tissue. Am J Physiol 276, R1569-1578.

Banke, E., Riva, M., Shcherbina, L., Wierup, N., and Degerman, E. (2013) Cocaine- and amphetamine-regulated transcript is expressed in adipocytes and regulate lipid- and glucose homeostasis. Regul Pept 182, 35-40.

Batterham, R.L., Cowley, M.A., Small, C.J., Herzog, H., Cohen, M.A., Dakin, C.L., Wren, A.M., Brynes, A.E., Low, M.J., Ghatei, M.A., Cone, R.D., and Bloom, S.R. (2002) Gut hormone PYY(3-36) physiologically inhibits food intake. Nature 418, 650-654.

Batterham, R.L., Heffron, H., Kapoor, S., Chivers, J.E., Chandarana, K., Herzog, H., Le Roux, C.W., Thomas, E.L., Bell, J.D., and Withers, D.J. (2006) Critical role for peptide YY in protein-mediated satiation and body-weight regulation. Cell Metab 4, 223-233.

Beck, B., Stricker-Krongrad, A., Nicolas, J.P., and Burlet, C. (1992) Chronic and continuous intracerebroventricular infusion of neuropeptide Y in Long-Evans rats mimics the feeding behaviour of obese Zucker rats. Int J Obes Relat Metab Disord 16, 295-302.

Begg, D.P. and Woods, S.C. (2012) The central insulin system and energy balance. Handb Exp Pharmacol, 111-129.

Benford, H., Bolborea, M., Pollatzek, E., Lossow, K., Hermans-Borgmeyer, I., Liu, B., Meyerhof, W., Kasparov, S., and Dale, N. (2017) A sweet taste receptor-dependent mechanism of glucosensing in hypothalamic tanycytes. Glia 65, 773-789.

Berger, U.V. and Hediger, M.A. (2001) Differential distribution of the glutamate transporters GLT-1 and GLAST in tanycytes of the third ventricle. J Comp Neurol 433, 101-114.

Bernardis, L.L. and Bellinger, L.L. (1998) The dorsomedial hypothalamic nucleus revisited: 1998 update. Proc Soc Exp Biol Med 218, 284-306.

Berthoud, H.R. (2008) Vagal and hormonal gut-brain communication: from satiation to satisfaction. Neurogastroenterol Motil 20 Suppl 1, 64-72.

Berthoud, H.R. and Powley, T.L. (1992) Vagal Afferent Innervation of the Rat Fundic Stomach - Morphological Characterization of the Gastric Tension Receptor. J Comp Neurol 319, 261-276.

Bewick, G.A., Gardiner, J.V., Dhillo, W.S., Kent, A.S., White, N.E., Webster, Z., Ghatei, M.A., and Bloom, S.R. (2005) Post-embryonic ablation of AgRP neurons in mice leads to a lean, hypophagic phenotype. FASEB J 19, 1680-1682.

Bicknell, A.B. (2016) 60 YEARS OF POMC: N-terminal POMC peptides and adrenal growth. J Mol Endocrinol 56, T39-48.

Bitsch, P. and Schiebler, T.H. (1979) [Postnatal development of the median eminence in the rat]. Z Mikrosk Anat Forsch 93, 1-20.

Blomstrand, F. and Giaume, C. (2006) Kinetics of endothelin-induced inhibition and glucose permeability of astrocyte gap junctions. J Neurosci Res 83, 996-1003.

Blouet, C., Jo, Y.H., Li, X., and Schwartz, G.J. (2009) Mediobasal hypothalamic leucine sensing regulates food intake through activation of a hypothalamus-brainstem circuit. J Neurosci 29, 8302-8311.

Blouet, C. and Schwartz, G.J. (2010) Hypothalamic nutrient sensing in the control of energy homeostasis. Behav Brain Res 209, 1-12.

Bolborea, M. and Dale, N. (2013) Hypothalamic tanycytes: potential roles in the control of feeding and energy balance. Trends Neurosci 36, 91-100.

Boucher, J., Kleinridders, A., and Kahn, C.R. (2014) Insulin receptor signaling in normal and insulin-resistant states. Cold Spring Harb Perspect Biol 6.

Brawer, J.R. (1972) The fine structure of the ependymal tanycytes at the level of the arcuate nucleus. J Comp Neurol 145, 25-41.

Broberger, C., Landry, M., Wong, H., Walsh, J.N., and Hokfelt, T. (1997) Subtypes Y1 and Y2 of the neuropeptide Y receptor are respectively expressed in pro-opiomelanocortin- and neuropeptide-Y-containing neurons of the rat hypothalamic arcuate nucleus. Neuroendocrinology 66, 393-408.

Brody, D.S., Hahn, S.R., Spitzer, R.L., Kroenke, K., Linzer, M., deGruy, F.V., 3rd, and Williams, J.B. (1998) Identifying patients with depression in the primary care setting: a more efficient method. Arch Intern Med 158, 2469-2475.

Bruni, J.E. (1974) Scanning and transmission electron microscopy of the ependymal lining of the third ventricle. Can J Neurol Sci 1, 59-73.

Burdyga, G., de Lartigue, G., Raybould, H.E., Morris, R., Dimaline, R., Varro, A., Thompson, D.G., and Dockray, G.J. (2008) Cholecystokinin regulates expression of Y2 receptors in vagal afferent neurons serving the stomach. J Neurosci 28, 11583-11592.

Butler, A.A., Kesterson, R.A., Khong, K., Cullen, M.J., Pelleymounter, M.A., Dekoning, J., Baetscher, M., and Cone, R.D. (2000) A unique metabolic syndrome causes obesity in the melanocortin-3 receptor-deficient mouse. Endocrinology 141, 3518-3521.

Cawley, N.X., Li, Z., and Loh, Y.P. (2016) 60 YEARS OF POMC: Biosynthesis, trafficking, and secretion of pro-opiomelanocortin-derived peptides. J Mol Endocrinol 56, T77-97.

Challis, B.G., Coll, A.P., Yeo, G.S., Pinnock, S.B., Dickson, S.L., Thresher, R.R., Dixon, J., Zahn, D., Rochford, J.J., White, A., Oliver, R.L., Millington, G., Aparicio, S.A., Colledge, W.H., Russ, A.P., Carlton, M.B., and O'Rahilly, S. (2004) Mice lacking pro-opiomelanocortin are sensitive to high-fat feeding but respond normally to the acute anorectic effects of peptide-YY(3-36). Proc Natl Acad Sci U S A 101, 4695-4700.

Challis, B.G., Pritchard, L.E., Creemers, J.W.M., Delplanque, J., Keogh, J.M., Luan, J., Wareham, N.J., Yeo, G.S.H., Bhattacharyya, S., Froguel, P., White, A., Farooqi, I.S., and O'Rahilly, S. (2002) A missense mutation disrupting a dibasic prohormone processing site in pro-opiomelanocortin (POMC) increases susceptibility to early-onset obesity through a novel molecular mechanism. Hum Mol Genet 11, 1997-2004.

Chen, H.Y., Trumbauer, M.E., Chen, A.S., Weingarth, D.T., Adams, J.R., Frazier, E.G., Shen, Z., Marsh, D.J., Feighner, S.D., Guan, X.M., Ye, Z., Nargund, R.P., Smith, R.G., Van der Ploeg, L.H., Howard, A.D., MacNeil, D.J., and Qian, S. (2004) Orexigenic action of peripheral ghrelin is mediated by neuropeptide Y and agouti-related protein. Endocrinology 145, 2607-2612.

Cheng, X., Broberger, C., Tong, Y., Yongtao, X., Ju, G., Zhang, X., and Hokfelt, T. (1998) Regulation of expression of neuropeptide Y Y1 and Y2 receptors in the arcuate nucleus of fasted rats. Brain Res 792, 89-96.

Chitravanshi, V.C., Kawabe, K., and Sapru, H.N. (2016) Stimulation of the hypothalamic arcuate nucleus increases brown adipose tissue nerve activity via hypothalamic paraventricular and dorsomedial nuclei. Am J Physiol Heart Circ Physiol 311, H433-444.

Ciofi, P. (2011) The arcuate nucleus as a circumventricular organ in the mouse. Neurosci Lett 487, 187-190.

Clark, J.T., Kalra, P.S., and Kalra, S.P. (1985) Neuropeptide Y stimulates feeding but inhibits sexual behavior in rats. Endocrinology 117, 2435-2442.

Cone, R.D. (2005) Anatomy and regulation of the central melanocortin system. Nat Neurosci 8, 571-578.

Coniglio, S.J., Eugenin, E., Dobrenis, K., Stanley, E.R., West, B.L., Symons, M.H., and Segall, J.E. (2012) Microglial stimulation of glioblastoma invasion involves epidermal growth factor receptor (EGFR) and colony stimulating factor 1 receptor (CSF-1R) signaling. Mol Med 18, 519-527.

Corander, M.P. and Coll, A.P. (2011) Melanocortins and body weight regulation: glucocorticoids, Agouti-related protein and beyond. Eur J Pharmacol 660, 111-118.

Cork, S.C., Richards, J.E., Holt, M.K., Gribble, F.M., Reimann, F., and Trapp, S. (2015) Distribution and characterisation of Glucagon-like peptide-1 receptor expressing cells in the mouse brain. Mol Metab 4, 718-731.

Cowley, M.A., Smart, J.L., Rubinstein, M., Cerdan, M.G., Diano, S., Horvath, T.L., Cone, R.D., and Low, M.J. (2001) Leptin activates anorexigenic POMC neurons through a neural network in the arcuate nucleus. Nature 411, 480-484.

Cullinan, W.E., Day, N.C., Schafer, M.K., Day, R., Seidah, N.G., Chretien, M., Akil, H., and Watson, S.J. (1991) Neuroanatomical and functional studies of peptide precursor-processing enzymes. Enzyme 45, 285-300.

Cummings, D.E., Purnell, J.Q., Frayo, R.S., Schmidova, K., Wisse, B.E., and Weigle, D.S. (2001) A preprandial rise in plasma ghrelin levels suggests a role in meal initiation in humans. Diabetes 50, 1714-1719.

Dagher, N.N., Najafi, A.R., Kayala, K.M., Elmore, M.R., White, T.E., Medeiros, R., West, B.L., and Green, K.N. (2015) Colony-stimulating factor 1 receptor inhibition prevents microglial plaque association and improves cognition in 3xTg-AD mice. J Neuroinflammation 12, 139.

Dailey, M.J. and Moran, T.H. (2013) Glucagon-like peptide 1 and appetite. Trends Endocrinol Metab 24, 85-91.

Dale, N. (2011) Purinergic signaling in hypothalamic tanycytes: potential roles in chemosensing. Semin Cell Dev Biol 22, 237-244.

Date, Y., Kojima, M., Hosoda, H., Sawaguchi, A., Mondal, M.S., Suganuma, T., Matsukura, S., Kangawa, K., and Nakazato, M. (2000) Ghrelin, a novel growth hormone-releasing acylated peptide, is synthesized in a distinct endocrine cell type in the gastrointestinal tracts of rats and humans. Endocrinology 141, 4255-4261.

Davies, J.S., Kotokorpi, P., Eccles, S.R., Barnes, S.K., Tokarczuk, P.F., Allen, S.K., Whitworth, H.S., Guschina, I.A., Evans, B.A., Mode, A., Zigman, J.M., and Wells, T. (2009) Ghrelin induces abdominal obesity via GHS-R-dependent lipid retention. Mol Endocrinol 23, 914-924.

De Souza, C.T., Araujo, E.P., Bordin, S., Ashimine, R., Zollner, R.L., Boschero, A.C., Saad, M.J., and Velloso, L.A. (2005) Consumption of a fat-rich diet activates a proinflammatory response and induces insulin resistance in the hypothalamus. Endocrinology 146, 4192-4199.

Dheen, S.T., Kaur, C., and Ling, E.A. (2007) Microglial activation and its implications in the brain diseases. Curr Med Chem 14, 1189-1197.

Dhillo, W.S., Small, C.J., Stanley, S.A., Jethwa, P.H., Seal, L.J., Murphy, K.G., Ghatei, M.A., and Bloom, S.R. (2002) Hypothalamic interactions between neuropeptide Y, agouti-related protein, cocaine- and amphetamine-regulated transcript and alpha-

melanocyte-stimulating hormone in vitro in male rats. J Neuroendocrinol 14, 725-730.

Dib, L., San-Jose, L.M., Ducrest, A.L., Salamin, N., and Roulin, A. (2017) Selection on the Major Color Gene Melanocortin-1-Receptor Shaped the Evolution of the Melanocortin System Genes. Int J Mol Sci 18.

Djogo, T., Robins, S.C., Schneider, S., Kryzskaya, D., Liu, X., Mingay, A., Gillon, C.J., Kim, J.H., Storch, K.F., Boehm, U., Bourque, C.W., Stroh, T., Dimou, L., and Kokoeva, M.V. (2016) Adult NG2-Glia Are Required for Median Eminence-Mediated Leptin Sensing and Body Weight Control. Cell Metab 23, 797-810.

Douglass, J. and Daoud, S. (1996) Characterization of the human cDNA and genomic DNA encoding CART: a cocaine- and amphetamine-regulated transcript. Gene 169, 241-245.

Douglass, J., McKinzie, A.A., and Couceyro, P. (1995) PCR differential display identifies a rat brain mRNA that is transcriptionally regulated by cocaine and amphetamine. J Neurosci 15, 2471-2481.

Douglass, J.D., Dorfman, M.D., Fasnacht, R., Shaffer, L.D., and Thaler, J.P. (2017) Astrocyte IKKbeta/NF-kappaB signaling is required for diet-induced obesity and hypothalamic inflammation. Mol Metab 6, 366-373.

Ebina, Y., Ellis, L., Jarnagin, K., Edery, M., Graf, L., Clauser, E., Ou, J.H., Masiarz, F., Kan, Y.W., Goldfine, I.D., and et al. (1985) The human insulin receptor cDNA: the structural basis for hormone-activated transmembrane signalling. Cell 40, 747-758.

Edwards, C.M., Stanley, S.A., Davis, R., Brynes, A.E., Frost, G.S., Seal, L.J., Ghatei, M.A., and Bloom, S.R. (2001) Exendin-4 reduces fasting and postprandial glucose and decreases energy intake in healthy volunteers. Am J Physiol Endocrinol Metab 281, E155-161.

Elias, C.F., Aschkenasi, C., Lee, C., Kelly, J., Ahima, R.S., Bjorbaek, C., Flier, J.S., Saper, C.B., and Elmquist, J.K. (1999) Leptin differentially regulates NPY and POMC neurons projecting to the lateral hypothalamic area. Neuron 23, 775-786.

Ellacott, K.L. and Cone, R.D. (2006) The role of the central melanocortin system in the regulation of food intake and energy homeostasis: lessons from mouse models. Philos Trans R Soc Lond B Biol Sci 361, 1265-1274.

Elmore, M.R., Najafi, A.R., Koike, M.A., Dagher, N.N., Spangenberg, E.E., Rice, R.A., Kitazawa, M., Matusow, B., Nguyen, H., West, B.L., and Green, K.N. (2014) Colony-stimulating factor 1 receptor signaling is necessary for microglia viability, unmasking a microglia progenitor cell in the adult brain. Neuron 82, 380-397.

Elmquist, J.K., Maratos-Flier, E., Saper, C.B., and Flier, J.S. (1998) Unraveling the central nervous system pathways underlying responses to leptin. Nat Neurosci 1, 445-450.

Erickson, J.C., Clegg, K.E., and Palmiter, R.D. (1996a) Sensitivity to leptin and susceptibility to seizures of mice lacking neuropeptide Y. Nature 381, 415-421.

Erickson, J.C., Hollopeter, G., and Palmiter, R.D. (1996b) Attenuation of the obesity syndrome of ob/ob mice by the loss of neuropeptide Y. Science 274, 1704-1707.

Eyigor, O. and Jennes, L. (1998) Identification of kainate-preferring glutamate receptor subunit GluR7 mRNA and protein in the rat median eminence. Brain Res 814, 231-235.

Fang, C.X., Dong, F., Thomas, D.P., Ma, H., He, L., and Ren, J. (2008) Hypertrophic cardiomyopathy in high-fat diet-induced obesity: role of suppression of forkhead transcription factor and atrophy gene transcription. Am J Physiol Heart Circ Physiol 295, H1206-H1215.

Faouzi, M., Leshan, R., Bjornholm, M., Hennessey, T., Jones, J., and Munzberg, H. (2007) Differential accessibility of circulating leptin to individual hypothalamic sites. Endocrinology 148, 5414-5423.

Farooqi, I.S., Drop, S., Clements, A., Keogh, J.M., Biernacka, J., Lowenbein, S., Challis, B.G., and O'Rahilly, S. (2006) Heterozygosity for a POMC-null mutation and increased obesity risk in humans. Diabetes 55, 2549-2553.

Farooqi, I.S. and O'Rahilly, S. (2008) Mutations in ligands and receptors of the leptin-melanocortin pathway that lead to obesity. Nat Clin Pract Endocrinol Metab 4, 569-577.

Farooqi, I.S., Yeo, G.S., Keogh, J.M., Aminian, S., Jebb, S.A., Butler, G., Cheetham, T., and O'Rahilly, S. (2000) Dominant and recessive inheritance of morbid obesity associated with melanocortin 4 receptor deficiency. J Clin Invest 106, 271-279.

Farooqi, S., Rau, H., Whitehead, J., and O'Rahilly, S. (1998) ob gene mutations and human obesity. Proc Nutr Soc 57, 471-475.

Fekete, C. and Lechan, R.M. (2014) Central regulation of hypothalamic-pituitary-thyroid axis under physiological and pathophysiological conditions. Endocr Rev 35, 159-194.

Fekete, C., Legradi, G., Mihaly, E., Huang, Q.H., Tatro, J.B., Rand, W.M., Emerson, C.H., and Lechan, R.M. (2000a) alpha-Melanocyte-stimulating hormone is contained in nerve terminals innervating thyrotropin-releasing hormone-synthesizing neurons in the hypothalamic paraventricular nucleus and prevents fasting-induced suppression of prothyrotropin-releasing hormone gene expression. J Neurosci 20, 1550-1558.

Fekete, C., Marks, D.L., Sarkar, S., Emerson, C.H., Rand, W.M., Cone, R.D., and Lechan, R.M. (2004) Effect of Agouti-related protein in regulation of the hypothalamic-pituitary-thyroid axis in the melanocortin 4 receptor knockout mouse. Endocrinology 145, 4816-4821.

Fekete, C., Mihaly, E., Herscovici, S., Salas, J., Tu, H., Larsen, P.R., and Lechan, R.M. (2000b) DARPP-32 and CREB are present in type 2 iodothyronine deiodinase-producing tanycytes: implications for the regulation of type 2 deiodinase activity. Brain Res 862, 154-161.

Fekete, C., Mihaly, E., Luo, L.G., Kelly, J., Clausen, J.T., Mao, Q., Rand, W.M., Moss, L.G., Kuhar, M., Emerson, C.H., Jackson, I.M., and Lechan, R.M. (2000c) Association of cocaine- and amphetamine-regulated transcript-immunoreactive elements with thyrotropin-releasing hormone-synthesizing neurons in the

hypothalamic paraventricular nucleus and its role in the regulation of the hypothalamic-pituitary-thyroid axis during fasting. J Neurosci 20, 9224-9234.

Fekete, C., Singru, P.S., Sanchez, E., Sarkar, S., Christoffolete, M.A., Riberio, R.S., Rand, W.M., Emerson, C.H., Bianco, A.C., and Lechan, R.M. (2006) Differential effects of central leptin, insulin, or glucose administration during fasting on the hypothalamic-pituitary-thyroid axis and feeding-related neurons in the arcuate nucleus. Endocrinology 147, 520-529.

Finkbeiner, S. (1992) Calcium waves in astrocytes-filling in the gaps. Neuron 8, 1101-1108.

Firth, J.A. and Bock, R. (1976) Distribution and properties of an adenosine triphosphatase in the tanycyte ependyma of the IIIrd ventricle of the rat. Histochemistry 47, 145-157.

Flament-Durand, J. and Brion, J.P. (1985) Tanycytes: morphology and functions: a review. Int Rev Cytol 96, 121-155.

Flier, J.S. (1998) Lowered leptin slims immune response. Nat Med 4, 1124-1125.

Flier, J.S. (2006) AgRP in energy balance: Will the real AgRP please stand up? Cell Metab 3, 83-85.

Frayling, C., Britton, R., and Dale, N. (2011) ATP-mediated glucosensing by hypothalamic tanycytes. J Physiol 589, 2275-2286.

Freire-Regatillo, A., Argente-Arizon, P., Argente, J., Garcia-Segura, L.M., and Chowen, J.A. (2017) Non-Neuronal Cells in the Hypothalamic Adaptation to Metabolic Signals. Front Endocrinol (Lausanne) 8, 51.

Gaisano, G.G., Park, S.J., Daly, D.M., and Beyak, M.J. (2010) Glucagon-like peptide-1 inhibits voltage-gated potassium currents in mouse nodose ganglion neurons. Neurogastroenterol Motil 22, 470-479, e111.

Gallyas, F. and Merchenthaler, I. (1988) Copper-H2O2 oxidation strikingly improves silver intensification of the nickel-diaminobenzidine (Ni-DAB) end-product of the peroxidase reaction. J Histochem Cytochem 36, 807-810.

Gao, Q. and Horvath, T.L. (2007) Neurobiology of feeding and energy expenditure. Annu Rev Neurosci 30, 367-398.

Garcia, M., Millan, C., Balmaceda-Aguilera, C., Castro, T., Pastor, P., Montecinos, H., Reinicke, K., Zuniga, F., Vera, J.C., Onate, S.A., and Nualart, F. (2003) Hypothalamic ependymal-glial cells express the glucose transporter GLUT2, a protein involved in glucose sensing. J Neurochem 86, 709-724.

Garcia, M.A., Carrasco, M., Godoy, A., Reinicke, K., Montecinos, V.P., Aguayo, L.G., Tapia, J.C., Vera, J.C., and Nualart, F. (2001) Elevated expression of glucose transporter-1 in hypothalamic ependymal cells not involved in the formation of the brain-cerebrospinal fluid barrier. J Cell Biochem 80, 491-503.

Gautvik, K.M., deLecea, L., Gautvik, V.T., Danielson, P.E., Tranque, P., Dopazo, A., Bloom, F.E., and Sutcliffe, J.G. (1996) Overview of the most prevalent hypothalamus-specific mRNAs, as identified by directional tag PCR subtraction. P Natl Acad Sci USA 93, 8733-8738.

Giaume, C. and Theis, M. (2010) Pharmacological and genetic approaches to study connexin-mediated channels in glial cells of the central nervous system. Brain Res Rev 63, 160-176.

Glatzle, J., Wang, Y., Adelson, D.W., Kalogeris, T.J., Zittel, T.T., Tso, P., Wei, J.Y., and Raybould, H.E. (2003) Chylomicron components activate duodenal vagal afferents via a cholecystokinin A receptor-mediated pathway to inhibit gastric motor function in the rat. J Physiol 550, 657-664.

Goebel-Stengel, M., Stengel, A., Wang, L., Ohning, G., Tache, Y., and Reeve, J.R., Jr. (2012) CCK-8 and CCK-58 differ in their effects on nocturnal solid meal pattern in undisturbed rats. Am J Physiol Regul Integr Comp Physiol 303, R850-860.

Gomez-Nicola, D., Fransen, N.L., Suzzi, S., and Perry, V.H. (2013) Regulation of microglial proliferation during chronic neurodegeneration. J Neurosci 33, 2481-2493.

Goto, K., Inui, A., Takimoto, Y., Yuzuriha, H., Asakawa, A., Kawamura, Y., Tsuji, H., Takahara, Y., Takeyama, C., Katsuura, G., and Kasuga, M. (2003) Acute intracerebroventricular administration of either carboxyl-terminal or amino-terminal fragments of agouti-related peptide produces a long-term decrease in energy expenditure in rats. Int J Mol Med 12, 379-383.

Graeber, M.B. (2010) Changing face of microglia. Science 330, 783-788.

Graeber, M.B., Li, W., and Rodriguez, M.L. (2011) Role of microglia in CNS inflammation. FEBS Lett 585, 3798-3805.

Gropp, E., Shanabrough, M., Borok, E., Xu, A.W., Janoschek, R., Buch, T., Plum, L., Balthasar, N., Hampel, B., Waisman, A., Barsh, G.S., Horvath, T.L., and Bruning, J.C. (2005) Agouti-related peptide-expressing neurons are mandatory for feeding. Nat Neurosci 8, 1289-1291.

Gutzwiller, J.P., Goke, B., Drewe, J., Hildebrand, P., Ketterer, S., Handschin, D., Winterhalder, R., Conen, D., and Beglinger, C. (1999) Glucagon-like peptide-1: a potent regulator of food intake in humans. Gut 44, 81-86.

Haan, N., Goodman, T., Najdi-Samiei, A., Stratford, C.M., Rice, R., El Agha, E., Bellusci, S., and Hajihosseini, M.K. (2013) Fgf10-expressing tanycytes add new neurons to the appetite/energy-balance regulating centers of the postnatal and adult hypothalamus. J Neurosci 33, 6170-6180.

Hahn, T.M., Breininger, J.F., Baskin, D.G., and Schwartz, M.W. (1998) Coexpression of Agrp and NPY in fasting-activated hypothalamic neurons. Nat Neurosci 1, 271-272.

Hakansson, M.L., Hulting, A.L., and Meister, B. (1996) Expression of leptin receptor mRNA in the hypothalamic arcuate nucleus--relationship with NPY neurones. Neuroreport 7, 3087-3092.

Halaas, J.L., Gajiwala, K.S., Maffei, M., Cohen, S.L., Chait, B.T., Rabinowitz, D., Lallone, R.L., Burley, S.K., and Friedman, J.M. (1995) Weight-reducing effects of the plasma protein encoded by the obese gene. Science 269, 543-546.

Hanisch, U.K. and Kettenmann, H. (2007) Microglia: active sensor and versatile effector cells in the normal and pathologic brain. Nat Neurosci 10, 1387-1394.

Hatton, J.D. and Ellisman, M.H. (1982) The distribution of orthogonal arrays in the freeze-fractured rat median eminence. J Neurocytol 11, 335-349.

Havrankova, J., Roth, J., and Brownstein, M. (1978) Insulin receptors are widely distributed in the central nervous system of the rat. Nature 272, 827-829.

Hayes, M.R., Kanoski, S.E., Alhadeff, A.L., and Grill, H.J. (2011) Comparative effects of the long-acting GLP-1 receptor ligands, liraglutide and exendin-4, on food intake and body weight suppression in rats. Obesity (Silver Spring) 19, 1342-1349.

Herrmann, C., Goke, R., Richter, G., Fehmann, H.C., Arnold, R., and Goke, B. (1995) Glucagon-like peptide-1 and glucose-dependent insulin-releasing polypeptide plasma levels in response to nutrients. Digestion 56, 117-126.

Hewson, A.K. and Dickson, S.L. (2000) Systemic administration of ghrelin induces Fos and Egr-1 proteins in the hypothalamic arcuate nucleus of fasted and fed rats. J Neuroendocrinol 12, 1047-1049.

Hillebrand, J.J., de Wied, D., and Adan, R.A. (2002) Neuropeptides, food intake and body weight regulation: a hypothalamic focus. Peptides 23, 2283-2306.

Hofmann, K., Lamberz, C., Piotrowitz, K., Offermann, N., But, D., Scheller, A., Al-Amoudi, A., and Kuerschner, L. (2017) Tanycytes and a differential fatty acid metabolism in the hypothalamus. Glia 65, 231-249.

Hokfelt, T., Foster, G., Schultzberg, M., Meister, B., Schalling, M., Goldstein, M., Hemmings, H.C., Jr., Ouimet, C., and Greengard, P. (1988) DARPP-32 as a marker for D-1 dopaminoceptive cells in the rat brain: prenatal development and presence in glial elements (tanycytes) in the basal hypothalamus. Adv Exp Med Biol 235, 65-82.

Holst, J.J. (2007) The physiology of glucagon-like peptide 1. Physiol Rev 87, 1409-1439.

Horvath, T.L., Sarman, B., Garcia-Caceres, C., Enriori, P.J., Sotonyi, P., Shanabrough, M., Borok, E., Argente, J., Chowen, J.A., Perez-Tilve, D., Pfluger, P.T., Bronneke, H.S., Levin, B.E., Diano, S., Cowley, M.A., and Tschop, M.H. (2010) Synaptic input organization of the melanocortin system predicts diet-induced hypothalamic reactive gliosis and obesity. Proc Natl Acad Sci U S A 107, 14875-14880.

Huang, W., Ramsey, K.M., Marcheva, B., and Bass, J. (2011) Circadian rhythms, sleep, and metabolism. J Clin Invest 121, 2133-2141.

Hunter, K. and Holscher, C. (2012) Drugs developed to treat diabetes, liraglutide and lixisenatide, cross the blood brain barrier and enhance neurogenesis. BMC Neurosci 13, 33.

Huszar, D., Lynch, C.A., Fairchild-Huntress, V., Dunmore, J.H., Fang, Q., Berkemeier, L.R., Gu, W., Kesterson, R.A., Boston, B.A., Cone, R.D., Smith, F.J., Campfield, L.A., Burn, P., and Lee, F. (1997) Targeted disruption of the melanocortin-4 receptor results in obesity in mice. Cell 88, 131-141.

Ibrahim, N., Bosch, M.A., Smart, J.L., Qiu, J., Rubinstein, M., Ronnekleiv, O.K., Low, M.J., and Kelly, M.J. (2003) Hypothalamic proopiomelanocortin neurons are glucose responsive and express K(ATP) channels. Endocrinology 144, 1331-1340.

Ito, D., Imai, Y., Ohsawa, K., Nakajima, K., Fukuuchi, Y., and Kohsaka, S. (1998) Microglia-specific localisation of a novel calcium binding protein, Iba1. Brain Res Mol Brain Res 57, 1-9.

Iwakura, H., Kangawa, K., and Nakao, K. (2015) The regulation of circulating ghrelin - with recent updates from cell-based assays. Endocr J 62, 107-122.

Jha, M.K. and Suk, K. (2013) Glia-based biomarkers and their functional role in the CNS. Expert Rev Proteomics 10, 43-63.

Kalra, S.P., Dube, M.G., Fournier, A., and Kalra, P.S. (1991) Structure-function analysis of stimulation of food intake by neuropeptide Y: effects of receptor agonists. Physiol Behav 50, 5-9.

Kanoski, S.E., Alhadeff, A.L., Fortin, S.M., Gilbert, J.R., and Grill, H.J. (2014) Leptin signaling in the medial nucleus tractus solitarius reduces food seeking and willingness to work for food. Neuropsychopharmacology 39, 605-613.

Kentish, S.J. and Page, A.J. (2014) Plasticity of gastro-intestinal vagal afferent endings. Physiol Behav 136, 170-178.

Kesterson, R.A., Huszar, D., Lynch, C.A., Simerly, R.B., and Cone, R.D. (1997) Induction of neuropeptide Y gene expression in the dorsal medial hypothalamic nucleus in two models of the agouti obesity syndrome. Mol Endocrinol 11, 630-637.

Kishi, T., Aschkenasi, C.J., Lee, C.E., Mountjoy, K.G., Saper, C.B., and Elmquist, J.K. (2003) Expression of melanocortin 4 receptor mRNA in the central nervous system of the rat. J Comp Neurol 457, 213-235.

Kofuji, P. and Newman, E.A. (2004) Potassium buffering in the central nervous system. Neuroscience 129, 1045-1056.

Kojima, M., Hosoda, H., Date, Y., Nakazato, M., Matsuo, H., and Kangawa, K. (1999) Ghrelin is a growth-hormone-releasing acylated peptide from stomach. Nature 402, 656-660.

Kong, W., Stanley, S., Gardiner, J., Abbott, C., Murphy, K., Seth, A., Connoley, I., Ghatei, M., Stephens, D., and Bloom, S. (2003) A role for arcuate cocaine and amphetamine-regulated transcript in hyperphagia, thermogenesis, and cold adaptation. FASEB J 17, 1688-1690.

Korner, J., Wissig, S., Kim, A., Conwell, I.M., and Wardlaw, S.L. (2003) Effects of agouti-related protein on metabolism and hypothalamic neuropeptide gene expression. J Neuroendocrinol 15, 1116-1121.

Kozlowski, G.P. and Coates, P.W. (1985) Ependymoneuronal specializations between LHRH fibers and cells of the cerebroventricular system. Cell Tissue Res 242, 301-311.

Krashes, M.J., Koda, S., Ye, C., Rogan, S.C., Adams, A.C., Cusher, D.S., Maratos-Flier, E., Roth, B.L., and Lowell, B.B. (2011) Rapid, reversible activation of AgRP neurons drives feeding behavior in mice. J Clin Invest 121, 1424-1428.

Kriegstein, A.R. and Gotz, M. (2003) Radial glia diversity: a matter of cell fate. Glia 43, 37-43.

Kristensen, P., Judge, M.E., Thim, L., Ribel, U., Christjansen, K.N., Wulff, B.S., Clausen, J.T., Jensen, P.B., Madsen, O.D., Vrang, N., Larsen, P.J., and Hastrup, S. (1998) Hypothalamic CART is a new anorectic peptide regulated by leptin. Nature 393, 72-76.

Krude, H., Biebermann, H., Luck, W., Horn, R., Brabant, G., and Gruters, A. (1998) Severe early-onset obesity, adrenal insufficiency and red hair pigmentation caused by POMC mutations in humans. Nat Genet 19, 155-157.

Lam, T.K., Schwartz, G.J., and Rossetti, L. (2005) Hypothalamic sensing of fatty acids. Nat Neurosci 8, 579-584.

Langlet, F., Levin, B.E., Luquet, S., Mazzone, M., Messina, A., Dunn-Meynell, A.A., Balland, E., Lacombe, A., Mazur, D., Carmeliet, P., Bouret, S.G., Prevot, V., and Dehouck, B. (2013) Tanycytic VEGF-A boosts blood-hypothalamus barrier plasticity and access of metabolic signals to the arcuate nucleus in response to fasting. Cell Metab 17, 607-617.

Lau, J. and Herzog, H. (2014) CART in the regulation of appetite and energy homeostasis. Front Neurosci 8, 313.

Laurent, V., Jaubert-Miazza, L., Desjardins, R., Day, R., and Lindberg, I. (2004) Biosynthesis of proopiomelanocortin-derived peptides in prohormone convertase 2 and 7B2 null mice. Endocrinology 145, 519-528.

Lazutkaite, G., Solda, A., Lossow, K., Meyerhof, W., and Dale, N. (2017) Amino acid sensing in hypothalamic tanycytes via umami taste receptors. Mol Metab 6, 1480-1492.

Lechan, R.M. and Fekete, C. (2007) Infundibular tanycytes as modulators of neuroendocrine function: hypothetical role in the regulation of the thyroid and gonadal axis. Acta Biomed 78 Suppl 1, 84-98.

Lee, D.A., Bedont, J.L., Pak, T., Wang, H., Song, J., Miranda-Angulo, A., Takiar, V., Charubhumi, V., Balordi, F., Takebayashi, H., Aja, S., Ford, E., Fishell, G., and Blackshaw, S. (2012) Tanycytes of the hypothalamic median eminence form a diet-responsive neurogenic niche. Nat Neurosci 15, 700-702.

Levine, A.S. and Morley, J.E. (1984) Neuropeptide Y: a potent inducer of consummatory behavior in rats. Peptides 5, 1025-1029.

Levitt, P. and Rakic, P. (1980) Immunoperoxidase localization of glial fibrillary acidic protein in radial glial cells and astrocytes of the developing rhesus monkey brain. J Comp Neurol 193, 815-840.

Li, Y. (2007) Sensory signal transduction in the vagal primary afferent neurons. Curr Med Chem 14, 2554-2563.

Lin, E.J., Sainsbury, A., Lee, N.J., Boey, D., Couzens, M., Enriquez, R., Slack, K., Bland, R., During, M.J., and Herzog, H. (2006) Combined deletion of Y1, Y2, and Y4 receptors prevents hypothalamic neuropeptide Y overexpression-induced hyperinsulinemia despite persistence of hyperphagia and obesity. Endocrinology 147, 5094-5101.

Liu, C.D., Aloia, T., Adrian, T.E., Newton, T.R., Bilchik, A.J., Zinner, M.J., Ashley, S.W., and McFadden, D.W. (1996) Peptide YY: a potential proabsorptive hormone for the treatment of malabsorptive disorders. Am Surg 62, 232-236.

Lovshin, J.A. and Drucker, D.J. (2009) Incretin-based therapies for type 2 diabetes mellitus. Nat Rev Endocrinol 5, 262-269.

Menyhert, J., Wittmann, G., Lechan, R.M., Keller, E., Liposits, Z., and Fekete, C. (2007) Cocaine- and amphetamine-regulated transcript (CART) is colocalized with the orexigenic neuropeptide Y and agouti-related protein and absent from the anorexigenic alpha-melanocyte-stimulating hormone neurons in the infundibular nucleus of the human hypothalamus. Endocrinology 148, 4276-4281.

Millan, C., Martinez, F., Cortes-Campos, C., Lizama, I., Yanez, M.J., Llanos, P., Reinicke, K., Rodriguez, F., Peruzzo, B., Nualart, F., and Garcia, M.A. (2010) Glial glucokinase expression in adult and post-natal development of the hypothalamic region. ASN Neuro 2, e00035.

Miller, R., Aaron, W., Toneff, T., Vishnuvardhan, D., Beinfeld, M.C., and Hook, V.Y. (2003) Obliteration of alpha-melanocyte-stimulating hormone derived from POMC in pituitary and brains of PC2-deficient mice. J Neurochem 86, 556-563.

Mitrou, P., Raptis, S.A., and Dimitriadis, G. (2013) Insulin action in morbid obesity: a focus on muscle and adipose tissue. Hormones (Athens) 12, 201-213.

Mizuno, T.M., Kelley, K.A., Pasinetti, G.M., Roberts, J.L., and Mobbs, C.V. (2003) Transgenic neuronal expression of proopiomelanocortin attenuates hyperphagic response to fasting and reverses metabolic impairments in leptin-deficient obese mice. Diabetes 52, 2675-2683.

Mizuno, T.M., Kleopoulos, S.P., Bergen, H.T., Roberts, J.L., Priest, C.A., and Mobbs, C.V. (1998) Hypothalamic pro-opiomelanocortin mRNA is reduced by fasting and [corrected] in ob/ob and db/db mice, but is stimulated by leptin. Diabetes 47, 294-297.

Monroe, B.G. and Paull, W.K. (1974) Ultrastructural changes in the hypothalamus during development and hypothalamic activity: the median eminence. Prog Brain Res 41, 185-208.

Morris, M.J., Tortelli, C.F., Filippis, A., and Proietto, J. (1998) Reduced BAT function as a mechanism for obesity in the hypophagic, neuropeptide Y deficient monosodium glutamate-treated rat. Regul Pept 75-76, 441-447.

Morton, G.J., Cummings, D.E., Baskin, D.G., Barsh, G.S., and Schwartz, M.W. (2006) Central nervous system control of food intake and body weight. Nature 443, 289-295.

Mullier, A., Bouret, S.G., Prevot, V., and Dehouck, B. (2010) Differential distribution of tight junction proteins suggests a role for tanycytes in blood-hypothalamus barrier regulation in the adult mouse brain. J Comp Neurol 518, 943-962.

Munzberg, H. and Myers, M.G., Jr. (2005) Molecular and anatomical determinants of central leptin resistance. Nat Neurosci 8, 566-570.

Muoio, D.M. and Newgard, C.B. (2008) Mechanisms of disease:Molecular and metabolic mechanisms of insulin resistance and beta-cell failure in type 2 diabetes. Nat Rev Mol Cell Biol 9, 193-205.

Murphy, B., Nunes, C.N., Ronan, J.J., Harper, C.M., Beall, M.J., Hanaway, M., Fairhurst, A.M., Van der Ploeg, L.H., MacIntyre, D.E., and Mellin, T.N. (1998) Melanocortin mediated inhibition of feeding behavior in rats. Neuropeptides 32, 491-497.

Nakazato, M., Murakami, N., Date, Y., Kojima, M., Matsuo, H., Kangawa, K., and Matsukura, S. (2001) A role for ghrelin in the central regulation of feeding. Nature 409, 194-198.

Nelson, G., Chandrashekar, J., Hoon, M.A., Feng, L., Zhao, G., Ryba, N.J., and Zuker, C.S. (2002) An amino-acid taste receptor. Nature 416, 199-202.

Neuwelt, E.A., Bauer, B., Fahlke, C., Fricker, G., Iadecola, C., Janigro, D., Leybaert, L., Molnar, Z., O'Donnell, M.E., Povlishock, J.T., Saunders, N.R., Sharp, F., Stanimirovic, D., Watts, R.J., and Drewes, L.R. (2011) Engaging neuroscience to advance translational research in brain barrier biology. Nat Rev Neurosci 12, 169-182.

Ollmann, M.M., Wilson, B.D., Yang, Y.K., Kerns, J.A., Chen, Y., Gantz, I., and Barsh, G.S. (1997) Antagonism of central melanocortin receptors in vitro and in vivo by agouti-related protein. Science 278, 135-138.

Orellana, J.A., Saez, P.J., Cortes-Campos, C., Elizondo, R.J., Shoji, K.F., Contreras-Duarte, S., Figueroa, V., Velarde, V., Jiang, J.X., Nualart, F., Saez, J.C., and Garcia, M.A. (2012) Glucose increases intracellular free Ca(2+) in tanycytes via ATP released through connexin 43 hemichannels. Glia 60, 53-68.

Ozcan, L., Ergin, A.S., Lu, A., Chung, J., Sarkar, S., Nie, D., Myers, M.G., Jr., and Ozcan, U. (2009) Endoplasmic reticulum stress plays a central role in development of leptin resistance. Cell Metab 9, 35-51.

Page, A.J., Martin, C.M., and Blackshaw, L.A. (2002) Vagal mechanoreceptors and chemoreceptors in mouse stomach and esophagus. J Neurophysiol 87, 2095-2103.

Paolicelli, R.C., Bolasco, G., Pagani, F., Maggi, L., Scianni, M., Panzanelli, P., Giustetto, M., Ferreira, T.A., Guiducci, E., Dumas, L., Ragozzino, D., and Gross, C.T. (2011) Synaptic pruning by microglia is necessary for normal brain development. Science 333, 1456-1458.

Pekny, M. and Nilsson, M. (2005) Astrocyte activation and reactive gliosis. Glia 50, 427-434.

Perez-Martin, M., Cifuentes, M., Grondona, J.M., Lopez-Avalos, M.D., Gomez-Pinedo, U., Garcia-Verdugo, J.M., and Fernandez-Llebrez, P. (2010) IGF-I stimulates neurogenesis in the hypothalamus of adult rats. Eur J Neurosci 31, 1533-1548.

Peruzzo, B., Pastor, F.E., Blazquez, J.L., Amat, P., and Rodriguez, E.M. (2004) Polarized endocytosis and transcytosis in the hypothalamic tanycytes of the rat. Cell Tissue Res 317, 147-164.

Peruzzo, B., Pastor, F.E., Blazquez, J.L., Schobitz, K., Pelaez, B., Amat, P., and Rodriguez, E.M. (2000) A second look at the barriers of the medial basal hypothalamus. Exp Brain Res 132, 10-26.

Phillips, R.J. and Powley, T.L. (2000) Tension and stretch receptors in gastrointestinal smooth muscle: re-evaluating vagal mechanoreceptor electrophysiology. Brain Res Brain Res Rev 34, 1-26.

Prevot, V. (2002) Glial-neuronal-endothelial interactions are involved in the control of GnRH secretion. J Neuroendocrinol 14, 247-255.

Prevot, V., Langlet, F., and Dehouck, B. (2013) Flipping the tanycyte switch: how circulating signals gain direct access to the metabolic brain. Aging (Albany NY) 5, 332-334.

Qian, S., Chen, H., Weingarth, D., Trumbauer, M.E., Novi, D.E., Guan, X., Yu, H., Shen, Z., Feng, Y., Frazier, E., Chen, A., Camacho, R.E., Shearman, L.P., Gopal-Truter, S., MacNeil, D.J., Van der Ploeg, L.H., and Marsh, D.J. (2002) Neither agouti-related protein nor neuropeptide Y is critically required for the regulation of energy homeostasis in mice. Mol Cell Biol 22, 5027-5035.

Qing, K. and Chen, Y. (2007) Central CART gene delivery by recombinant AAV vector attenuates body weight gain in diet-induced-obese rats. Regul Pept 140, 21-26.

Redecker, P. (1989) Postnatal development of glial fibrillary acidic protein (GFAP) immunoreactivity in pituicytes and tanycytes of the Mongolian gerbil (Meriones unguiculatus). Histochemistry 91, 507-515.

Rethelyi, M. (1984) Diffusional barrier around the hypothalamic arcuate nucleus in the rat. Brain Res 307, 355-358.

Robins, S.C., Stewart, I., McNay, D.E., Taylor, V., Giachino, C., Goetz, M., Ninkovic, J., Briancon, N., Maratos-Flier, E., Flier, J.S., Kokoeva, M.V., and Placzek, M. (2013a) alpha-Tanycytes of the adult hypothalamic third ventricle include distinct populations of FGF-responsive neural progenitors. Nat Commun 4, 2049.

Robins, S.C., Trudel, E., Rotondi, O., Liu, X., Djogo, T., Kryzskaya, D., Bourque, C.W., and Kokoeva, M.V. (2013b) Evidence for NG2-glia derived, adult-born functional neurons in the hypothalamus. PLoS One 8, e78236.

Rodriguez, E.M., Blazquez, J.L., Pastor, F.E., Pelaez, B., Pena, P., Peruzzo, B., and Amat, P. (2005) Hypothalamic tanycytes: a key component of brain-endocrine interaction. Int Rev Cytol 247, 89-164.

Rodriguez, E.M., Gonzalez, C.B., and Delannoy, L. (1979) Cellular organization of the lateral and postinfundibular regions of the median eminence in the rat. Cell Tissue Res 201, 377-408.

Rose, C.R. and Ransom, B.R. (1996) Intracellular sodium homeostasis in rat hippocampal astrocytes. J Physiol 491 (Pt 2), 291-305.

Rose, C.R. and Ransom, B.R. (1997) Gap junctions equalize intracellular Na+ concentration in astrocytes. Glia 20, 299-307.

Rottkamp, D.M., Rudenko, I.A., Maier, M.T., Roshanbin, S., Yulyaningsih, E., Perez, L., Valdearcos, M., Chua, S., Koliwad, S.K., and Xu, A.W. (2015) Leptin potentiates astrogenesis in the developing hypothalamus. Mol Metab 4, 881-889.

Rouach, N., Koulakoff, A., Abudara, V., Willecke, K., and Giaume, C. (2008) Astroglial metabolic networks sustain hippocampal synaptic transmission. Science 322, 1551-1555.

Rutzel, H. and Schiebler, T.H. (1980) Prenatal and early postnatal development of the glial cells in the median eminence of the rat. Cell Tissue Res 211, 117-137.

Saez, J.C., Berthoud, V.M., Branes, M.C., Martinez, A.D., and Beyer, E.C. (2003) Plasma membrane channels formed by connexins: their regulation and functions. Physiol Rev 83, 1359-1400.

Salgado, M., Tarifeno-Saldivia, E., Ordenes, P., Millan, C., Yanez, M.J., Llanos, P., Villagra, M., Elizondo-Vega, R., Martinez, F., Nualart, F., Uribe, E., and de Los Angeles Garcia-Robles, M. (2014) Dynamic localization of glucokinase and its regulatory protein in hypothalamic tanycytes. PLoS One 9, e94035.

Saltiel, A.R. and Kahn, C.R. (2001) Insulin signalling and the regulation of glucose and lipid metabolism. Nature 414, 799-806.

Sayegh, A.I. (2013) The role of cholecystokinin receptors in the short-term control of food intake. Prog Mol Biol Transl Sci 114, 277-316.

Schafer, M.K., Day, R., Cullinan, W.E., Chretien, M., Seidah, N.G., and Watson, S.J. (1993) Gene expression of prohormone and proprotein convertases in the rat CNS: a comparative in situ hybridization analysis. J Neurosci 13, 1258-1279.

Schmelz, S. and Naismith, J.H. (2009) Adenylate-forming enzymes. Curr Opin Struct Biol 19, 666-671.

Schuit, F.C., Huypens, P., Heimberg, H., and Pipeleers, D.G. (2001) Glucose sensing in pancreatic beta-cells: a model for the study of other glucose-regulated cells in gut, pancreas, and hypothalamus. Diabetes 50, 1-11.

Schwartz, M.W., Woods, S.C., Porte, D., Jr., Seeley, R.J., and Baskin, D.G. (2000) Central nervous system control of food intake. Nature 404, 661-671.

Semenkovich, C.F. (2006) Insulin resistance and atherosclerosis. J Clin Invest 116, 1813-1822.

Shechter, R., London, A., Kuperman, Y., Ronen, A., Rolls, A., Chen, A., and Schwartz, M. (2013) Hypothalamic neuronal toll-like receptor 2 protects against age-induced obesity. Sci Rep 3, 1254.

Shoelson, S.E., Lee, J., and Goldfine, A.B. (2006) Inflammation and insulin resistance. J Clin Invest 116, 1793-1801.

Shukla, C., Britton, S.L., Koch, L.G., and Novak, C.M. (2012) Region-specific differences in brain melanocortin receptors in rats of the lean phenotype. Neuroreport 23, 596-600.

Smart, J.L. and Low, M.J. (2003) Lack of proopiomelanocortin peptides results in obesity and defective adrenal function but normal melanocyte pigmentation in the murine C57BL/6 genetic background. Ann N Y Acad Sci 994, 202-210.

Smith, G.M. and Shine, H.D. (1992) Immunofluorescent labeling of tight junctions in the rat brain and spinal cord. Int J Dev Neurosci 10, 387-392.

Smith, G.P., Gibbs, J., Jerome, C., Pi-Sunyer, F.X., Kissileff, H.R., and Thornton, J. (1981) The satiety effect of cholecystokinin: a progress report. Peptides 2 Suppl 2, 57-59.

Stengel, A. and Tache, Y. (2011) Interaction between gastric and upper small intestinal hormones in the regulation of hunger and satiety: ghrelin and cholecystokinin take the central stage. Curr Protein Pept Sci 12, 293-304.

Stewart, W.W. (1981) Lucifer dyes--highly fluorescent dyes for biological tracing. Nature 292, 17-21.

Stuber, G.D. and Wise, R.A. (2016) Lateral hypothalamic circuits for feeding and reward. Nat Neurosci 19, 198-205.

Szalay, G., Martinecz, B., Lenart, N., Kornyei, Z., Orsolits, B., Judak, L., Csaszar, E., Fekete, R., West, B.L., Katona, G., Rozsa, B., and Denes, A. (2016) Microglia protect against brain injury and their selective elimination dysregulates neuronal network activity after stroke. Nature Communications 7.

Szilvasy-Szabo, A., Varga, E., Beliczai, Z., Lechan, R.M., and Fekete, C. (2017) Localization of connexin 43 gap junctions and hemichannels in tanycytes of adult mice. Brain Res 1673, 64-71.

Takahashi, K.A. and Cone, R.D. (2005) Fasting induces a large, leptin-dependent increase in the intrinsic action potential frequency of orexigenic arcuate nucleus neuropeptide Y/Agouti-related protein neurons. Endocrinology 146, 1043-1047.

Tang-Christensen, M., Larsen, P.J., Goke, R., Fink-Jensen, A., Jessop, D.S., Moller, M., and Sheikh, S.P. (1996) Central administration of GLP-1-(7-36) amide inhibits food and water intake in rats. Am J Physiol 271, R848-856.

Tatemoto, K. (1982) Isolation and characterization of peptide YY (PYY), a candidate gut hormone that inhibits pancreatic exocrine secretion. Proc Natl Acad Sci U S A 79, 2514-2518.

Tatro, J.B. (1990) Melanotropin receptors in the brain are differentially distributed and recognize both corticotropin and alpha-melanocyte stimulating hormone. Brain Res 536, 124-132.

Thaler, F., Varasi, M., Carenzi, G., Colombo, A., Abate, A., Bigogno, C., Boggio, R., Carrara, S., Cataudella, T., Dal Zuffo, R., Reali, V., Vultaggio, S., Dondio, G., Gagliardi, S., Minucci, S., and Mercurio, C. (2012a) Spiro[chromane-2,4'-piperidine]-based histone deacetylase inhibitors with improved in vivo activity. ChemMedChem 7, 709-721.

Thaler, J.P., Yi, C.X., Schur, E.A., Guyenet, S.J., Hwang, B.H., Dietrich, M.O., Zhao, X., Sarruf, D.A., Izgur, V., Maravilla, K.R., Nguyen, H.T., Fischer, J.D., Matsen, M.E., Wisse, B.E., Morton, G.J., Horvath, T.L., Baskin, D.G., Tschop, M.H., and Schwartz, M.W. (2012b) Obesity is associated with hypothalamic injury in rodents and humans. J Clin Invest 122, 153-162.

Thaler, R., Spitzer, S., Karlic, H., Klaushofer, K., and Varga, F. (2012c) DMSO is a strong inducer of DNA hydroxymethylation in pre-osteoblastic MC3T3-E1 cells. Epigenetics 7, 635-651.

Thomzig, A., Laube, G., Pruss, H., and Veh, R.W. (2005) Pore-forming subunits of K-ATP channels, Kir6.1 and Kir6.2, display prominent differences in regional and cellular distribution in the rat brain. J Comp Neurol 484, 313-330.

Thomzig, A., Wenzel, M., Karschin, C., Eaton, M.J., Skatchkov, S.N., Karschin, A., and Veh, R.W. (2001) Kir6.1 is the principal pore-forming subunit of astrocyte but not neuronal plasma membrane K-ATP channels. Mol Cell Neurosci 18, 671-690.

Tran, D.Q., Tse, E.K., Kim, M.H., and Belsham, D.D. (2016) Diet-induced cellular neuroinflammation in the hypothalamus: Mechanistic insights from investigation of neurons and microglia. Mol Cell Endocrinol 438, 18-26.

Tschop, M., Smiley, D.L., and Heiman, M.L. (2000) Ghrelin induces adiposity in rodents. Nature 407, 908-913.

Tschop, M., Weyer, C., Tataranni, P.A., Devanarayan, V., Ravussin, E., and Heiman, M.L. (2001) Circulating ghrelin levels are decreased in human obesity. Diabetes 50, 707-709.

Tschop, M.H., Speakman, J.R., Arch, J.R., Auwerx, J., Bruning, J.C., Chan, L., Eckel, R.H., Farese, R.V., Jr., Galgani, J.E., Hambly, C., Herman, M.A., Horvath, T.L., Kahn, B.B., Kozma, S.C., Maratos-Flier, E., Muller, T.D., Munzberg, H., Pfluger, P.T., Plum, L., Reitman, M.L., Rahmouni, K., Shulman, G.I., Thomas, G., Kahn, C.R., and Ravussin, E. (2011) A guide to analysis of mouse energy metabolism. Nat Methods 9, 57-63.

Tu, H.M., Kim, S.W., Salvatore, D., Bartha, T., Legradi, G., Larsen, P.R., and Lechan, R.M. (1997) Regional distribution of type 2 thyroxine deiodinase messenger ribonucleic acid in rat hypothalamus and pituitary and its regulation by thyroid hormone. Endocrinology 138, 3359-3368.

Ullrich, A., Bell, J.R., Chen, E.Y., Herrera, R., Petruzzelli, L.M., Dull, T.J., Gray, A., Coussens, L., Liao, Y.C., Tsubokawa, M., and et al. (1985) Human insulin receptor and its relationship to the tyrosine kinase family of oncogenes. Nature 313, 756-761.

Valdearcos, M., Douglass, J.D., Robblee, M.M., Dorfman, M.D., Stifler, D.R., Bennett, M.L., Gerritse, I., Fasnacht, R., Barres, B.A., Thaler, J.P., and Koliwad, S.K. (2017) Microglial Inflammatory Signaling Orchestrates the Hypothalamic Immune Response to Dietary Excess and Mediates Obesity Susceptibility. Cell Metab 26, 185-197 e183.

Valdearcos, M., Robblee, M.M., Benjamin, D.I., Nomura, D.K., Xu, A.W., and Koliwad, S.K. (2014) Microglia dictate the impact of saturated fat consumption on hypothalamic inflammation and neuronal function. Cell Rep 9, 2124-2138.

van Houten, M., Khan, M.N., Khan, R.J., and Posner, B.I. (1981) Blood-borne adrenocorticotropin binds specifically to the median eminence-arcuate region of the rat hypothalamus. Endocrinology 108, 2385-2387.

Van Houten, M., Khan, M.N., Walsh, R.J., Baquiran, G.B., Renaud, L.P., Bourque, C., Sgro, S., Gauthier, S., Chretien, M., and Posner, B.I. (1985) NH2-terminal specificity

and axonal localization of adrenocorticotropin binding sites in rat median eminence. Proc Natl Acad Sci U S A 82, 1271-1275.

Vauthier, V., Derviaux, C., Douayry, N., Roux, T., Trinquet, E., Jockers, R., and Dam, J. (2013) Design and validation of a homogeneous time-resolved fluorescence-based leptin receptor binding assay. Anal Biochem 436, 1-9.

Vong, L., Ye, C., Yang, Z., Choi, B., Chua, S., Jr., and Lowell, B.B. (2011) Leptin action on GABAergic neurons prevents obesity and reduces inhibitory tone to POMC neurons. Neuron 71, 142-154.

Wang, H., Storlien, L.H., and Huang, X.F. (2002a) Effects of dietary fat types on body fatness, leptin, and ARC leptin receptor, NPY, and AgRP mRNA expression. Am J Physiol Endocrinol Metab 282, E1352-1359.

Wang, L., Saint-Pierre, D.H., and Tache, Y. (2002b) Peripheral ghrelin selectively increases Fos expression in neuropeptide Y - synthesizing neurons in mouse hypothalamic arcuate nucleus. Neurosci Lett 325, 47-51.

Wierup, N., Richards, W.G., Bannon, A.W., Kuhar, M.J., Ahren, B., and Sundler, F. (2005) CART knock out mice have impaired insulin secretion and glucose intolerance, altered beta cell morphology and increased body weight. Regul Pept 129, 203-211.

Willesen, M.G., Kristensen, P., and Romer, J. (1999) Co-localization of growth hormone secretagogue receptor and NPY mRNA in the arcuate nucleus of the rat. Neuroendocrinology 70, 306-316.

Wittmann, G., Farkas, E., Szilvasy-Szabo, A., Gereben, B., Fekete, C., and Lechan, R.M. (2017) Variable proopiomelanocortin expression in tanycytes of the adult rat hypothalamus and pituitary stalk. J Comp Neurol 525, 411-441.

Wittmann, G., Hrabovszky, E., and Lechan, R.M. (2013) Distinct glutamatergic and GABAergic subsets of hypothalamic pro-opiomelanocortin neurons revealed by in situ hybridization in male rats and mice. J Comp Neurol 521, 3287-3302.

Wittmann, G., Mohacsik, P., Balkhi, M.Y., Gereben, B., and Lechan, R.M. (2015) Endotoxin-induced inflammation down-regulates L-type amino acid transporter 1 (LAT1) expression at the blood-brain barrier of male rats and mice. Fluids Barriers CNS 12, 21.

Woods, S.C. (2013) Metabolic signals and food intake. Forty years of progress. Appetite 71, 440-444.

Woods, S.C., Lotter, E.C., McKay, L.D., and Porte, D., Jr. (1979) Chronic intracerebroventricular infusion of insulin reduces food intake and body weight of baboons. Nature 282, 503-505.

Wren, A.M., Seal, L.J., Cohen, M.A., Brynes, A.E., Frost, G.S., Murphy, K.G., Dhillo, W.S., Ghatei, M.A., and Bloom, S.R. (2001) Ghrelin enhances appetite and increases food intake in humans. J Clin Endocrinol Metab 86, 5992.

Wu, Q. and Palmiter, R.D. (2011) GABAergic signaling by AgRP neurons prevents anorexia via a melanocortin-independent mechanism. Eur J Pharmacol 660, 21-27.

Xu, Y., Tamamaki, N., Noda, T., Kimura, K., Itokazu, Y., Matsumoto, N., Dezawa, M., and Ide, C. (2005) Neurogenesis in the ependymal layer of the adult rat 3rd ventricle. Exp Neurol 192, 251-264.

Yaswen, L., Diehl, N., Brennan, M.B., and Hochgeschwender, U. (1999) Obesity in the mouse model of pro-opiomelanocortin deficiency responds to peripheral melanocortin. Nat Med 5, 1066-1070.

Young, A.A. (2012) Brainstem sensing of meal-related signals in energy homeostasis. Neuropharmacology 63, 31-45.

Zaborszky, L. and Schiebler, T.H. (1978) [Glia of median eminence. Electron microscopic studies of normal, adrenalectomized and castrated rats]. Z Mikrosk Anat Forsch 92, 781-799.

Zhang, K. and Kaufman, R.J. (2008) From endoplasmic-reticulum stress to the inflammatory response. Nature 454, 455-462.

Zhang, X., Zhang, G., Zhang, H., Karin, M., Bai, H., and Cai, D. (2008) Hypothalamic IKKbeta/NF-kappaB and ER stress link overnutrition to energy imbalance and obesity. Cell 135, 61-73.

Zhang, Y., Proenca, R., Maffei, M., Barone, M., Leopold, L., and Friedman, J.M. (1994) Positional cloning of the mouse obese gene and its human homologue. Nature 372, 425-432.

Zhou, Y. and Rui, L. (2013) Leptin signaling and leptin resistance. Front Med 7, 207-222.

10. List of publications

10.1. List of publications the thesis is based on

<u>Szilvásy-Szabó A</u>, Varga E, Beliczai Z, Lechan RM, Fekete C. (2017) Localization of connexin 43 gap junctions and hemichannels in tanycytes of adult mice. Brain Research, 1673:64-71.

Wittmann G, Farkas E, <u>Szilvásy-Szabó A</u>, Gereben B, Fekete C, Lechan RM. (2016) Variable proopiomelanocortin expression in tanycytes of the adult rat hypothalamus and pituitary stalk. J Comp Neurol, 525:411-441

10.2. Other publications

Kalló I, Vida B, Bardóczi Z, <u>Szilvásy-Szabó A</u>, Rabi F, Molnár T, Farkas I, Caraty A, Mikkelsen J, Coen CW, Hrabovszky E, Liposits Z. (2013) Gonadotropin-releasing hormone neurones innervate kisspeptin neurones in the female mouse brain. Neuroendocrinology, 98(4):281-289.

Mohácsik P, Füzesi T, Doleschall M, <u>Szilvásy-Szabó A</u>, Vancamp P, Hadadi É, Darras VM, Fekete C, Gereben B. (2016). Increased thyroid hormone activation accompanies the formation of thyroid hormone-dependent negative feedback in developing chicken hypothalamus. Endocrinology, 157:1211-1221.

Zséli G, Vida B, <u>Szilvásy-Szabó A</u>, Tóth M, Lechan RM, Fekete C. (2017) Neuronal connections of the central amygdalar nucleus with refeeding-activated brain areas in rats. Brain Struct Funct, 223(1):391-414

11. Acknowledgements